MSC ENGINEERING DISSERTATION

CHARACTERISING ELECTRICAL TREES IN NANOCOMPOSITE EPOXY-RESIN USING PARTIAL DISCHARGE DETECTION METHODS

Darryn Ryan Cornish

A dissertation submitted to the Faculty of Engineering and the Built Environment, University of the Witwatersrand, Johannesburg, in fulfilment of the requirements for the degree of Master of Science in Engineering.

Johannesburg, 2014

DECLARATION

I declare that this dissertation is my own unaided work except where specifically acknowledged. It is being submitted for a Degree of Master of Science to the University of the Witwatersrand, Johannesburg. It has not previously been submitted for any degree or examination to any other university.

Darryn Ryan Cornish	Date

ABSTRACT

Modern polymer based solid electrical insulation technologies, whilst highly optimal for their function, have been shown to have a major flaw: susceptibility to electrical treeing failure mode. This dissertation investigates the possibility of using Partial Discharge (PD) detection techniques to monitor and characterise electrical trees in nanocomposite epoxy insulation. The experimentation is done by creating highly divergent electric stress in nanocomposite samples and monitoring PD magnitudes over time until failure. Furthermore, a remote monitoring system was designed to allow for constant monitoring from anywhere with an internet connection. The experimental results revealed several interesting findings. Electrical trees in unfilled insulation behave differently from those in nanocomposite insulation. The electrical trees that form in unfilled epoxy are of bush/branch type with the corresponding PDs comprising of both big (greater than 10 pC) and small (less than 10 pC) pulses throughout the lifetime of the tree. In nanodielectrics however, the PD magnitudes are generally smaller than in the unfilled dielectric. Moreover the PD patterns evolve through distinct phases as the trees propagate from inception to complete failure. These distinct phases show new behaviour not seen in unfilled insulation, with phases of complete silence and some displaying patterns similar to corona. The resulting patterns are analysed and auto-classified, using a program written for this purpose, before being used to develop a model to explain the observed behaviour.

To my family,
without whom I would not have made it.

ACKNOWLEDGEMENTS

The author would like to acknowledge with gratitude the role rendered by both Dr. Cuthbert Nyamupangadengu and Prof. Iakovos Sigalas. Gratitude is given to Eskom for their support of the High Voltage Engineering Research Group at Wits University through TESP. The author would also like to express gratitude to the Department of Trade and Industry (DTI) for THRIP funding and to thank the National Research Foundation (NRF) for direct funding of these postgraduate studies. Lastly, the aid of the Technical University of Delft (TUDelft) was paramount to the completion of this research, due to their aid in the manufacturing of samples.

CONTENTS

DECLARATION i

ABSTRACT ii

ACKNOWLEDGEMENTS iv

LIST OF FIGURES ix

LIST OF SYMBOLS xii

NOMENCLATURE xiii

1 INTRODUCTION 1

1.1 Problem Statement 1
1.2 The Research Methodology 2
1.3 The Dissertation Structure 2
1.3.1 A review of electrical insulation technology (Chapter 2) 3
1.3.2 Composite material technology overview (Chapter 3) . 4
1.3.3 The experimental work (Chapter 4) 4
1.3.4 Results, analysis and conclusions (Chapters 5-8) 5

2 A REVIEW OF ELECTRICAL INSULATION TECHNOLOGY 6

2.1 Modern Electrical Insulators 6
2.1.1 Polyvinyl chloride (PVC) 7
2.1.2 Oil impregnated paper in power cables 7

2.1.3 Cross-linked polyethylene (XLPE) 8
2.1.4 Ethylene propylene rubber (EPR) 9
2.1.5 Silicone rubber (SIR) 9
2.1.6 Epoxy-resin 9
2.2 Failure Problems of Electrical Insulation 10
2.3 Electric Fields and Insulation 11
2.4 Partial Discharges 12
2.4.1 Types of partial discharges 13
2.4.2 Inception and extinction voltage 14
2.4.3 Detection of partial discharges 15
2.4.4 Implications of partial discharges on insulation integrity 17
2.5 Corona Discharges 17
2.5.1 Types of corona 18
2.5.2 Corona inception and extinction voltage 19
2.5.3 Detection of corona 19
2.6 Electrical Tree Insulation Failure Mechanism 19
2.6.1 The electrical tree life-cycle 20
2.6.2 Types of electrical trees 22
2.6.3 Detection of electrical trees 25
2.7 Summary 26

3 COMPOSITE MATERIAL TECHNOLOGY 27
3.1 Composite Material 28
3.2 Composite Material Models 30
3.2.1 Multi-core model 30
3.2.2 Polymer Chain Alignment Model (PCAM) 31
3.3 Simplifications of the Models 34
3.4 Summary 35

4 EXPERIMENTAL WORK 36
4.1 The Electrical Tree PD Detection 36
4.2 The Test Samples 38
4.2.1 Sample geometry 38

4.2.2 Sample material manufacturing . . . 40
4.3 Experimental Procedure . . . 42
4.4 Data Processing . . . 44
4.4.1 Data conditioning . . . 45
4.4.2 Data collation . . . 46
4.4.3 Data analysis and auto-classification . . . 50
4.4.4 Correcting the auto-classification . . . 55
4.4.5 Program implementation . . . 56
4.5 Summary . . . 57

5 RESULTS AND DISCUSSION 58
5.1 Unfilled (Clean) Epoxy . . . 59
5.2 Al_2O_3/Epoxy Samples . . . 61
5.2.1 Al_2O_3 0.5 %wt . . . 61
5.2.2 Al_2O_3 2 %wt . . . 66
5.2.3 Al_2O_3 5 %wt . . . 70
5.2.4 Al_2O_3 Trends . . . 74
5.3 MgO/Epoxy Samples . . . 74
5.3.1 MgO 0.5 %wt . . . 74
5.3.2 MgO 2 %wt . . . 78
5.3.3 MgO 5 %wt . . . 81
5.3.4 MgO Trends . . . 81
5.4 Si_2O/Epoxy Samples . . . 85
5.4.1 Si_2O 0.5 %wt . . . 85
5.4.2 Si_2O 2 %wt . . . 88
5.4.3 Si_2O 5 %wt . . . 92
5.4.4 Si_2O Trends . . . 92
5.5 Overall Comparison of the Trends . . . 96
5.6 Summary . . . 97

6 GENERALISED MODEL OF OBSERVED BEHAVIOUR 98
6.1 Basic Model . . . 99
6.1.1 Class A and B . . . 99

6.1.2 Class C . . . 100
6.1.3 Class D . . . 101
6.1.4 Class E . . . 103
6.1.5 Cycles . . . 105
6.2 Complications in the Model . . . 106
6.2.1 Consistency . . . 106
6.2.2 Dead zones . . . 107
6.3 Summary . . . 107

7 FUTURE WORK 108
7.1 Samples . . . 108
7.2 Model and Auto-Classification . . . 109
7.3 Summary . . . 110

8 CONCLUSION 111

REFERENCES 112

A AUTO-CLASSIFICATION MATLAB CODE 122
A.1 Collation Program . . . 122
A.2 Analysis and Auto-Classification Program . . . 125

B SAUPEC 2013 PUBLICATION 146

C ISH 2013 PUBLICATION 152

D SAUPEC 2014 PUBLICATION 158

LIST OF FIGURES

2.1 Rod-plane electrode configuration. 11
2.2 Void with no residual charge. 13
2.3 An example of a Phase Resolved Partial Discharge Pattern. . . 13
2.4 PD residual charge mechanics. 14
2.5 Basic PD detection circuit in accordance with IEC 60270 . . . 16
2.6 An example of a PRPDP for a corona discharge. 18
2.7 Causes of electrical treeing. 20
2.8 Electrical tree inception phase's push-pull mechanism. 21
2.9 Diagram of an electrical bush tree. 23
2.10 An example of a PRPDP for a bush electrical tree. 23
2.11 Diagram of an electrical branch tree. 23
2.12 An example of a PRPDP for a branch electrical tree. 24
2.13 Diagram of an electrical combination tree. 24
2.14 An example of a PRPDP for a combination electrical tree. . . 25

3.1 Multi-core model diagram. 30
3.2 Perpendicular chain alignment at particle surface 32
3.3 Effect of surface conditioning. 32
3.4 Electron-hole recombination. 34

4.1 Schematic of test circuit based off of IEC60270. 37
4.2 Diagram of sample geometry. 39
4.3 Photograph of the complete test sample assembly configuration that is submerged in oil during testing. 39

4.4 Photograph of custom connector to hold samples that smooth out electric fields. 40
4.5 Flowchart of sample synthesis. 41
4.6 Photograph of actual nanocomposite samples used in research. 42
4.7 Diagram illustrating the remote desktop configuration developed. 44
4.8 Collation program flow diagram. 47
4.9 Required directory tree structure 48
4.10 UML class diagram of auto-classification program. 51
4.11 Flow diagram of the main part of the auto-classification program. 52
4.12 Relationship of various means in a PD time evolution plot. . . 53
4.13 Flow diagram of the portion of the auto-classification program which actually segments and classifies. 54
4.14 Flow of dialogue boxes for correction protocol. 56

5.1 Clean epoxy PD time evolution plot 60
5.2 AL0.5-1 PD time evolution plot with PRPDPs. 62
5.3 AL0.5-2 PD time evolution plot with PRPDPs. 63
5.4 AL0.5-3 PD time evolution plot with PRPDPs. 64
5.5 AL2-1 PD time evolution plot with PRPDPs. 67
5.6 AL2-2 PD time evolution plot with PRPDPs. 68
5.7 AL2-3 PD time evolution plot with PRPDPs. 69
5.8 AL5-1 PD time evolution plot with PRPDPs 71
5.9 AL5-2 PD time evolution plot with PRPDPs 72
5.10 AL5-3 PD time evolution plot with PRPDPs 73
5.11 MG0.5-1 PD time evolution plot with PRPDPs. 75
5.12 MG0.5-2 PD time evolution plot with PRPDPs. 76
5.13 MG0.5-3 PD time evolution plot with PRPDPs. 77
5.14 MG2-1 PD time evolution plot with PRPDPs. 78
5.15 MG2-2 PD time evolution plot with PRPDPs. 79
5.16 MG2-3 PD time evolution plot with PRPDPs. 80
5.17 MG5-1 PD time evolution plot with PRPDPs. 82
5.18 MG5-2 PD time evolution plot with PRPDPs. 83

5.19 MG5-3 PD time evolution plot with PRPDPs. 84
5.20 SI0.5-1 PD time evolution plot with PRPDPs. 85
5.21 SI0.5-2 PD time evolution plot with PRPDPs. 86
5.22 SI0.5-3 PD time evolution plot with PRPDPs. 87
5.23 SI2-1 PD time evolution plot with PRPDPs. 89
5.24 SI2-2 PD time evolution plot with PRPDPs. 90
5.25 SI2-3 PD time evolution plot with PRPDPs. 91
5.26 SI5-1 PD time evolution plot with PRPDPs. 93
5.27 SI5-2 PD time evolution plot with PRPDPs. 94
5.28 SI5-3 PD time evolution plot with PRPDPs. 95

6.1 Model of class A and B behaviour. 99
6.2 Termination mechanic. 100
6.3 Model of the class C mechanics. 101
6.4 Model behind class D behaviour. 101
6.5 Change in the rod-plane model due to carbonisation. 102
6.6 Model behind class E mechanics. 103
6.7 Model of the cause of corona behaviour in class E. 104
6.8 TEM image of protrusions 105
6.9 Cyclical model. 106

LIST OF SYMBOLS

Symbol	Description	Units
E_{max}	Maximum electric field strength	Volts/metre [V/m]
V	Applied voltage difference	Volts [V]
r	Radius of rod tip	metres [m]
d	Distance between two electrodes	metres [m]
$V_{inception}$	PD or corona inception voltage	Volts [V]
$V_{extinction}$	PD or corona extinction voltage	Volts [V]
V_{app}	Applied voltage for experiment	Volts [V]
Q_{p-avg}	Average PD magnitude over sample interval	Coloumbs [C]
Q_{p-max}	Maximum PD magnitude over sample interval	Coloumbs [C]
Q_{p-min}	PD magnitude over sample interval	Coloumbs [C]
U_{RMS}	RMS voltage from ICMcompact	Volts [V]
$\hat{U}/\sqrt{2}$	Peak calculated RMS voltage from ICMcompact	Volts [V]

NOMENCLATURE

Term	**Description**
EPR	Ethylene Propylene Rubber
GIS	Gas Insulated Systems
GUI	Graphical User Interface
HV	High Voltage
OO	Object Orientated
PCAM	Polymer Chain Alignment Model
PD	Partial Discharge
PILC	Paper Insulated and Lead Covered
PRPDP	Phase Resolved Partial Discharge Pattern
PVC	PolyVinyl Chloride
SIR	Silicone Rubber
SSH	Secure Shell
TDR	Time Domain Reflectometry
TEM	Transmission Electron Microscopy
TUDelft	Technical University of Delft
UML	Unified Modelling Language
XLPE	Cross-Linked PolyEthylene

Chapter 1

INTRODUCTION

Advancements in technology and knowledge in a specific discipline are often developed through the cross-fertilization of methodologies, technologies or knowledge from other disciplines. An example of such a case is where the technology available for several centuries in material sciences [1] has only relatively recently found application in electrical insulation and this is the improvement of modern insulation materials through nanocomposite technology.

1.1 Problem Statement

Modern insulation materials, such as epoxy, Cross-Linked PolyEthylene (XLPE) and Ethylene Propylene Rubber (EPR), have proven to be relatively more effective insulators. Epoxy is one of the polymer dielectrics commonly used in electric machines such as generators, motors and cable joints. Unfortunately these polymeric based insulation have a major flaw: susceptibility to electrical treeing. Attempts to improve the insulation properties of epoxy and possibly negate this flaw are being explored using nanotechnology.

Given that electrical trees have also been shown to be the main mode of final failure of most insulation defects [2, 3], any solution to this phenomena would be useful. One possible solution to this problem is the use of nanoparticles in an insulator host material. Nanocomposite material should show improved behaviour of electrical trees when compared to unfilled epoxy. The focus of this dissertation work is to search for answers to the questions:

"How do electrical trees in nanocomposite insulation differ from electrical trees in clean insulation? Furthermore, can Partial Discharge (PD) detection techniques be used to both monitor and offer insight into the electrical treeing process?"

1.2 The Research Methodology

This dissertation explores a method to characterise a degradation mechanism of nanocomposite epoxy. The degradation mechanism of interest in this case is electrical treeing in various types of nanocomposite epoxy. The type variation in nanocomposite epoxy is realised through different filler materials (Al_2O_3, MgO and Si_2O) with different filler loading levels for each filler material. The electrical treeing degradation phenomena is monitored through PD measurements.

The following methodology was conceived to answer the research questions. The basic method was to monitor PD parameters of interest until the sample fails. The PD parameters were then analysed, compared and contrasted to extract trends and information from the data.

A standard PD detection circuit was used to measure the PD magnitudes and Phase Resolved Partial Discharge Patterns (PRPDPs) of each sample. The circuit is based on the basic detection circuit of IEC 60270 [4]. The resulting data was then analysed to generate information about the electrical trees behaviour over time. The information was then used to compare and contrast the treeing mechanism in the nanocomposite and the unfilled material.

1.3 The Dissertation Structure

The following sections summarise the content of each chapter of the dissertation and, in essence, provide an overview of the dissertation.

1.3.1 A review of electrical insulation technology (Chapter 2)

Electrical distribution systems have been a major component of electrical power systems since their invention. Furthermore the use of High Voltage (HV) in transmission and distribution networks is essential with ever higher voltages being achieved and implemented all over the world [5]. The HV systems require substantial insulation for both safety and economic design considerations and this has motivated ongoing research into developing better insulation materials [6]. The definition of a better insulator has several aspects that will be discussed further in the chapter and is often context dependent.

The contemporary generation of insulators (other than fluid based insulation systems) are primarily polymer based rubbers and epoxies such as Cross-Linked PolyEthylene (XLPE), epoxy resin and Ethylene Propylene Rubber (EPR). Solid polymer insulations have proven to be lighter and more flexible whilst improving on the electric field breakdown strength of older insulation technologies. These solid insulations have however displayed a problem attributable to their unique molecular structure: a susceptibility to the electrical treeing phenomenon. It is therefore necessary to find a means of retarding or preventing electrical trees so as to unlock the potential of an otherwise robust insulation technology.

An understanding of electric fields leads to an understanding of the behaviour of electrical insulators from standard operation to the associated phenomena, ranging from defects to final failure. Chapter 2 discusses the physics behind the behaviour of insulators, which is encapsulated in electric field theory. Phenomena such as Partial Discharges (PDs), corona discharges and electrical trees are agencies of insulation failure and recent research has shown that there are inextricable links between all these phenomena [3]. These problems, especially electrical trees, have become a major concern since the advent of modern solid polymer insulation technologies.

1.3.2 Composite material technology overview (Chapter 3)

One of the directions taken by researchers world-wide is the investigation of composite insulation and lately nanocomposite insulation. There already exists a wealth of knowledge on composite material for mechanical functions, which is briefly covered in Chapter 3, but electrical property modifications have not had the same attention thus far. The application of composite techniques to the modification of the electrical properties of a material had not been possible before the invention of microscale (and smaller) particle manufacturing capabilities. Before this scale had been achieved, experiments had proven that almost all particles inside a polymer matrix acted as a contaminant, distorting the electric field and actually reducing the life-span and breakdown strength of the material [7]. The electrical phenomena in composite materials requires more research effort to reach the same level as that currently enjoyed by those interested in the mechanical property modifications. The research progress so far has shown developments that bode well for the burgeoning technology in the field of electrical engineering [8].

1.3.3 The experimental work (Chapter 4)

There are two main intentions to these experiments: to ascertain whether the behaviour of electrical trees in nanocomposite insulation differs from unfilled insulation; and verify whether PD detection is a useful method for tracking electrical treeing. To investigate the different behaviour of nanocomposites, three filler materials (MgO, Al_2O_3 and Si_2O) with various filler loading levels (0.5 to 5 % by weight) in epoxy resin are experimented with. The experiment attempts to monitor the growth of electrical trees using the PD magnitude over time. A rod-plane electrode geometry cast in the solid polymer insulation is used in these experiments. The rod-plane configuration is a commonly used method in studying the electrical tree phenomena [2, 3, 9, 10]. The resulting patterns are of interest in providing information on the state of the electrical tree over time. The information will give insights on the ability the nanocomposites to retard the electrical tree growth. The experimental work (incorporating the experimental configuration, procedure and the data processing) is covered in detail in Chapter 4.

1.3.4 Results, analysis and conclusions (Chapters 5-8)

Each sample's results are analysed, interpreted and discussed on a case by case basis in Chapter 5. Furthermore as new behaviour patterns are encountered, the underlying physical mechanisms responsible for the behaviour are suggested and discussed. Any trends that can be determined are delineated in relation to both filler material and loading level. All of these observations and mechanics are collated and an overarching model developed in Chapter 6. The model is further supported with specific instances and a critique as to the possible flaws in the model. There are various possible directions the research can be pursued at higher levels in future, which are covered in Chapter 7. An example of a specific direction is the further refinement of the pattern classification program developed in this work. Finally, the conclusion that can be drawn from the work presented in this dissertation is given in Chapter 8. Appendix A contains the code of the program developed to automatically classify the PD patterns. Lastly, Appendices B to D provides copies of the articles published elsewhere on various aspects of the work presented in the dissertation.

Chapter 2

A REVIEW OF ELECTRICAL INSULATION TECHNOLOGY

This chapter reviews the basics of electrical insulation, and by extension, the electric field. The degradation phenomena to be retarded in electrical insulation such as partial discharges, corona discharges and electrical trees are explained to ensure a basis for later analysis. Electrical trees are covered in relatively more detail, as they are a focus of this dissertation.

2.1 Modern Electrical Insulators

A variety of insulation materials are currently in widespread use in industry, with their use often dependent upon context. For power cables, the three most common used insulation types currently are PolyVinyl Chloride (PVC), oil impregnated paper and Cross-Linked PolyEthylene (XLPE). Other insulation materials include Silicone Rubber (SIR), oil, glass, ceramics and epoxy. These are often used in specific applications such as transformers, rotating machines and line insulators. Gas Insulated Systems (GIS) are not discussed as these fall outside the scope of this project.

2.1.1 Polyvinyl chloride (PVC)

PVC is the standard solid insulation used for household wiring and is used because of the low price attached to it [11]. Its breakdown strength however, is much lower than other insulation. PVC's use is therefore primarily a design decision based around cost rather than electric breakdown strength. Using PVC will require a thicker layer than other technologies, meaning that beyond a certain length, it becomes more economically feasible to employ an insulation with a higher breakdown strength. Industry usually requires large lengths or high breakdown strengths, meaning other insulations technologies are used.

2.1.2 Oil impregnated paper in power cables

Oil impregnated paper insulation cables were popular a few decades ago and many legacy cable systems still employ them in their distribution system [12]. Furthermore many systems still use Paper Insulated - Lead Covered (PILC) cables specifically, due to their reliable track record. As the name implies, oil impregnated paper is used as an insulation medium and is both contained, and mechanically shielded, in a lead sheath [13]. The oil makes the insulation partially self-healing, as PDs are generally swamped with oil if they occur. Maintenance and connections are however, major drawbacks for this technology due to the use of oil [13]. The inclusion of oil makes leaks the main cause of electric breakdown of the cables systems. Connectors (cable joints) have to be made air tight to ensure air and other contaminants do not enter the oil, as these contaminants can form a single conductive path between layers of paper insulation, essentially lowering the breakdown strength [12, 13]. Another major drawback is the lead sheath that makes the cable both heavy and reduces its flexibility by a large margin. In search of alternatives to correct the shortfalls in PILC cables, XLPE insulation was developed and has since dominated.

2.1.3 Cross-linked polyethylene (XLPE)

XLPE is a polymer based rubber insulation that uses the phenomenon of cross-linking of molecular bonds [14]. Various forms of PolyEthylene (PE) are employed with either vulcanization or Silane-linking [14] to form XLPE. In broad terms, Silane-linking makes use of an inorganic compound (Silicon chain based) to brake a section of the polymer strand and form an OH bond. The OH bond, in the presence of the catalyst, causes a bond, referred to as a cross-link, to form between the two polymer strands. Due to the cross-linking, the insulator hardens but retains its flexibility and enjoys a large improvement to its breakdown strength [14]. The quality of the insulator is directly linked to the degree of cross-linking [13, 14].

XLPE is currently one of the most commonly used insulations for power cables around the world due to its breakdown strength, flexibility, low weight and economic price [15]. XLPE does have one flaw due to its unique molecular structure: a susceptibility to electrical treeing [15, 16]. The cross-linking bonds are especially vulnerable to the damage experienced by the push-pull effect of the treeing mechanism described later in Section 2.6 [16]. Once these links have been damaged enough, the polymer chains connected are partially unstable and reduce the breakdown strength of the material in that region. This results in XLPE lasting only hours, or even minutes, once an electrical tree has been formed and the propagation phase starts [16]. The cross-linked bonds are especially vulnerable to damage from the electron and ion collisions that occur during the inception phase of an electrical tree [16]. One figure of merit important to design consideration is the operating temperature range of the insulation. For extreme environments, such as desserts and snow, XLPE is not as effective an insulation material for cables due to the limitation in its operating temperature. As polymer insulation appears to have many benefits, research was conducted to find a polymer insulator that could be used in extreme environments.

2.1.4 Ethylene propylene rubber (EPR)

EPR is a very similar insulator to XLPE but has a higher breakdown strength and a much wider range of operating temperature [15]. For this reason, it is viewed as a specialised insulation material and is relatively more costly. Its main usage is in extreme environments such as desserts and locations that experience snow frequently. It also shares the same flaws as discussed for XLPE [15]. These flaws include the vulnerability to electrical discharge based insulation degradation. XLPE and EPR are primarily used for cable insulation as there are more appropriate insulation materials for other applications.

2.1.5 Silicone rubber (SIR)

SIR insulators are often used for isolation of an electric power transmission line tower from the transmission conductors [17]. SIR composite insulators are popular as they are hydrophobic, reducing the problems associated with pollution. Currently microcomposite SIR insulators are employed in a variety of utilities, due to its improved hydrophobicity [6, 17]. Silicone insulation, like other polymers, has weak resistance to electrical discharges.

2.1.6 Epoxy-resin

Epoxy-resin is a binary mixture material that can also be referred to as epoxy [18]. It is a base monomer, or short polymer, that is mixed with a hardener or curing agent [18]. The hardener or curing agent causes the monomer or polymer to undergo polymerisation and thereby harden [18]. The product is usually hard and has a relatively high breakdown strength. Its usage is very common in dry transformer windings, motor windings, cable joints and terminations [18]. Common problems with epoxy are also associated with discharges as with other polymer based insulation materials. Most experiments involving nancomposites use epoxy as the host material as it is much simpler to create nanocomposites using epoxy [19, 20]. It is hoped that once suitable materials are found in epoxy, they should behave similarly in other polymer based insulations as has been shown in cases thus far [21].

A consistent flaw covered for the above insulation materials is a susceptibility to discharge related degradation. Some background is necessary to understand the mechanisms behind these discharges and how they cause the enhanced degradation in polymer based insulation.

2.2 Failure Problems of Electrical Insulation

Electrical insulation engineering is a broad field of study, which is itself a specialisation of material sciences. A material is an electrical insulator if its electric charges do not flow freely unless certain criteria are met [22]. These criteria are derived from the breakdown field strength of the material which is dependent upon the applied voltage and other environmental factors such as pressure [13]. Once the electric field strength has exceeded a certain value, determined by the material's permittivity, in a region of the insulator, this region of the insulator changes into a conductor, allowing current to flow freely [13]. An electrical insulator is said to have failed when a conductive path between the two conductors is formed. The resulting current flow damages the material, severely reducing its electrical breakdown strength and continued breakdowns are inevitable. The conductive region formed by a non-linear electric field however, may not bridge the insulator between the conductors (electrodes). This implies that the breakdown may not occur between the two electrodes, but in some region of the insulator that does not include the boundaries in contact with the electrodes.

Some types of insulation, such as oil, are self-healing by their nature. Self-healing means that if any discharge phenomena, such as PD, occur; the insulation recovers after the degrading event. The insulator then experiences no lasting damage, effectively healing itself. Self-healing is an advantageous property to have but is generally limited to gas and liquid insulation. Air is a relatively good insulator and has the self-healing property. An understanding of electric fields is necessary in studying the behaviour of electrical insulation materials.

2.3 Electric Fields and Insulation

The electric field is an essential concept of electromagnetic physics. This section only introduces the core ideas behind electric field models. An electric field is created between two or more surfaces that have different charge levels. A large concern in insulation coordination is ensuring that the electric fields in and around the HV equipment are as linear as possible to avoid discharge phenomena, which degrade performance and equipment.

In order to experimentally study the effect of highly divergent, enhanced electric fields, a rod-plane configuration, as shown in Figure 2.1, is commonly used. Such a setup is convenient in treeing mechanism studies for solid dielectrics. In the work presented in the this dissertation, the rod-plane electrode system was cast in epoxy insulation. This configuration was chosen for use in this work primarily to ensure that electrical trees would develop before the insulation under test experiences complete breakdown. A secondary benefit exists in that this configuration has a well-known analytical expression, the Laplacian model, to calculate the maximum electric field at the rod's tip. The Laplacian model uses Equation (2.1) [23–25] with reference to Figure 2.1.

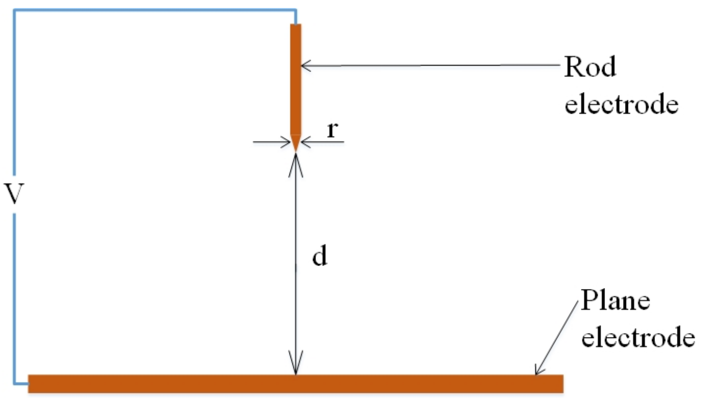

Figure 2.1: Rod-plane electrode configuration.

$$E_{max} = \frac{2V}{r\ln(1+\frac{4d}{r})} \tag{2.1}$$

Where V represents the RMS voltage, in Volts [V], applied between the two electrodes. d represents the distance between the rod tip and the plane and r is the rod tip radius both expressed in metres [m]. E_{max} represents the maximum electric field strength, which occurs at the rod tip, and is measured in Volts per metre [V/m]. The electric field on the rod tip is an enhanced and highly non-linear electric field, owing to the geometry of the electrodes. In gas or liquid insulation, the electric field strength can easily cause ionisation of air molecules resulting in discharges. In solid insulation, the highly divergent field initiates electrical trees which are micro-channels that support partial discharges.

2.4 Partial Discharges

PD is the phenomenon when breakdown of a region of an insulation material occurs that does not bridge one electrode to another [3, 26]. In this dissertation, a PD refers specifically to an internal PD and not a surface PD. A surface PD is a discharge that occurs along the outer surface of the insulator. Surface PDs share many similarities with internal PDs but are not covered in this work. The experiments focused on internal PDs as these are the type that occur inside electrical tree microtubules. PDs are measured in many ways but the most common measurement parameter of interest is the PD magnitude in Coloumbs [C]. Internal PDs are commonly caused by voids in the material as shown in Figure 2.2. Prior to any discharges, there is no residual charge present in the void, and therefore the resultant electric field in the void is only due to the electric field in the insulation, as in Figure 2.2.

The difference in permittivity between the gas in the void and the material causes electric stress enhancement in the void and if this stress exceeds the PD inception voltage level, a discharge occurs that deposits charge on the walls of the void. This is directly linked to the voltage applied to the electrodes, as the greater the voltage, the higher the enhanced stress in the void. Once a PD has occurred, the likelihood of further PDs increases. Figure 2.3 shows an example of a measured PD signal with reference to sinusoidal phase. This is referred to as a Phase Resolved Partial Discharge Pattern (PRPDP), which gives information as to where in the sinusoidal waveform the PD oc-

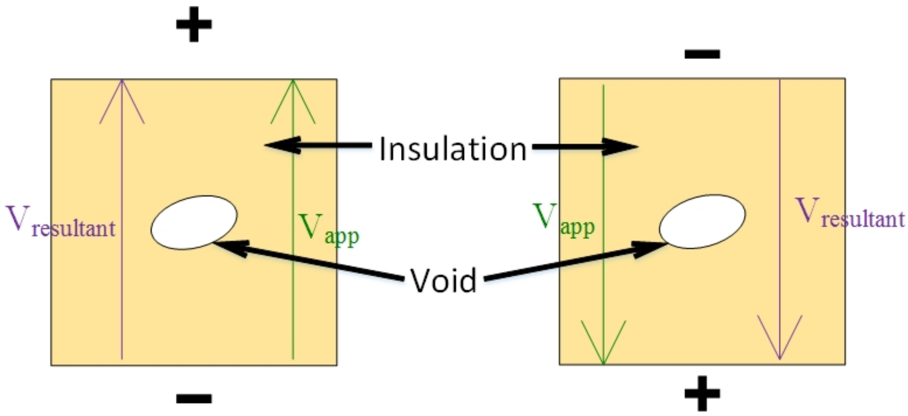

Figure 2.2: Void with no residual charge.

curred. PRPDPs have several benefits as this information can help further classify the PD event.

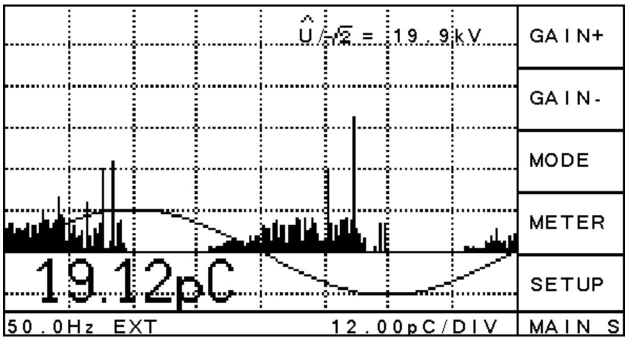

Figure 2.3: An example of a Phase Resolved Partial Discharge Pattern.

2.4.1 Types of partial discharges

From the PRPDP in Figure 2.3, two important aspects are evident. First, the PDs start just after the zero crossing of the waveform. Secondly, after a period where no PDs are experienced, the PDs can also occur just before the zero crossing. The mechanism is explained as follows; once a PD has occurred, residual charge that opposes the electric field due to the applied voltage will be formed, ostensibly reducing the resultant electric field [26, 27]. An example of this effect is shown in Figure 2.4 where $V_{resultant} = V_{app} - V_{residual}$ and $V_{residual}$ is the electric field that is created due to the residual charge in the void. As the discharge occurs much faster (in the order of nanoseconds) than the sinusoidal signal (assuming 50 Hz signal), the pulse will recur multiple times within one quarter-cycle [26]. This leads to the resultant field across the void being reduced with each discharge, until the resultant electric field strength is lower than the breakdown strength of the void. This is the period when no discharges can be observed. Once the voltage waveform enters the second quarter cycle, the voltage starts to drop and the resultant electric field strength increases in negative polarity. The breakdown strength of the void will be reached at a lower voltage, albeit with opposite polarity, before the third quarter-cycle starts. This mechanism accounts for the observation of PDs before a zero crossing. The same pattern occurs for the transition from negative to positive half-cycles as well.

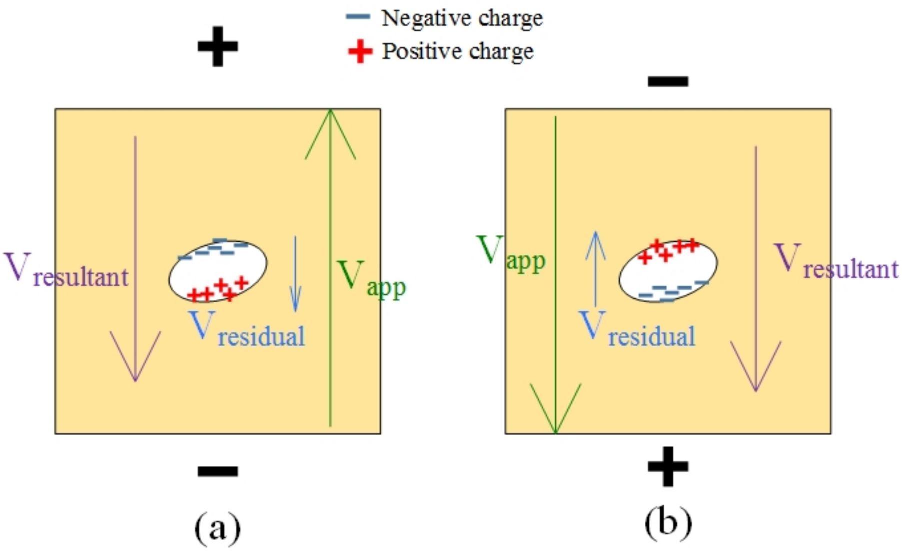

Figure 2.4: Mechanics behind PD that results in discharges occurring before zero-crossing for (a) positive and (b) negative polarities.

2.4.2 Inception and extinction voltage

Two further parameters of interest for PDs are the PD inception and PD extinction voltage [3, 26, 27]. Given a specific type of insulation material, PDs will only start at a certain voltage, $V_{inception}$, dependent upon the geometry of the PD defect. At and above $V_{inception}$, PDs will occur. The PD extinction voltage, $V_{extinction}$, is the voltage below which PD activity has ceased after $V_{inception}$ has been reached. It is important to note that $V_{extinction} \leq V_{inception}$ [3, 26]. This occurs because the PD activity that was started lowers the energy necessary for continued breakdown allowing PD activity to continue below the PD inception voltage. The space charge that is deposited on the cavity walls during the PD event causes the PD activity to extinguish at a voltage lower than $V_{inception}$.

2.4.3 Detection of partial discharges

There exist a number of methods for measuring partial discharges, but the predominant method employed is measurement of the momentary voltage drop across the electrodes caused by the discharge [26, 27]. This method allows relatively easy measurement without sacrificing accuracy and is recommended by IEC 60270, whose basic circuit is displayed in Figure 2.5, due to its ease and accuracy [4, 26]. The basic principle is to use the coupling capacitor to measure the PD voltage drops due to discharges in the device under test. The voltage of the capacitor decays slower than the time a discharge can occur in [26, 27]. This implies the voltage drop experienced by the sample when a discharge occurs will cause a current to flow, which is measured using the measurement box allowing for an accurate voltage measurement with reference to the point of the waveform it occurred. The detected current can be converted to the PD magnitude using the measured voltage [26, 27]. This methodology is only appropriate where the PD source is near the point of connection of the test set, as the magnitude of the current decays rapidly with distance from the point of discharge [28].

Another popular insulation testing method is applying standard tanδ testing. Tanδ testing is a method that essentially measures the ratio of the capacitive and resistive current components in the insulation material. As the voltage is gradually increased, the tanδ value should remain constant until PDs start to occur. When PDs occur, the tanδ increases due to the discharges changing the the insulation impedance. This behaviour is referred

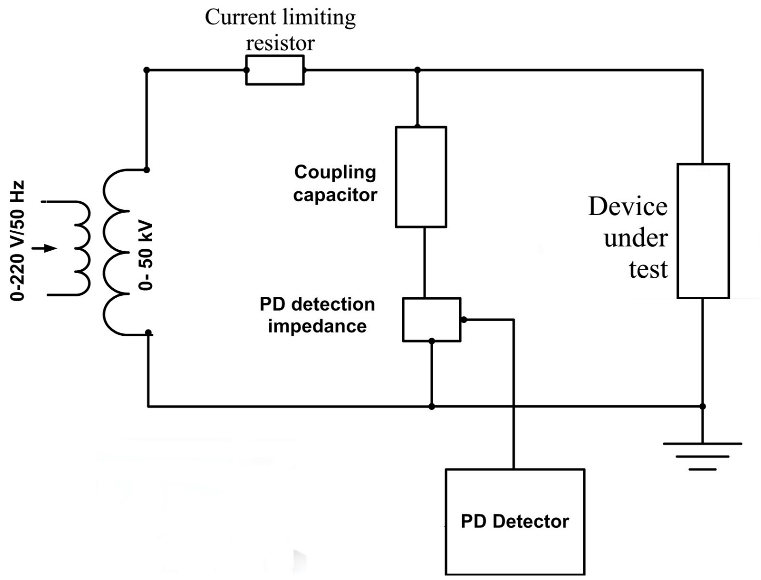

Figure 2.5: Basic PD detection circuit in accordance with IEC 60270 [4]

to as tip-up and is used to detect the presence of PD defects using tanδ measurement. Tanδ testing is useful for testing long lengths and large volumes of insulation [29]. Small defects, such as voids, in large amounts of insulation are sometimes too small to cause a bulk change in the dielectric loss angle of the insulator. This renders tanδ testing only useful to confirm the existence of a defect not to declare an insulator as defect free.

Other than the electrical methods of PD detection, there are other techniques based on PD phenomena such as temperature and light emission. PDs emit ultraviolet light, which allows detection through specific frequency ultra-violet light detection [26]. The main limitation with light detection techniques and other non-electrical techniques is that they can only monitor small sections of an insulator at any one time, rendering large scale detection impractical, which limits them to verification methods. The non-electrical detection methods can however yield information that cannot be extracted from pure electrical detection methods alone and therefore can be used in combination for a greater amount of PD information [26].

2.4.4 Implications of partial discharges on insulation integrity

PDs are unwanted for several reasons, but the primary concern is the damage to the insulation in which they occur [26, 27]. The discharges cause degradation of the insulator material as well as generating several chemical by-products [26, 27]. These by-products are dependent upon the composition of the material, but generally include corrosive and conductive liquids and gases. These by-products also degrade the insulation material and also increase the pressure inside the void, further damaging any molecular bonds in the material [3]. It is for this reason that a sample that has experienced PD activity previously can experience a lowering of its PD inception and extinction voltages [26, 27]. Furthermore, recent research has found that these chemicals crystalise inside the void and cause a rod-like extrusion into the surrounding insulation [3]. This crystal rod will create a rod-plane configuration, which can result in an electrical tree forming.

The above information is specific to internal PDs but much of the theory also applies to surface PDs. The mechanisms behind discharges in air, also called corona discharges, share many similarities with PDs but are slightly different in some aspects.

2.5 Corona Discharges

The corona discharge phenomenon, also referred to as just corona, is a form of partial discharge, but is defined as the localised breakdown of a gas or liquid [26]. This occurs, most frequently in air, when a sharp point acts as a geometric electrical stress point. From Equation (2.1), it is clear that the electrical stress experienced by the gas around the tip of the rod is very high for a sharp point. It is quite possible that for a very small tip radius, the electric field strength can exceed the breakdown strength of the surrounding air. For example, if a rod with a 1 mm tip radius is suspended 10 mm from a plane. Applying 20 kV across these electrodes will produce a maximum electric field strength of 10.8 MV/m at the rod tip. This causes the region of air that experiences the enhanced stress to breakdown.

2.5.1 Types of corona

There are two types of corona that show different PRPDPs: positive corona and negative corona. Positive corona arises due to positive voltage polarity of the discharge point and negative corona occurs due to negative voltage. As displayed in Figure 2.6, the PRPDP for corona, created by AC voltage, shows discharges occurring around the peak and trough of the waveform. The negative corona, often referred to as Trichel pulses, show uniform and small amplitude pulses, whereas the positive corona discharges are much larger and do not appear uniform [26].

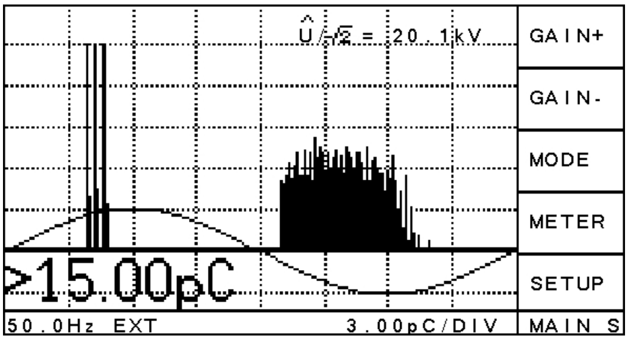

Figure 2.6: An example of a PRPDP for a corona discharge.

The clustering about the peaks and troughs is distinctive for corona, as only once the electric field strength reaches the breakdown strength of the fluid (gas or liquid), do the corona discharges occur. For a given geometry, the voltage waveform is directly responsible for the electric field strength with no influence of residual space charge as in cavity PDs. Therefore, an absence of discharges around the zero crossing implies that the discharge occurring is corona discharge and not PD in a void. This absence is due to there being no residual space charge to interact with the applied electric field. The width of the discharge pattern about the peak and trough increases proportional to the voltage as the electric field breakdown strength is reached sooner for a higher peak voltage.

2.5.2 Corona inception and extinction voltage

Corona also has an inception and extinction voltage with similar definitions as PDs, but the extinction voltage is not necessarily lower than the inception voltage [26]. This difference occurs due to the nature of gas, which is a self-healing insulation. Logically, if the air experiences breakdown, the ionization of the air will dissipate, eventually returning to a normal state. It must be noted that any by-products will disperse as well but this can lead to complications for multiple breakdowns occurring due to the accumulation of these by-products. This means that the reduction in energy may not apply as it does for PDs. In a closed environment, the ionized air would allow breakdowns to occur at lower voltages but in open air this ionization disperses relatively rapidly reducing the likelihood of further breakdowns.

2.5.3 Detection of corona

Corona discharge detection is almost identical to PD detection methods, but corona is somewhat easier to detect as it often occurs in open air environs. This creates new opportunities for detection such as using acoustic energy or UV cameras to detect the location of the corona. It also invalidates certain techniques such as tanδ testing, which specifically measures the dielectric loss tangent of the insulation, that would not experience the tip-up effect due to external discharges as the discharge occurs on the outside of the insulation and does not affect the impedance of the insulation. Corona occurs due to discharges at a point of enhanced stress in gas or liquid; in solid insulation, the mechanism becomes electrical treeing.

2.6 Electrical Tree Insulation Failure Mechanism

Electrical trees are insulation failure mechanisms where a small part of the insulation undergoes electric stress beyond its electric breakdown strength. This is most commonly caused by defects such as contaminant particles and sharp point intrusions into the insulation as shown in Figure 2.7. Once the trees are formed, PDs are responsible for the propagation and expansion of the electrical tree.

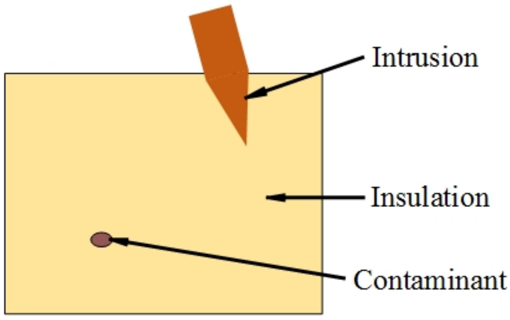

Figure 2.7: Causes of electrical treeing.

2.6.1 The electrical tree life-cycle

The electrical tree life-cycle can be divided into 3 distinct phases [2]:

- Inception phase:
  As the electric field strength increases, an electrostatic push-pull force is generated within the material [30]. For a negative polarity voltage, the electric field will cause any free electrons within the material to be pushed away from the cathode and free ions to be attracted to the cathode. For a positive voltage polarity, the opposite occurs with the tip as the anode attracting electrons and repulsing ions. Both instances are shown in Figure 2.8.

  For AC conditions, this causes a constant movement of electrons and ions back and forth within the material. This motion causes electron and ion collisions with the molecules and polymer bonds that comprise the material [30]. These collisions lead to the phenomenon known as electroluminescence, which is essentially light being emitted due to the excitation from collisions [31]. Eventually, the damage exceeds the capability of the molecular bonds to remain cohesive, breaking to form a micro-gap. At this point the propagation mechanism takes over.

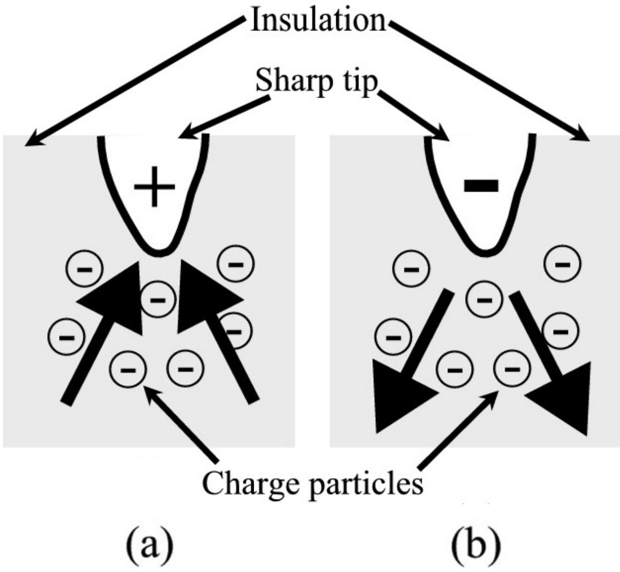

Figure 2.8: Push-pull mechanism for different polarities experienced during the electrical tree inception phase. The polarity causes the tip to act as (a) a cathode and (b) an anode.

- Propagation phase:
  Once a gap of sufficient size (generally microscale) has formed, PDs start to occur in the formed gap [2]. PDs have multiple side-effects including corrosive chemical evolution, pressure increases and material degradation. These side-effects cause the gap to slowly increase in size and propagate into microtubules towards the general direction of the opposite electrode. The overall shape of the tree is determined by several factors and will be discussed below. Electrical trees have been shown to follow the fractal pattern called a Lichtenberg figure, which is common to many electrical phenomena [26]. The treeing pattern exhibits both stochastic and deterministic growth patterns when a new tubule forms. It is difficult to measure and keep track of all variables simultaneously to predict the next tubule growth direction. Furthermore, the location of the PD in the electrical tree and therefore all the ancillary effects such as pressure spikes, are similarly difficult to measure. The complicated and interdependent nature of these effects are best modelled as probabilistic due to the inherent difficulty.

- Failure phase:
  Once the tree has propagated far enough into the material, the material fails and breakdown occurs. At this point the insulation will continually breakdown. In a failed state, the insulation becomes useless as it will no longer isolate two conductors. The question exists as to how far should the electrical tree grow into the insulation before causing complete failure. Recent findings by Toshikatsu Tanaka show that the tree length may not be as important as the channel width [10]. This implies that a tree can fully bridge the insulation material without failure occurring until the channel reaches a certain width, which has been shown to be true by Toshikatsu Tanaka in [10] and [32]. His experiments show fully bridged insulation by an electrical tree tubule, without failure occurring until several hours have passed. This behaviour could occur if the channel is not wide enough to support a consistent current stream to form a fully ionized pathway, also referred to as plasma.

2.6.2 Types of electrical trees

There are various types of electrical trees [33] but only the main types will be described here.

- Bush electrical tree:
  Bush trees display a fan type pattern with the short tubules radiating out from the inception point as in Figure 2.9. This type of tree develops as a result of a very high, localised electric field. This can be described as the strength of the field causing so many collisions, in multiple locations, that many tubules form in various directions. A bush tree typically displays a PRPDP as shown in Figure 2.10. The PRPDP is characterised by a dense group of approximately uniform magnitudes. These characteristics are due to the large number of tubules of similar lengths all experiencing PDs.

- Branch electrical tree:
  A branch tree develops due to a less intensive electric field strength than

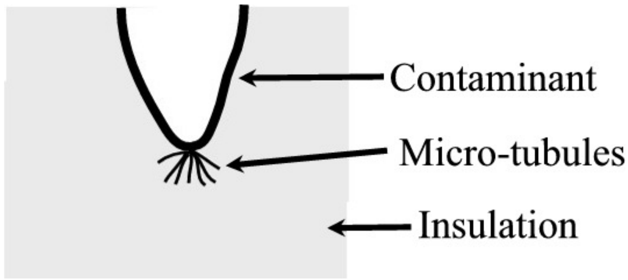

Figure 2.9: Diagram of an electrical bush tree.

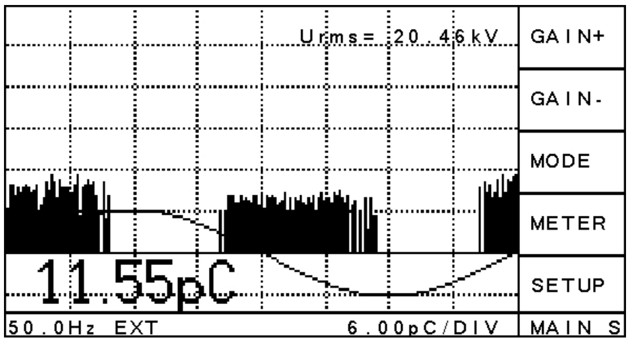

Figure 2.10: An example of a PRPDP for a bush electrical tree.

a bush tree. It is characterised by long primary roots that extend from the inception point, in the general direction of the opposite electrode, with many smaller branches developing along the primary roots. An example of this pattern is displayed below in Figure 2.11.

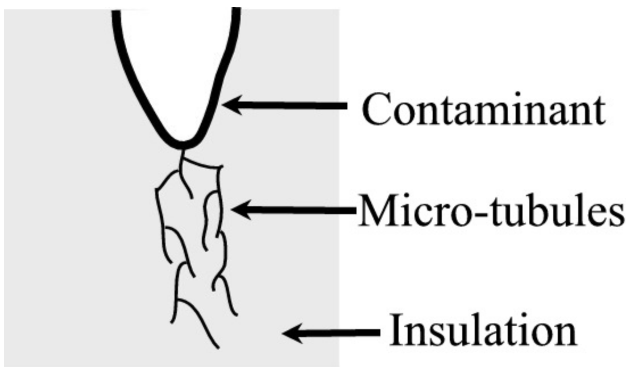

Figure 2.11: Diagram of an electrical branch tree.

Branch type electrical trees display a PRPDP similar to the example shown in Figure 2.12. A branch electrical tree's PRPDP is characterised by the large variation of magnitudes and positions of the PDs. It is almost the complete opposite of the bush electrical tree's characteristics.

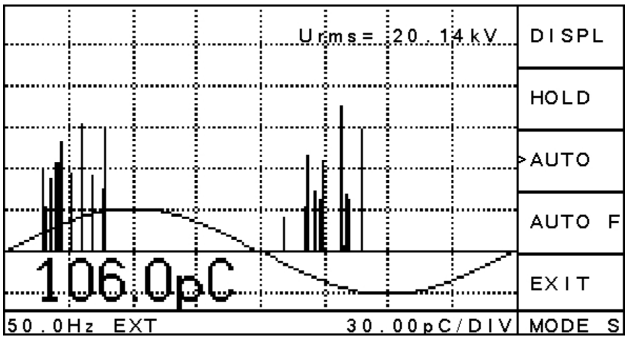

Figure 2.12: An example of a PRPDP for a branch electrical tree.

- Combination (bush/branch) electrical tree:
  In certain circumstances both a bush and a branch tree can develop simultaneously. Very often a bush electrical tree is initiated first, before one or more of the branches of the bush tree propagates further into the insulation as a branch tree. An example is shown in Figure 2.13.

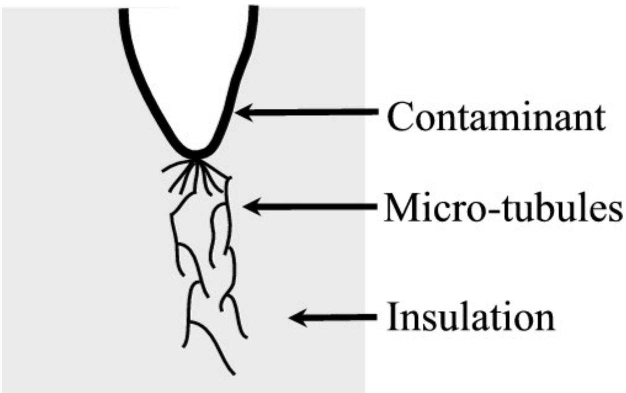

Figure 2.13: Diagram of an electrical combination tree.

The PRPDP for a combination tree resembles a superposition of both a bush and a branch electrical tree's PRPDPs, as in Figure 2.14. There are distinct families of small PDs (bush electrical tree) and large PDs (branch electrical tree). This occurs because the branch PDs are larger than the bush and will obscure the smaller bush PDs. The bush may be experiencing PDs but this is difficult to observe due to the branch PDs masking the smaller PDs.

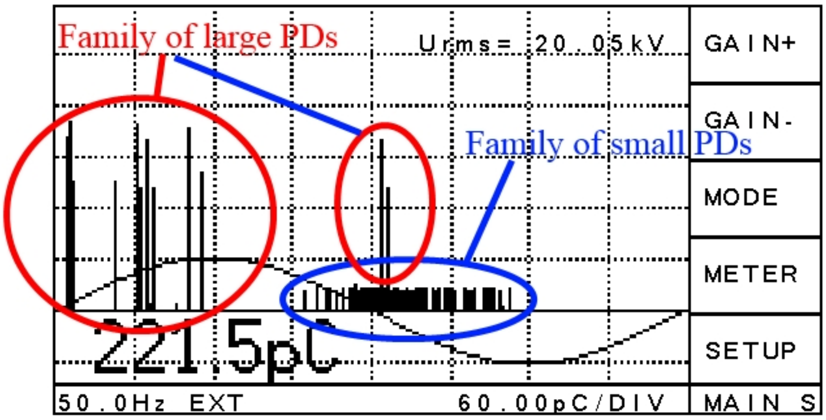

Figure 2.14: An example of a PRPDP for a combination electrical tree.

The three types of electrical tree are generally results of an intrusion into the insulation such as a sharp point piercing the insulation of a cable. It is further noted that electrical trees can only develop in solid insulation as fluid insulation displays the self-healing property, not allowing damage to accrue enough to cause tubules to form.

2.6.3 Detection of electrical trees

Detection of electrical trees is much harder to accomplish than partial discharge detection. The main method of detection is visual verification under a microscope but this requires that the insulation is transparent. Visual techniques can still be used for opaque insulation if the insulation is sectioned in some way, but this completely destroys the samples and makes it difficult to reconstruct the overall pattern. Tanδ testing does show some results, especially if the electrical tree started as a water tree. Tanδ is a bulk test technique and as an electrical tree's volume is much smaller than the insulator volume by a factor of many thousands, the increased losses due to trees is negligible. Using PD detection techniques offers the capability of detecting electrical trees regardless of the opacity of the insulation material.

2.7 Summary

As the dissertation work is motivated by correcting the drawbacks of certain types of insulation material, an understanding of electrical insulation is necessary. Electrical insulation has been defined in general before the specific insulation materials of interest are covered in detail. The detail covers the basis of each insulation material and their advantages and weaknesses. The basics of electric field theory are covered along with the specific electrode configuration used in this work. From this basis, degradation phenomena such as PDs, corona and electrical trees, are explained in detail. Specific attention is given to the electrical trees, as they are the phenomena of primary interest, and the recent findings regarding electrical treeing. Electrical treeing is currently the main problem with conventional insulation material, but a solution to this problem may lie in the application of composite material technology.

Chapter 3

COMPOSITE MATERIAL TECHNOLOGY

Composite material is a field that was initially concerned with the modification of a material's mechanical properties. The technology has since changed to incorporate modification of other material characteristics such as electrical properties. The introduction of smaller filler material size has offered possibilities that allow for improvements in conventional insulation. The mechanics behind these improvements (and changes in general) are not fully understood yet, but models have been developed that could offer insight. These models, the multi-core model and Polymer Chain Alignment Model, are discussed and reviewed from an electrical property modification perspective.

To improve an insulator, an understanding of the basic physics and chemistry of material sciences is necessary. This will allow for explanations of the behaviour of the composite insulation when compared to the unfilled insulation. Material science is largely concerned with investigating, discovering and developing materials for use in technological applications [1]. Solid materials can be broadly classified into one of four types: ceramics; metals; polymers; and composites. Composite materials arise from combinations of the other three types. The area of interest in this research is composite insulators, with specific focus on nanocomposite insulation material.

3.1 Composite Material

Composite material technology has been in use for several centuries already, if not millennia [1], with the most recent development being the use of micro-composites and nanocomposites. One of the earliest examples of a composite materials was the use of straw in baking bricks. This was however most likely only for temperature modification rather than durability unlike more recent composites such as steel reinforced concrete and carbon fibre reinforced polymers [34]. For this reason, microcomposites and nanocomposites for use in construction, and other physical systems, have been available commercially for some time already [34].

These composite materials have been found to possess unique characteristics, often utilising a useful characteristic of the base material, but negating some unwanted property or enhancing a secondary characteristic through the use of a filler. This filler material is usually bonded to the host material using a surface conditioner or surface functionalizer. The surface conditioner or functionalizer serves to allow for bonds to form between the filler particles and host material and forms an interface region. It is currently thought this interface region is responsible for the modifications seen in composite materials [35].

A composite material consists of two or more parts: a base material; and one or more filler material particles. The base material can also be referred to as the host material or host matrix. More than one filler material can be used with one filler material being referred to as a binary composite, two filler materials being referred to as a ternary composite, and so forth. The micro or nano prefix merely refers to the size of the filler material particles. One concern is what size is meant by the micro or nano prefix. In this dissertation, particles between 10 nm and 100 nm are defined as nanoparticles [19].

The size of the filler material is an important parameter in composite materials. The improvements displayed in construction materials, such as improving the fire retardant capabilities of the material, show that the smaller the particles, the more pronounced the effect [21]. The reason behind these improvements are currently not fully understood, but investigations into the electrical property modification through the use of nanofillers have offered insight. It is currently believed that the size-effect relationship exists due to the existence of an interface region [35]. This region is the area around the particle that is bonded to the surrounding host matrix, resulting in a region that is distinct from both the host material and the filler particles [35]. As shown in a mathematical model discussed in [36], the smaller the size of the filler particles, the greater the interface region. If the interface region is responsible for the electrical modifications in composite materials, the size of this region would certainly affect the strength of the modifications.

Composites are not new in electrical engineering, with semiconductors being a fundamental component of almost every electronic circuit. Beyond this however, composites as insulators are almost certain to behave worse than their unfilled (clean) polymer or ceramic counterparts. This is due to the filler material acting as a geometrical electrical stress enhancement for any applied electric field. Indeed some nanocomposites and microcomposites still behave in this manner but others have shown useful effects with very little downside [6].

The most common usage of composite material in an electrical engineering context, is in 'composite insulators'. A 'composite insulator', as used in industry, usually refers to a microcomposite insulator, with the host material being Silicone Rubber (SIR) and the filler dependant upon usage. The most common usage of these composite insulators is to enhance the hydrophobicity of SIR through the use of microparticles. Significant improvements have been shown in both laboratory and practical testing, but the reason behind this improvement is not fully understood [37–39].

It should be noted that the electrical dynamics of binary composites are already complex and not yet fully understood; ternary and greater composites offer an even greater level of complexity and are beyond the scope of this research currently. All composites in this dissertation are binary composites, unless otherwise specified.

3.2 Composite Material Models

There are many models available to represent composites in general, but only two will be discussed in this dissertation due to their applicability to the research. The models offer insights into the physics behind the modifications and the possible reasons for the improvements experienced by composites. All the models will be discussed in the context of nanocomposites, for ease of explanation but, unless otherwise stated, should hold for all filler materials that are significantly smaller than the host matrix structure.

3.2.1 Multi-core model

The multi-core model is a complex, but flexible, model first proposed by Toshikatsu Tanaka in [40]. This model essentially treats the interface region as comprising of three discrete layers around the particles, as illustrated in Figure 3.1. This model is primarily used as an analytical model, rather than a physics model used to describe the exact mechanisms, but draws from the same sources as Polymer Chain Alignment Model (PCAM), resulting in similar basis of reasoning.

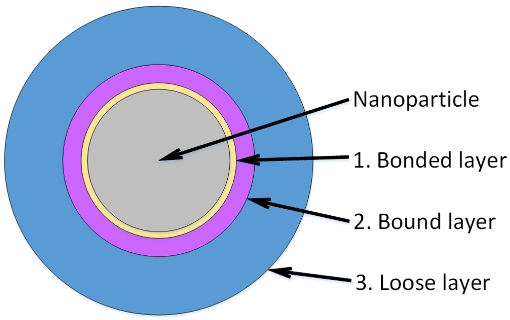

Figure 3.1: Illustration of the multi-core model. Illustration of multi-core model based off of [40].

The interface region is modelled to comprise of:

- Bonded layer: This layer consists of the actual bonds, either van der Waal's forces or hydrogen bonds, that connect the host material and the particle. This layer is the smallest region and is presumed to be 1 nm thick.

- Bound layer: This layer comprises of the polymer chain-ends that are bonded via the first layer. As these chains are directly bound via the bonded layer, they show strong bonds and interactions with the first layer. Since the chains are aligned perpendicular to the particle surface, chain mobility is restricted. This region is assumed to be between 2 to 9 times the size of the bonded layer.

- Loose layer: The loose layer is the thickest region by a factor of several 10's than the bonded layer. This region shows the general morphological changes that can occur from changes in chain formation, chain mobility, free space and crystallinity.

The multi-core model is not specific enough regarding the physics to allow for predictions of macroscopic effects, but is useful for explaining some of the phenomena seen in nanocomposites.

3.2.2 Polymer Chain Alignment Model (PCAM)

PCAM aims to describe the morphology of the nanocomposites and derive the consequent macroscopic material properties. Unlike the multi-core model, which does not focus on modelling the physics and chemistry of the reactions, the PCAM focuses on the physics behind the material modification. This is done by assuming the surface functionalized particles result in polymer chains being aligned perpendicular to the surface of the nanoparticle, as shown in Figure 3.2. This model includes a great amount of detail but only A qualitative treatment and basic sections of interest will be discussed.

The basis of PCAM is that the material properties of the nanocomposite are primarily dependent upon processes prior to and during polymerization [19]. Initial mixing of the monomer and surface conditioned nanoparticles will result in chains surrounding the surface conditioned nanoparticles, but no reactions will occur without the hardener or curing agent. Once the curing agent is added and polymerization occurs, the output polymer chains

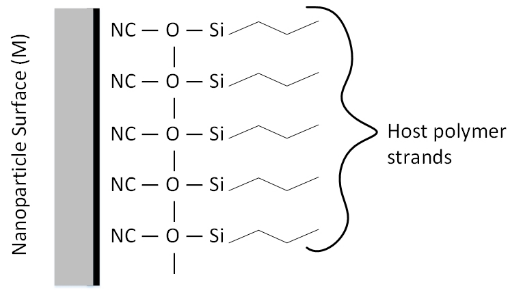

Figure 3.2: Display of the perpendicular alignment of chains that occurs at the surface of the surface conditioned nanoparticle. Diagram based on [19].

will bond with the surface conditioning agent. Assuming uniform dispersion of the bonds, the chains will align perpendicular to the surface as in Figure 3.2. This is a reasonable assumption, as single bonds between the surface conditioner and the polymer should result in inter-molecular forces, causing the polymer chains to arrange evenly.

An inter-penetrating polymer network will form between the polymer chains that possess physical properties unlike both host and filler material [41]. Figure 3.3 displays the difference between the interaction of nanoparticles without and with surface conditioner. As the aligned polymer chains are long with respect to the particle, a significant region surrounding the nanoparticle should experience these effects.

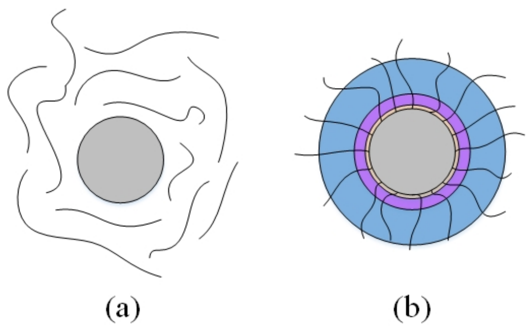

Figure 3.3: Effect of surface conditioning on nanoparticles: (a) no surface conditioning; (b) surface conditioning. Diagram based off [19].

The PCAM assumes that the material is homogeneous with spheres of the same size evenly dispersed throughout the host material [19]. The important part of the model is the ability to quantify the crystallinity of the material. Alignment generally implies crystallinity, which means that the increase in aligned material results in a more crystalline material. As the interface region is fixed per particle, the only way to increase crystallinity is to increase the number of particles. As nanocomposites have a relative larger interface region, the interface region volume is greater in a nanocomposite than a microcomposites. The difference in overall interface volume is the probable cause of the more pronounced improvements in nanocomposites.

Crystalline regions of polymers display anistropic behaviour, due to intra- and intermolecular forces [42]. This behaviour includes changes to thermal and electrical properties. The main modification of interest is that the crystalline regions display a much higher resistivity than the amorphous regions [43]. This results in conduction in the polymer occurring primarily in the amorphous region [44]. This causes an unintended but positive side-effect: as only amorphous regions act as conduction pathways, any electron that encounters the interface region would be funnelled down to the surface of the particles. This negatively charges the surface of the particle and as holes can travel along polymer chains [45], any stray holes are attracted towards the surface of the particle. This implies that the particle surface could act as a natural hole-electron well and recombination point as illustrated in Figure 3.4. The hole-electron recombination will result in the improved dissipation of space charge, which results in reduction of the damage to molecular bonds. The reduction in collisions and therefore damage will result in electrical trees initiating and propagating at a slower rate.

It has been shown experimentally that the beneficial effects of a nanocomposite do not scale linearly with filler loading level [46]. As the overall interface volume percentage increases (and the crystalline region with it), the amorphous volume percentage decreases. At a certain point the overall impedance of the material will be dominated by the crystalline volume's impedance, negating the positive effects that accompany crystallinity.

PCAM presents the best basis for developing the model evolved in this dissertation as it is primarily concerned with linking the mechanics to the behaviour displayed in experiments. This can then be correlated further with

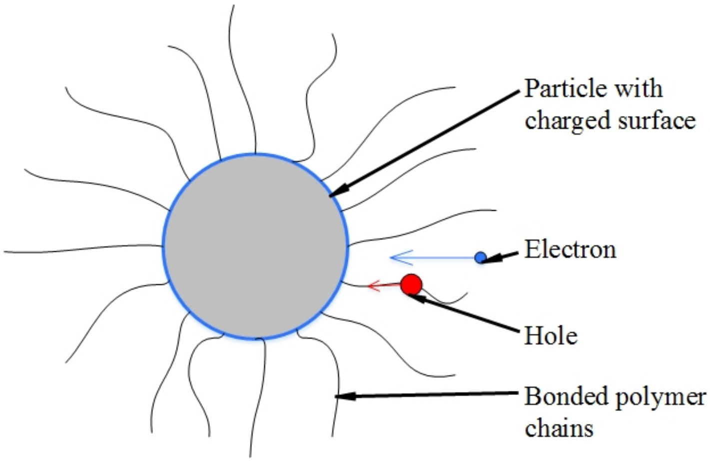

Figure 3.4: Diagram of electron-hole recombination effect.

the Partial Discharge (PD) time evolution behaviour. The multi-core model is not suited to discussions of the molecular structure modifications but is more useful as a simulation aid.

3.3 Simplifications of the Models

As one may notice with the models above, both the models assume even dispersion of the filler material. This is a very important aspect, as the clustering of filler material, referred to as agglomerations, causes unexpected behaviour. Homogeneous dispersion has been an important issue in composite materials with agglomerations since the beginning. Agglomerations often cause problems such as areas of lower mechanical strength which compromises the entire material structure. With microcomposites and nanocomposites, this is even more important and difficult to achieve as the size of the particles are inversely proportional to the force of attraction between them. This greater attraction due to the much smaller size results in a greater likelihood of agglomerations. For this reason, all nanocomposite synthesis processes involve a variety of dispersion techniques to minimize agglomerations. As for electrical properties, these agglomerations may negate the positive effects introduced by the nanoparticles when evenly dispersed. Furthermore, the agglomerations have the potential to act as space charge traps, which would in turn enhance the electric field, creating undesirable effects.

3.4 Summary

Until recently, composite material technology (micro and nanoscale filler), modification of the electrical properties of a material using composition was thought to be non-progressive. This was due to the filler material causing electric field enhancement rather than solving any problems. Nanofillers may alter the molecular structure at a low enough level that either the electric field stress enhancement is minor or can be utilised as a benefit instead of a hindrance. The modifications are most likely caused by the interface region, which is represented well by the PCAM, which has been reviewed with a focus on the possible effects the modified interface structure may have on the macroscale electrical properties. As these models often assume even dispersion, the complications that can arise when dispersion is not homogeneous, are also considered. From the information presented, the basis of the research experiment can now be explained in detail. All these aspects allow for an explanation of the experimental configuration that will be used to investigate the electrical property modifications possible with nanocomposite technology.

Chapter 4

EXPERIMENTAL WORK

The overall experimental setup is summarised before a discussion on each component is given. The sample geometry and manufacture is outlined in detail due to the importance of the sample quality on the results. The procedure followed is delineated along with the designed and implemented remote monitoring procedure necessary to capture all the data required. Finally, the output data is large and requires a fair amount of data processing innovations to allow for information extraction. This data processing is described in detail along with the program developed to perform automatic classification of the resultant PD patterns.

There are three primary points of interest for the experimental procedure: the experimental configuration; the samples manufacture; and data processing.

4.1 The Electrical Tree PD Detection

A diagram of the treeing PD detection circuit is shown in Figure 4.1 and is in accordance with IEC 60270 Partial Discharge (PD) measurement method. A deionized water resistor is used as a current limiting resistor to reduce the amount of current that flows during breakdown. The sample is connected in parallel with a coupling capacitor that is in turn in series with the measurement impedance. This coupling capacitor is necessary for three reasons:

- It decouples the voltage source from the sample.
- It acts as a 50 Hz filter to reduce noise for measurement purposes.
- It holds the voltage, V_1, during a PD to allow the momentary PD voltage difference, $V_1 - V_2$, to form between the sample and the capacitor.

Any discharge that occurs in the sample will cause V_2 to momentarily drop slightly. As the discharge time of the capacitor is much greater than the duration of a PD, the voltage difference formed $V_1 - V_2 \neq 0$ causing a current, i_c, to flow. This current is then measured using the PD detection impedance, which is converted to a PD magnitude in the PD detector.

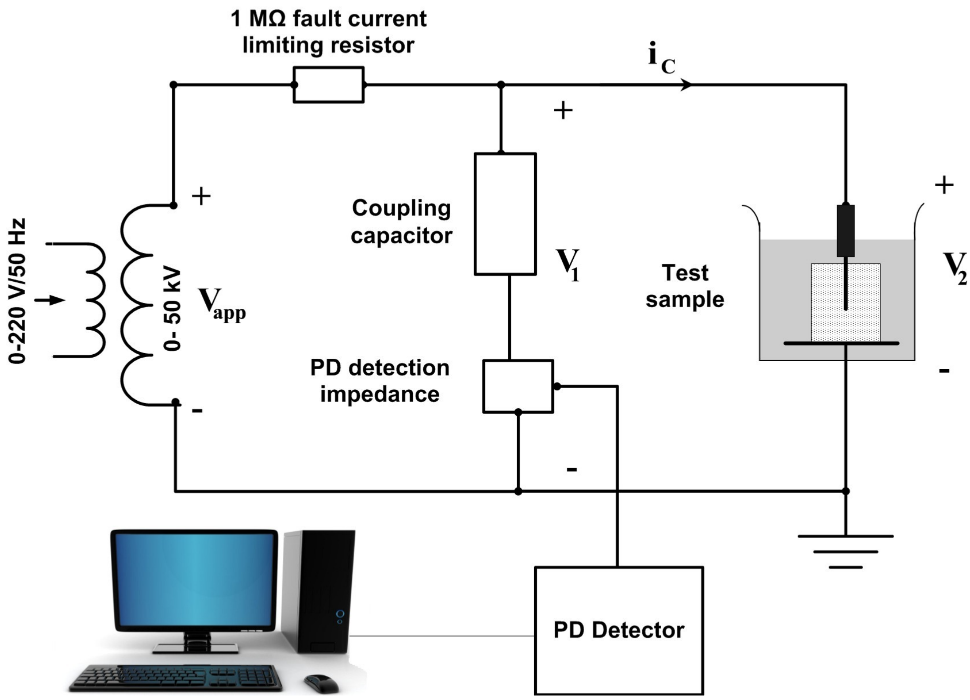

Figure 4.1: Schematic of test circuit based off of IEC60270.

The experiment was set up and run in an HV laboratory constructed as a double-shielded Faraday Cage, resulting in a noise level of approximately

0.3 pC. A notable component of the circuit is the inclusion of a computer for data logging of multiple parameters of interest available from the PD detector software. A computer also allows for far more complex operations around the data to be performed as a post-process.

4.2 The Test Samples

The test samples were manufactured at the Technical University of Delft (TUDelft). They consist of various nanofiller types, MgO, Si_2O and Al_2O_3, with varying loading levels. Clean epoxy samples were also tested to be used as a control group. This allows for comparison between nanofiller material types as well as variations across filler loading levels. The loading levels used in this dissertation are 0.5 %wt (% by weight), 2 %wt and 5 %wt. There are two important facets to the samples: geometry and manufacture.

4.2.1 Sample geometry

The general sample design is shown in Figure 4.2. The main features of merit are the Ogura™ needle [47] and the gap distance. An Ogura™ needle is used because it is manufactured from tungsten, allowing for a very well defined 5 μm, with a 30° angle, tip profile. This well-defined straight edge allows for accurate calculation of the electric field produced by the needle-plane gap, using the Laplacian model described in Section 2.3 of Chapter 2. The gap distance was set to 3 mm as this is the average distance between conductors in medium voltage insulated cable systems. Lastly, the bottom plane of the sample is coated in a conductive silver paint to ensure good contact and an even distribution of the charge across the plane. The test sample geometry, as illustrated in Figure 4.2, is consistent among the samples.

Precautions were taken in the test circuit to avoid external PDs and corona. This was achieved through the use of a custom made test sample assembly, illustrated in Figure 4.3, and a custom made connector as in Figure 4.4.

The sample is held by a smooth cylinder that can be screwed into copper

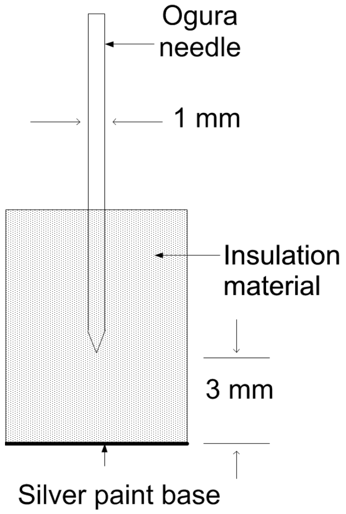

Figure 4.2: Diagram of sample geometry.

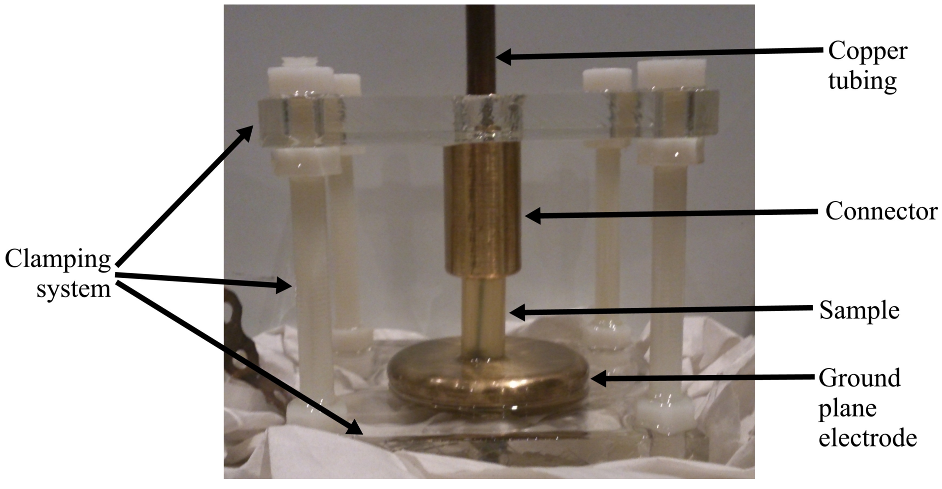

Figure 4.3: Photograph of the complete test sample assembly configuration that is submerged in oil during testing.

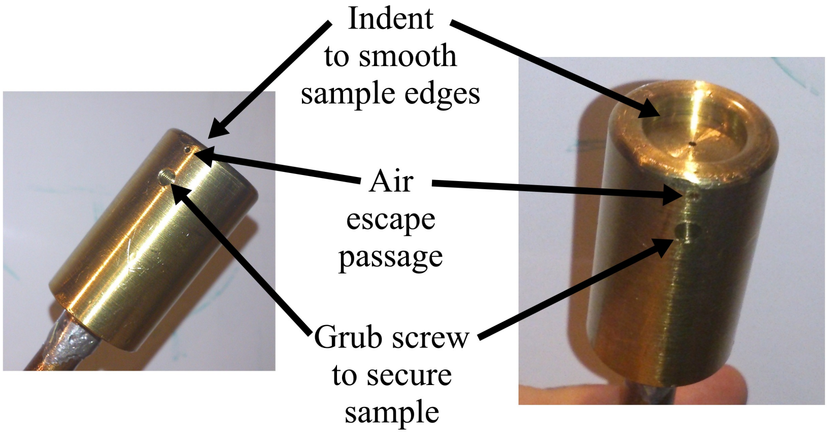

Figure 4.4: Photograph of custom connector to hold samples that smooth out electric fields.

tubing. The cylinder has a small hole into which the top of the needle of the sample can be inserted. Furthermore, the cylinder has a smooth bevel on its surface that is in contact with the sample to reduce any enhancement of the electric field. The needle is then secured with a grub screw. To avoid any electrical stress inducing air bubbles, a small hole connects the needle hollow to the outside of the cylinder, to allow for air to escape when submersed in transformer oil. Lastly a copper cylinder, that is much larger than the sample, is used as the ground plane that rests against the bottom of the sample. These features are highlighted in Figure 4.4.

4.2.2 Sample material manufacturing

The samples were manufactured at TUDelft following a procedure illustrated in Figure 4.5 and consists of the following steps:

- Nanoparticle dispersion: The nanoparticles are first introduced into a solution of ethanol and the surface conditioning agent, γ-glycidoxypropyl-trimethoxysilane. This solution then undergoes ultrasonification in an ultrasonic bath, which serves to force agglomerations to dissipate.

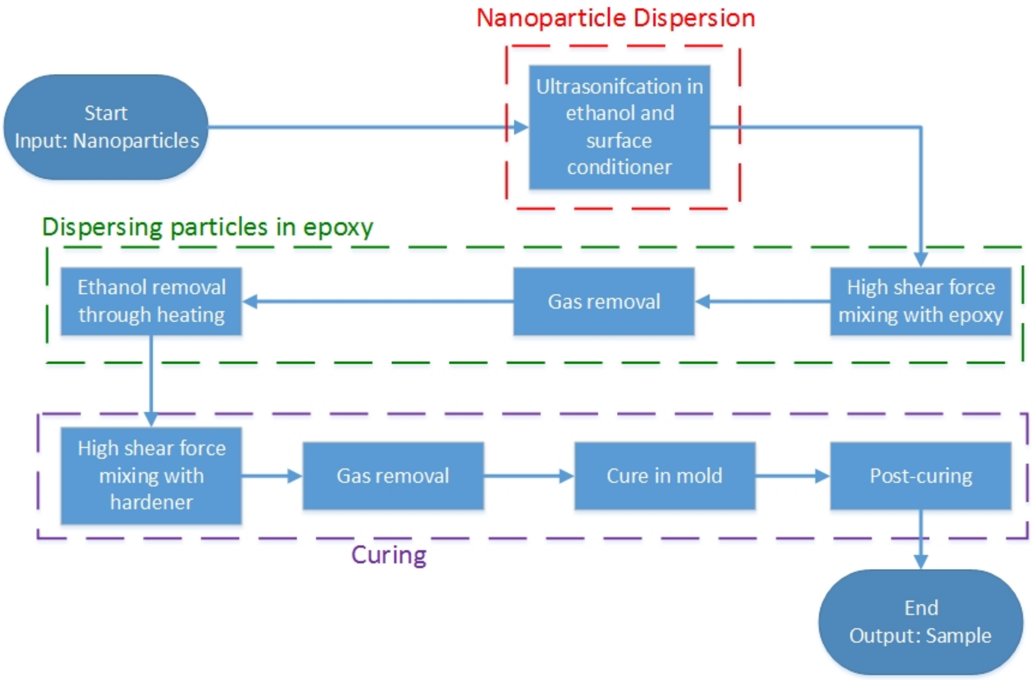

Figure 4.5: Flowchart of sample synthesis [3, 48].

- Dispersing nanoparticles in epoxy: The solution was then mixed with the epoxy, Huntsman type CY231, using a high shear force mixture technique to maintain the even dispersion achieved previously. High shear force mixing techniques are essentially based on the principle of causing motion of different portions of a mixture at different speeds resulting in a high shear force and turbulence that effectively disperses any concentrations. Such techniques are necessary due to the relatively high viscosity of the substances involved. The resulting mixture was then heated for half a day in a vacuum oven to remove the evolved gas and ethanol.

- Curing: The hardener, Huntsman curing agent HY925, was then shear force mixed with the epoxy. This mixture undergoes degassing before being placed in the sample mold. The mold was then placed in an oven at $100°C$ for 8 hours to cure and then post-cured at $140°C$ for a further 14 hours.

Every effort is made to minimise the amount of agglomerations present in the nanocomposite samples during manufacture. There are multiple researchers investigating new and better techniques for minimising agglomeration but it is still possible for agglomerations to occur within the material [49–52]. As delineated in Chapter 3, agglomerations have multiple drawbacks associated with their presence. Examples of the test samples used in this disseration work are shown in Figure 4.6.

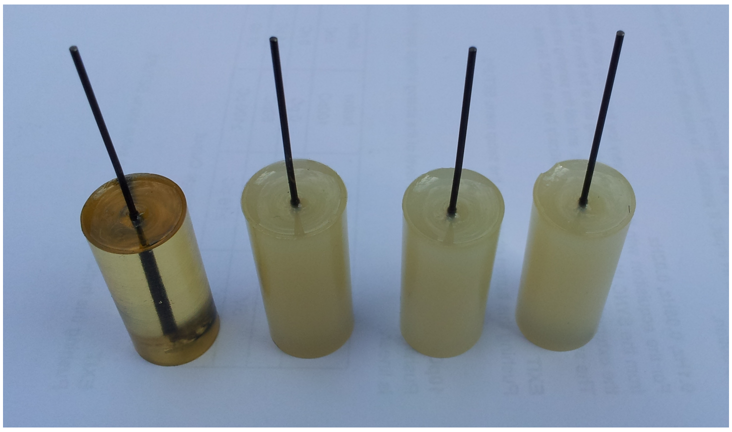

Figure 4.6: Photograph of actual nanocomposite samples used in research.

4.3 Experimental Procedure

The PD test experimental procedure consists of two stages:

- The initiation stage:
  The voltage applied across the sample, V_{app}, was slowly increased from $0\ V$ until $V_{app} = 20\ kV_{RMS}$ at 50 Hz has been achieved. An applied voltage of $V_{app} = 20\ kV_{RMS}$ was selected as this was well above the PD inception voltage of both the clean epoxy and the nanocomposite epoxy samples, ensuring that electrical trees would be initiated. The voltage must be increased slowly to allow for capture the PD inception voltage.

- Continuous PD data capture:
  Once V_{app} was reached the monitoring stage begins. It must be noted

that continuous data capture would have been ongoing since the beginning of the experiment but the build-up stage was relatively short and left out in the trending analysis. Monitoring was accomplished through use of an ICMcompact™ [53, 54], screen capture software and computer logging. The ICMcompact™ measures the PD parameters and logs these parameters of interest over the defined data logging period. The logging rate was set at 1 second and the parameters include minimum, maximum and average PD magnitude (Q_{p-min}, Q_{p-max} and Q_{p-avg}), as well as the RMS voltage, U_{RMS} and the peak calculated RMS voltage, $\hat{U}/\sqrt{2}$.

The Phase Resolved Partial Discharge Patterns (PRPDPs) are also monitored continuously by recording the screen using the freeware program Blueberry FlashBack Screen Recorder. This raises some challenges with synchronising (correlating) the video with the data logged by the ICMcompact™. The output of the screen recorder is also proprietary format, requiring conversion afterwards to allow portability with other software. The currently implemented system is such that the user must manually relate the PRPDPs with the logged data, which can be laborious.

To allow for remote monitoring after-hours, an autonomous monitoring method was implemented. An overview of the system setup is illustrated in Figure 4.7.

The autonomous monitoring system was accomplished using a Secure Shell (SSH) remote desktop connection. A remote desktop connection is essentially a connection that displays the lab computer's screen on another computer, along with the ability to control the inputs of that computer, such as the mouse and keyboard. A remote desktop connection can be initiated from anywhere that has internet access, allowing monitoring to be done from half-way around the world if necessary. This was possible using the Wits University's School of Electrical and Information Engineering's (EIE's) server, but this requires a pre-authenticated user. A second option was developed using the freeware

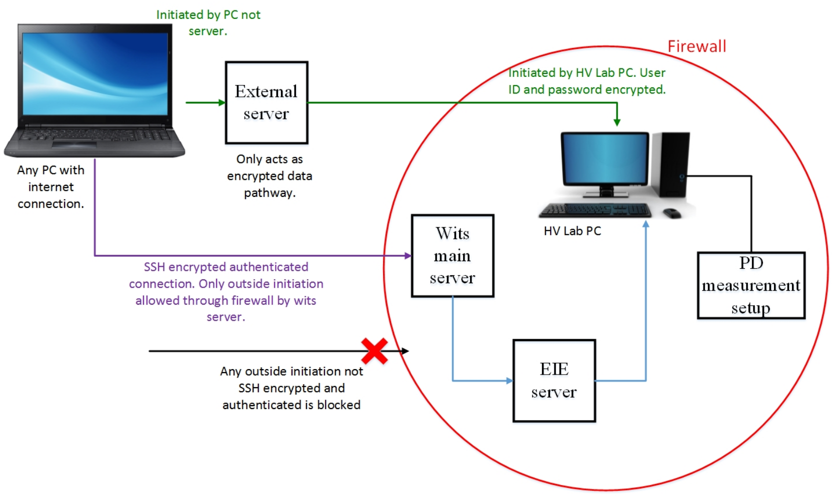

Figure 4.7: Diagram illustrating the remote desktop configuration developed.

program Ammyy Admin [55]. This is a program that accomplishes the same results as above but using a unique identification number for each computer and an external server to act as an encrypted data pathway. This way each computer communicates with the other through the external server in a similar manner to the method Skype™ uses. This allows for security to be maintained by the EIE server, with no firewall exceptions needed to allow access. The users of the HV Lab PC can then create username and password combinations on request, with no administrative processes being involved in authenticating new users. Thereby combining ease of access for multiple users without sacrificing security.

With these monitoring systems, the sample could be monitored even from off-site locations, until the sample experienced breakdown. Once failure occurred, the input to the system would be switched off, and the data logging and screen recording stopped.

4.4 Data Processing

The amount of data accumulated from the experiments was large as expected given their duration, with an average matrix size of approximately 7×10^4x10.

Once the PRPDP data is automatically included, the data would probably expand to (7×10^4)x10x360 at least. Manual processing of that volume of data is not feasible. Furthermore, due to the behaviour of the monitoring system, the recorded data was distributed across multiple Microsoft™ Excel® spreadsheet files (extension .xls or .xlsx) and therefore required three separate stages in the data processing procedure.

4.4.1 Data conditioning

The data had to be checked for spurious readings. Spurious data can occur when a voltage measurement shows a large voltage change for only a few samples and occurs due to corruption of the data either during transmission or storage. These false readings had to be dealt with for two reasons:

- The collation algorithm, detailed below, assumes that the first instance of V_{app} entering the tolerance region around 20 kV, and the first instance of V_{app} exiting this tolerance region, are the start and end points of the data of interest.
- The sample data, such as the various PD magnitudes, can not be fully trusted, as the spurious voltage reading may indicate a corruption in the data received or stored by the computer logging program.

There are several methodologies for dealing with these instances, such as interpolation or straight deletion. Interpolation is not necessarily an appropriate technique however, as the PD magnitude could, statistically, be almost anything [26]. For this reason, the most appropriate technique is data deletion. From the conditioning carried out on this set of data, the occurrence of these spurious readings was very low, and only a few sample for any occurrence. Of this current data set, no more than ten samples were found to have corrupt voltage readings. This loss of sample data was negligible and did not affect the overall pattern, which was the focus of the research. After the data set was conditioned, the data distributed amongst an unknown number of spreadsheet files at runtime, was collated for ease of access later.

Furthermore, any data that was not necessary for the analysis, such as the voltage ramp data and the data from after failure, was removed.

4.4.2 Data collation

A data collation algorithm was designed and implemented on the MATLAB® platform. In summary the collation program reads each sample's data that is distributed across multiple Microsoft™ Excel® spreadsheets, extracts the parameters of interest and concatenates the data into one Comma Separated Values (CSV) file as illustrated in a flow diagram in Figure 4.8 with the detailed program code in Appendix A.1. The collation was accomplished by first asking the user for the directory in which the spreadsheet files are stored. The collation program is dependent upon a certain structure applied to the storage of the conditioned data.

Modelling the directory tree as a tree data structure, the program assumes that the spreadsheet files are only located in the leaf-nodes of the directory structure. Furthermore, for simplicity, the program assumes the final folder name in the directory structure defines the sample code that the data applies to. A file naming convention was defined as follows: *MMF-S*p*N.ext*. *MM* is a 2 character code that defines the filler material, i.e. 'MG' corresponds to MgO, SI corresponds to Si_2O and AL corresponds to Al_2O_3. *F* is the filler loading level which is not limited to one character. *S* is the sample number and *N* is the 3 digit part number of the file, i.e. N=023 is the twenty third recording file for that sample. Finally, *ext* is the extension of the file which is limited to xls and xlsx extensions as this is the output of the ICMcompact device. As can be seen this is simply the sample code with the part code and file extension appended to it. An example of this structure is shown below in Figure 4.9.

First, the script requests the top level folder that contains the measurement data files. It then recursively searches through the subdirectories until a directory leaf-node is found. The script then iteratively reads in each spreadsheet file and extracts the Q_{p-avg} (average PD magnitude) and the U_{RMS} fields and concatenates each file's data into a large three column matrix.

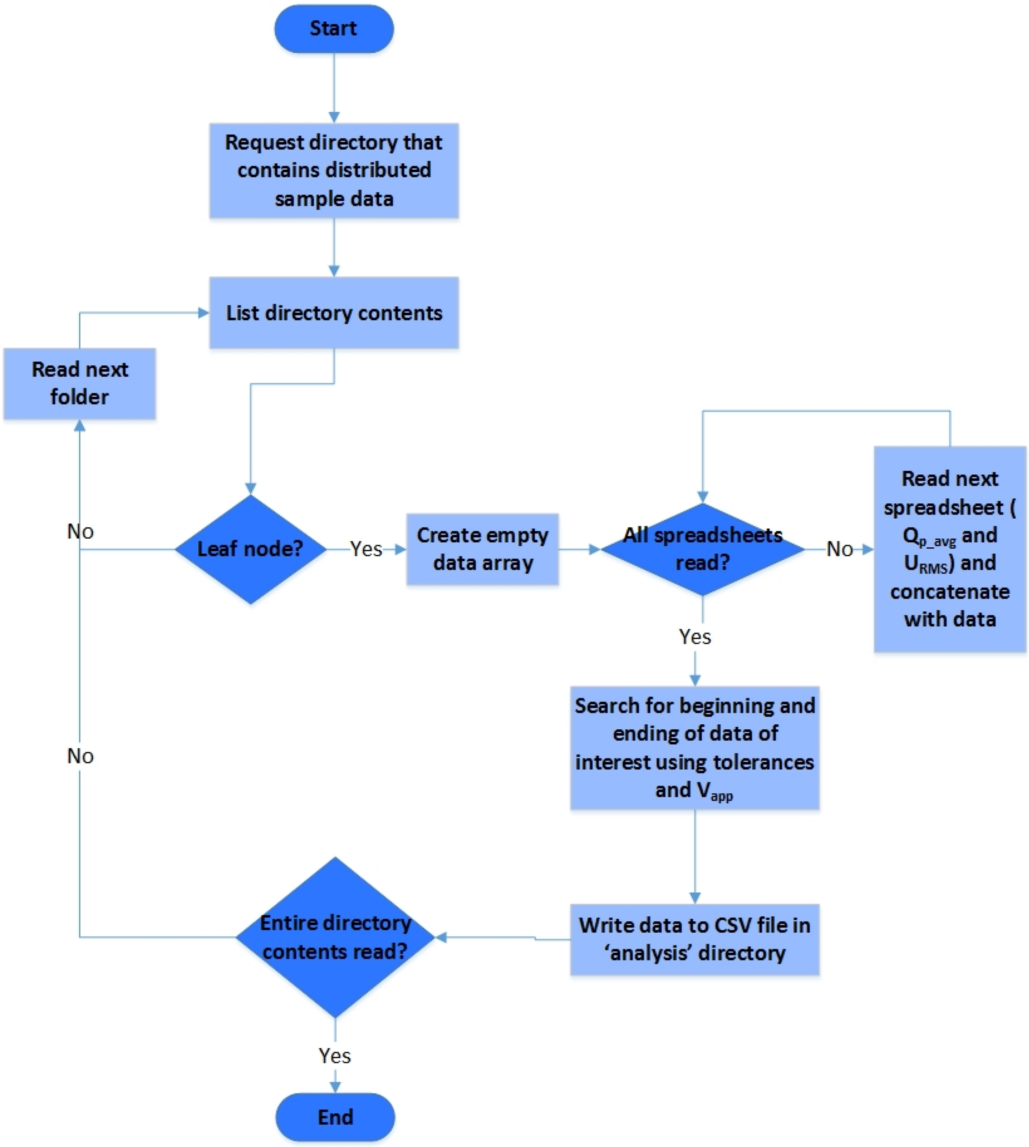

Figure 4.8: Collation program flow diagram.

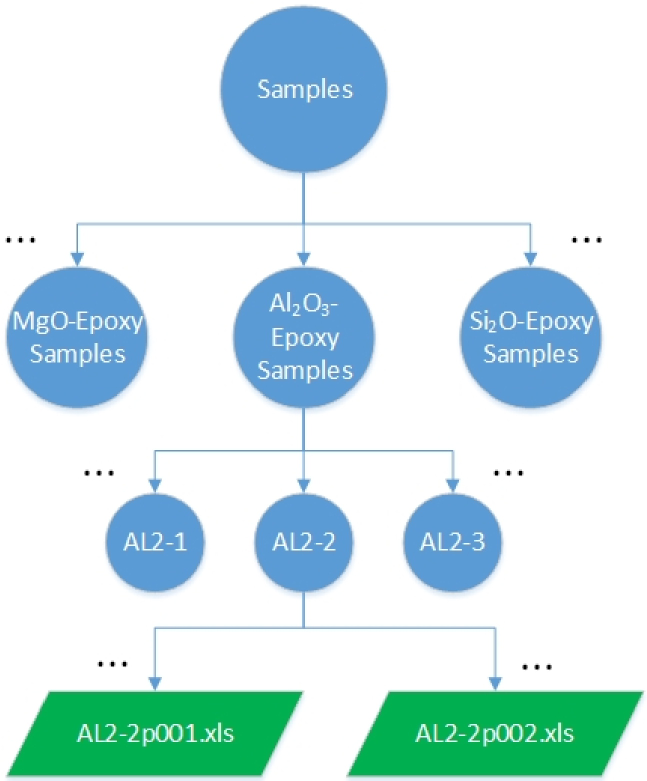

Figure 4.9: Tree diagram illustrating assumed structure by collation program.

Once all the data has been concatenated, the U_{RMS} was used to eliminate the initial voltage ramp, as it was not in scope, and the point of failure. This was done by using V_{app} with tolerance levels to determine these two points of interest. The start point of the data was defined as the the first sample that enters the tolerance region. The end point of the data was defined as the point, after the start point, where the sample voltage signal leaves the tolerance region again. It must be remembered that this was dependent upon data conditioning, as spurious samples often read as 0 V or extremely large voltages such as 100 kV. The PD data before the start point and after the end point was then ignored and discarded.

The program can easily detect the PD inception voltage that occurs during the voltage ramp at the beginning of the recorded data. This functionality was not untilised as it fell outside the scope of this dissertation, but the data was available, as the PD inception voltage was recorded for each sample.

The time vector, generated by using the sample time in combination with the vector length, and average PD magnitude vector are then written to a folder in the current working directory as '*sample_code.csv*'. The output CSV file was then used as the input to the analysis program, detailed below, that can be carried out at a later date. This collation script was written to be executed separately from the analysis, as the amount of data can result in collation taking anywhere from 30 minutes to an hour, dependant upon the capabilities of the processor used. The collation runtime will scale linearly at best, meaning an increase in the amount of data will result in significant amounts of time being needed for the collation script. Furthermore, the data being read in is of indeterminate size, creating difficulty in employing time-saving techniques such as preallocation. These factors led to the implementation of the recursive nature, as well as the rigidly defined structure. These two features allow for the user to easily select only subsets of samples that needed to be collated, saving significant time when new data was obtained that needs to be collated. This also allowed for collation to be done only when necessary, cutting down on collation time significantly.

4.4.3 Data analysis and auto-classification

Once the data had been collated, a program was written to allow for analysis and auto-classification. Its methodology is summarised in Figure 4.11 and detailed in Appendix A.2. Each sample's data is read in before it segments the data into different classes and plots the resulting segmented data. The program is currently being expanded during the language migration, described below, into a function that takes a string as an input to allow for specific filler material inclusion and exclusion at runtime, with the aid of Map data structures. The directory where the CSV files to be analysed are kept is first requested from the user. The program then iterates through the list of CSV files and creates a Sample object for each file. An assumption made for the program is that the CSV files are only in the directory passed by the user, and not in any of its subdirectories. A Unified Modelling Language (UML) class diagram for the analysis program is shown below in Figure 4.10. The salient features of this UML class diagram are the Sample and PDSignal classes. Sample uses a method, in combination with a Map data structure, to parse the CSV file name and retrieve the details for each sample. Furthermore every Sample is composed of a single Signal object.

The decision to implement a fully Object Orientated (OO) program was made due to the complexity of the analysis program. To facilitate understanding and to reduce complexity, the code could have been segmented into functions, however the problem fits OO logic, and allows for simple implementation of generalised functions that are dependent upon the the type of object running it. This is most evident in the implementation of the segmentation operation before classification occurs. The segmentation essentially looks for differences between groups of classes, which can then be classified using different criteria dependent upon the group the segment falls into. Furthermore, it simplifies the plotting operation as one plot command can be issued causing an iteration through the object arrays that compose each class, plotting each class in different colours and possibly placing division lines for further clarity. Not using OO programming would result in maintaining multiple vectors of values that must be carefully managed to

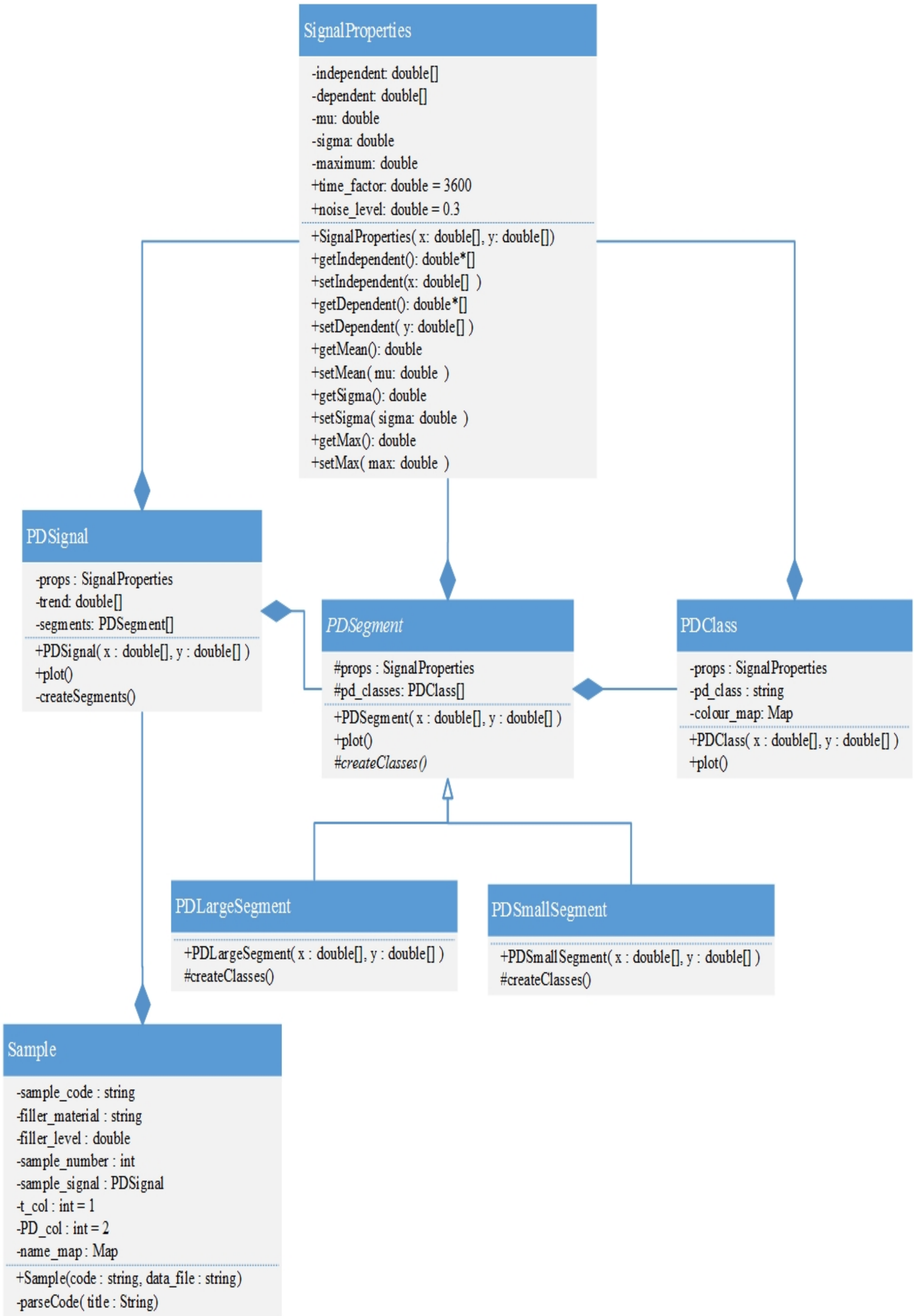

Figure 4.10: UML class diagram of auto-classification program.

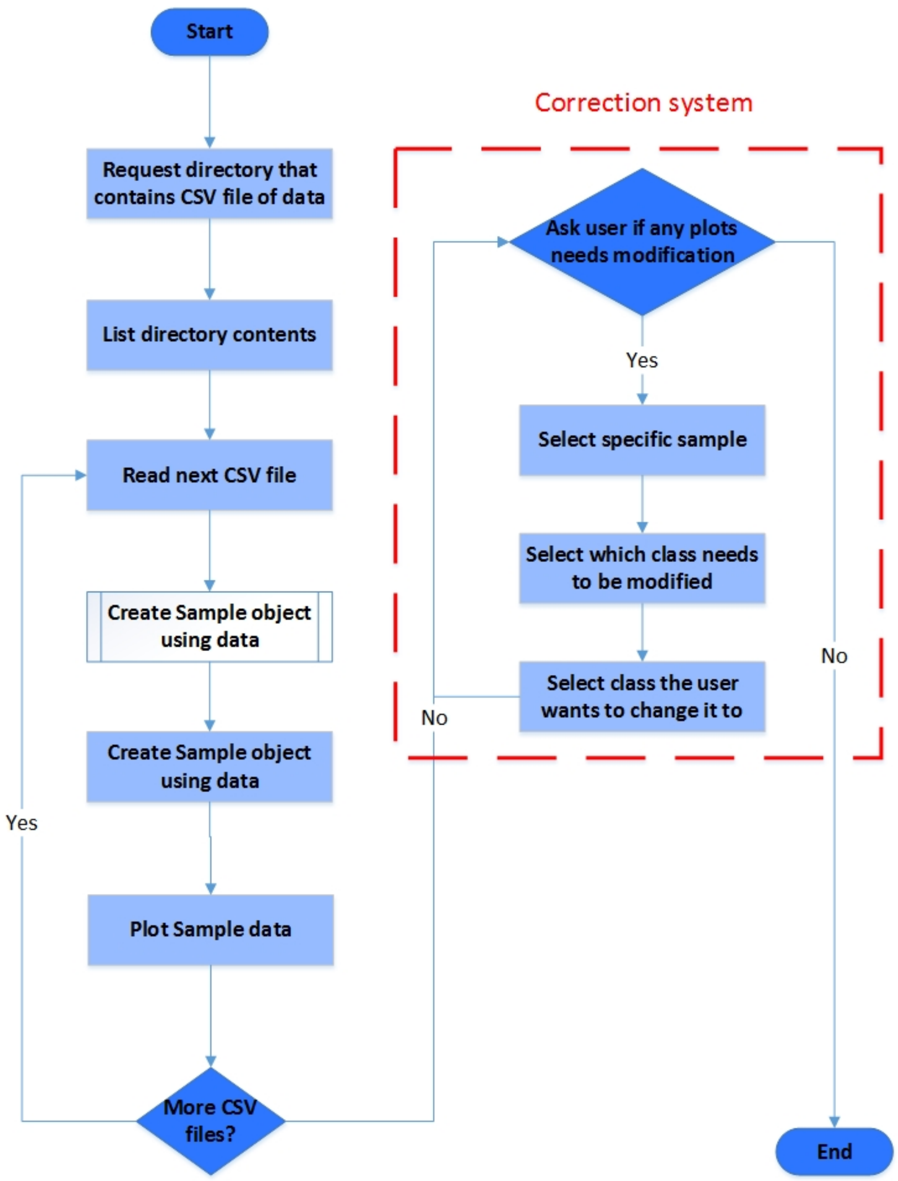

Figure 4.11: Flow diagram of the main part of the auto-classification program.

ensure the vectors are kept synchronised. OO programming also allows for easy expansion of the information export capabilities of the program. The overall complexity, clarity and efficiency of the OO implementation should be magnitudes greater than merely implementing multitudes of functions.

Segmentation of the electrical tree PD data for auto-classification

Two segment groups of the electrical tree PD parameter data captured throughout the tree's life have currently been identified: segments containing relatively small PD magnitudes; and segments containing relatively large PD magnitudes. The importance lies in the relative qualifier; the segments are identified relative to the maximum PD magnitude detected and the overall mean of the PD signal. Furthermore, the data used to quantify which type the segment adheres to is the trend, calculated using a moving average, instead of the average PD magnitude values. The use of the trend smooths out any spikes in magnitude that do not affect the overall pattern. An example of the relationships of means and magnitudes is shown in Figure 4.12. This segmentation and auto-classification scheme is illustrated in the flow diagram in Figure 4.13.

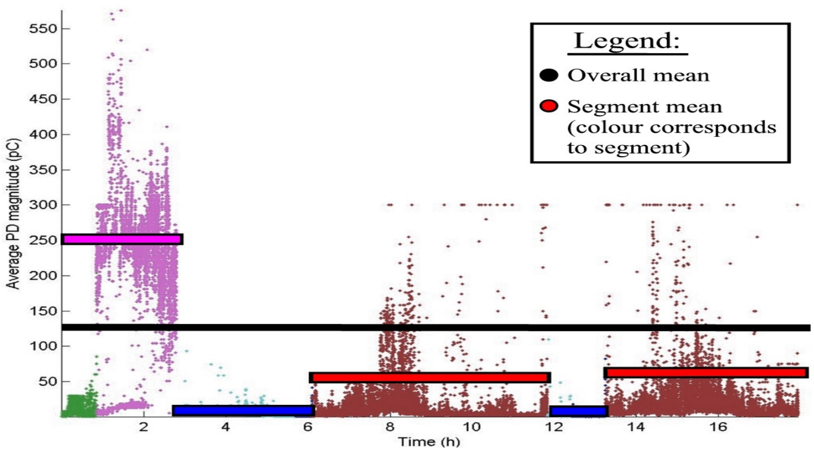

Figure 4.12: An illustration of the relationship between the various means used in the auto-classification program for segmentation.

Once the the signal has been segmented, each segment undergoes further segmentation into the classes that comprise that section. This is again based

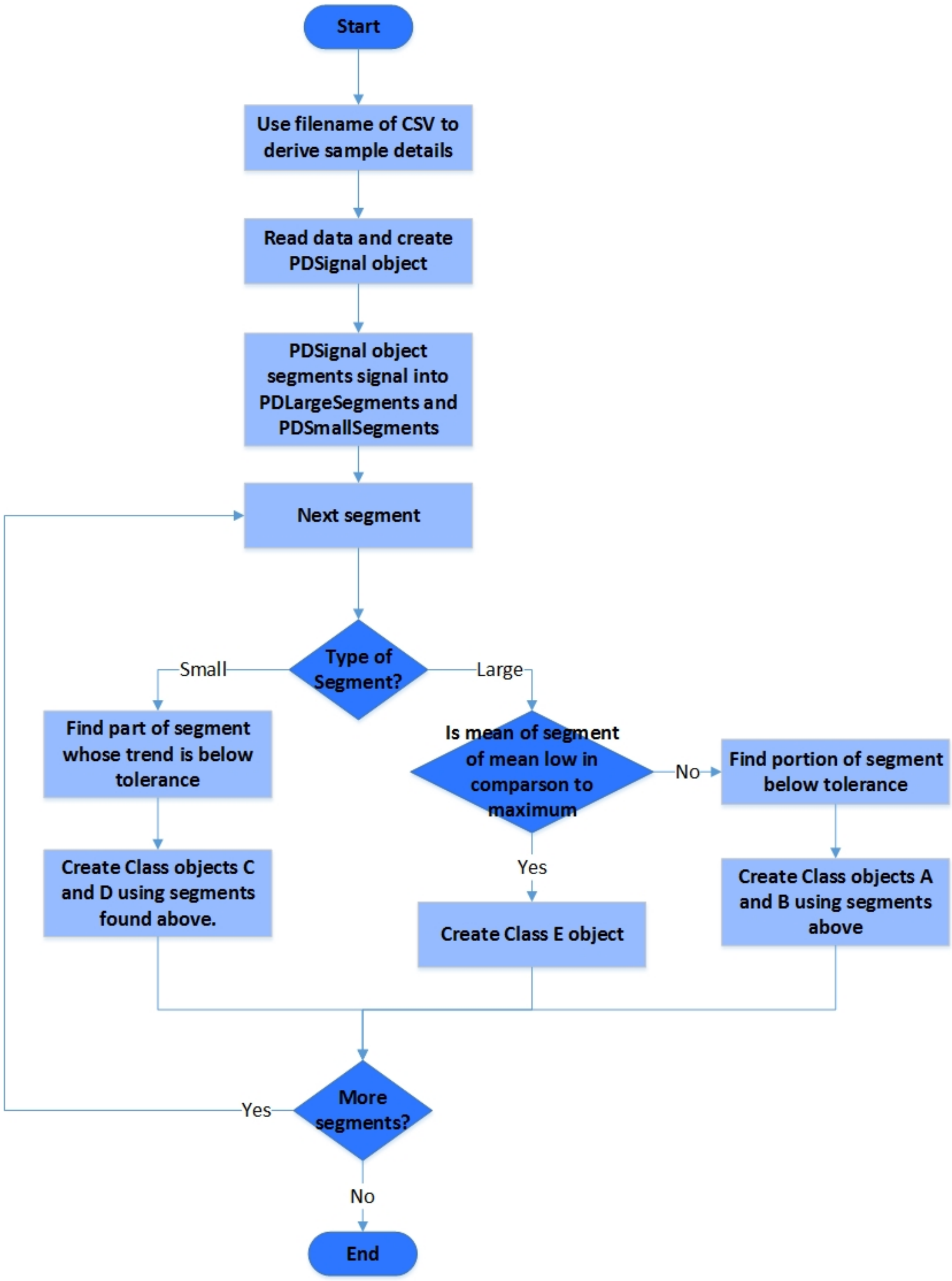

Figure 4.13: Flow diagram of the portion of the auto-classification program which actually segments and classifies.

on monitoring parameters of the segment, such as mean and standard deviation, with respect to the trend. Classes C and D are segmented by finding the section of the segment that exceeds a certain tolerance. This tolerance is calculated as a multiple of the segment mean. For classes A, B and E, it was noticed that instances of PD class B have a much higher mean and lower standard deviation than class E. It is assumed that, due to the definition described in the following sections, class A precedes class B. This classification works relatively well with only a few errors in the classification. Currently the program does require human intervention to review the plotted data and make corrections as necessary with the aid of the corresponding PRPDPs.

It must be noted that the tolerances were found by manual inspection of the general behaviour of each classes mean and standard deviation. This resulted in a rough range of values to work with, which was narrowed down by trial and error experimentation until the current values were found. This does not imply that the current set of tolerances are unique in their effectiveness, or are even the the best combination. Better tolerances could result in more accurate classification, with less errors that require corrections.

4.4.4 Correcting the auto-classification

To aid in easy correction, a Graphical User Interface (GUI) scheme was developed that prompts the user to review the plots and decide if they wish to modify any of the plots. The correction algorithm is displayed in the correction block of the flowchart in Figure 4.11. If the user does wish to modify the plots, a list of all the samples analysed is displayed from which the user can select a specific sample code as in Figure 4.14. A dialogue box asks which class of the the specific sample the user wishes to modify and a final dialogue box asks which class the user wishes to change it to. The chosen sample is then accessed, and the specific class accessed and modified as requested. The program then displays the plot and asks whether the modified plot should be saved. This can be done over and over until the user clicks cancel, or closes the dialogue boxes.

No modification of the segment lengths have been implemented as no

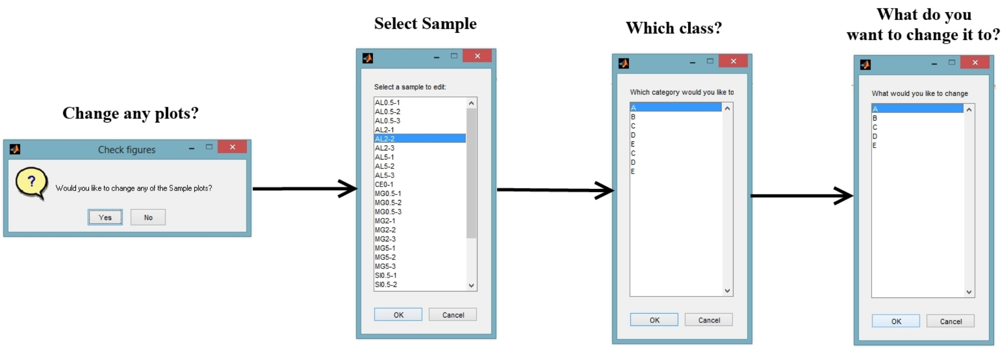

Figure 4.14: Flow of dialogue boxes for correction protocol.

significant errors have been detected in the segmentations. This is a necessary step, as the observations utilised in the design of the program may not apply to every sample, and the difference between classes B and E should be done using the PRPDPs of the sample. This data is not available to the program yet, requiring verification by the user to determine if the classification by metric parameters is correct. A difficulty does lie in the classification scheme, even for a human user, but this limitation will be discussed in the following sections as it is a general difficulty that is not unique to the auto-classification program.

4.4.5 Program implementation

The data processing programs described above were implemented in the MATLAB® programming language, and the detailed code is given in Appendix A. There are several idiosyncrasies to the MATLAB® programming language as object orientation is not a native part of the language. Rather, object orientation was developed as an addition to the language at a later stage. This is most obvious in the absence of native pointer and polymorphism support. These two standard facets of OO programming must be manually activated through inheritance of specific classes. For example, passing by reference for an object, can only be activated by inheriting from the abstract *handle* class. In fact, polymorphism can only be activated in this way from MATLAB® R2011a onwards, as the required code is not available below this version [56]. It is for these reasons, as well as portability concerns, that the program is currently being migrated to Python programming language [57]. Python was designed as an OO language from the beginning, negating many of these idiosyncrasies that MATLAB® displays. Furthermore, Python is natively supported on almost every UNIX based operating system, allowing for a much greater degree of portability. Lastly, Python is a commonly used language in the computational sciences, for data processing on a scale beyond the relatively small data set for these experiments [57].

4.5 Summary

At face value, the experimental methodology is relatively simple until each section is detailed. The sample geometry was specifically designed to ensure electrical trees were initiated. The sample manufacturing process is complicated and the resulting materials adhered to the necessary specification, although there is always a probability that agglomerations are present. The PD measurements continuous monitoring system implemented involved PD magnitude monitoring, video recording and remote desktop access to allow for after-hours monitoring. For analysis, the output data was collated and plotted as well as classified by an auto-classification program developed specifically for the function. This program was implemented in MATLAB®, but is being migrated to Python for future expansion and work. This chapter serves to construct a foundation from which to present the results of the experiments in the next chapter.

Chapter 5

RESULTS AND DISCUSSION

This chapter covers the results as well as analysis, interpretation and discussion. It is necessary to present the basic mechanics that underlie the behaviour seen in each case. These results, interpretation and discussion will serve as the foundation for a model that will be presented in the next chapter.

Many samples were tested and therefore the results and analysis will be discussed per sample group at a time. Each section will represent a specific filler material (either Al_2O_3, MgO and Si_2O) with subsections representing the results and analysis of each filler loading level (0.5 %wt, 2 %wt and 5 %wt). At the end of each section, any trends peculiar to the type of filler material will be discussed. After all the filler materials have been discussed in the respective sections, a final section will be included discussing the trends along filler loading levels. The results are discussed by using the Partial Discharge (PD) time evolution plot as described in Section 2.4 of Chapter 2. Each PD time evolution plot will be classified using a colouring scheme and displayed along with the Phase Resolved Partial Discharge Patterns (PRPDPs) for each class. For multiple instances of a class, only one of the instances will have a corresponding PRPDP shown due to space limitations, but the other instances of that class display similar behaviour. The explanations of the physical mechanisms in each class will be discussed as each class is encountered. A full comprehensive explanation of the proposed model will be suggested in the following chapter. It must be noted that whilst the auto-classification program was used to generate the coloured plots, the included PRPDPs were manually inserted for each figure.

5.1 Unfilled (Clean) Epoxy

A typical example of a clean epoxy's electrical tree PD time evolution plot is shown in Figure 5.1. The graph shows two different classes of the average PD magnitude, referred to as Q_{p-avg}, on the graph. A clean epoxy's PD time evolution graph displays two classes of PD magnitudes:

- Class A:
  With reference to Figure 5.1, the first class can be seen as a region of approximately linear increase in the Q_{p-avg}. This class shows relatively small Q_{p-avg}, although the magnitude increases within the class. Furthermore, the corresponding PRPDPs display a family of uniform, smaller PDs occurring. This can be seen as the inception and propagation of the bush tree. PDs in class A are associated with the formation of a bush electrical tree in this regard. This is expected as the electric field stress around the needle tip is very high and divergent, which would result the formation of a bush electrical tree.

- Class B:
  After class A has occurred (about 20 % of the total time, 15 minutes for this example), the Q_{p-avg} enters a stage of much greater Q_{p-avg}. Furthermore, the Q_{p-avg} displays wide variations for this segment. The mean of this section is also at least double the mean of class A. Class B could be attributed to the development of a branch trees, creating much larger PDs within the longer tubules. The corresponding PRPDPs, an example of which is pictured in Figure 5.1, further support this proposal as they display larger, random PDs occurring.

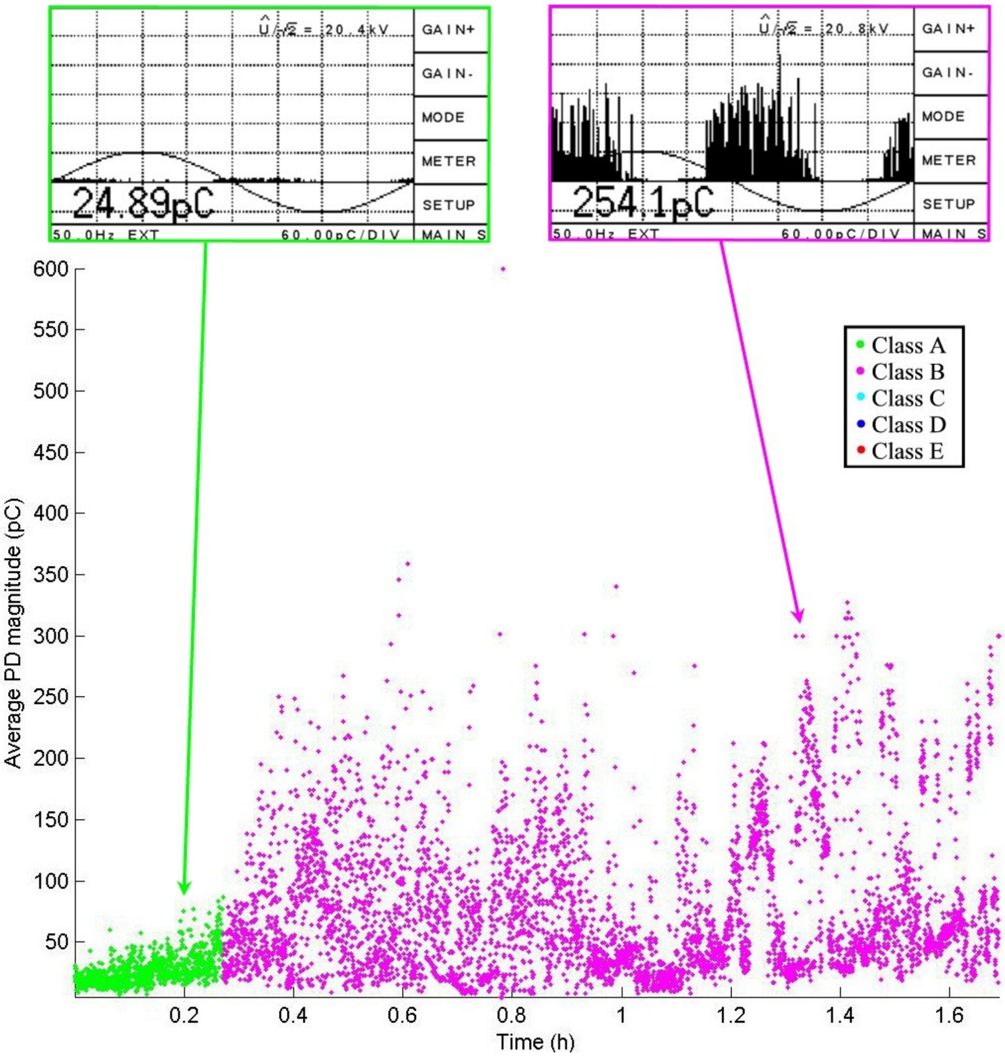

Figure 5.1: Example of a clean epoxy's PD time evolution pattern with classification and PRPDPs.

All clean epoxy samples exhibit this basic pattern of class A followed by class B. Specifically, a period of linear growth with small, uniform PDs in the PRPDPs and then a second stage of much larger, random PDs in the PRPDPs. In literature, no one appears to have monitored the PD magnitudes in this manner over the entire life-cycle of the electrical tree. The most notable feature of these two classes is the transition. Class B shows a much greater overall mean than class A. Furthermore class A constitutes a much smaller part, almost a tenth of the time to failure, than class B does. This is to be expected given the mechanics described above.

Note must be taken of the relative y-axis scale for the following plots as they do not have the same range as Figure 5.1. The change in scale is necessary to retain detail but the scale is mentioned in each analysis to ensure cognizance of the fact. Furthermore, some of the samples' PD time evolution plots may show a clamping effect in certain sections. This is an effect introduced by the auto-ranging feature of the ICMcompact™. If large, infrequent PD magnitude pulses occur, the auto-ranging feature will not compensate before the pulses stop or cease for a short period. This results in the measurements saturating at the maximum for the range at the time.

5.2 Al_2O_3/Epoxy Samples

5.2.1 Al_2O_3 0.5 %wt

With regard to the number of classes, most Al_2O_3/Epoxy 0.5 %wt have only two classes as in clean epoxy, but in both classes the PD magnitudes were noticeably smaller than in clean epoxy. One of the Al_2O_3/Epoxy 0.5 %wt samples however, displayed additional classes C, D and E as shown in Figure 5.4. The samples' PD time evolution plots are displayed in Figures 5.2, 5.3 and 5.4.

Each sample displays a distinct class A and B except for sample AL0.5-2, in Figure 5.3, which displays very low Q_{p-avg} with many data points within the noise mask of 0.3 pC.

The third sample in Figure 5.4, AL0.5-3, however displays a further three classes, as well as the usual class A and B, as detailed below. The PD time evolution plots were all classified using the auto-classification program with no manual corrections necessary.

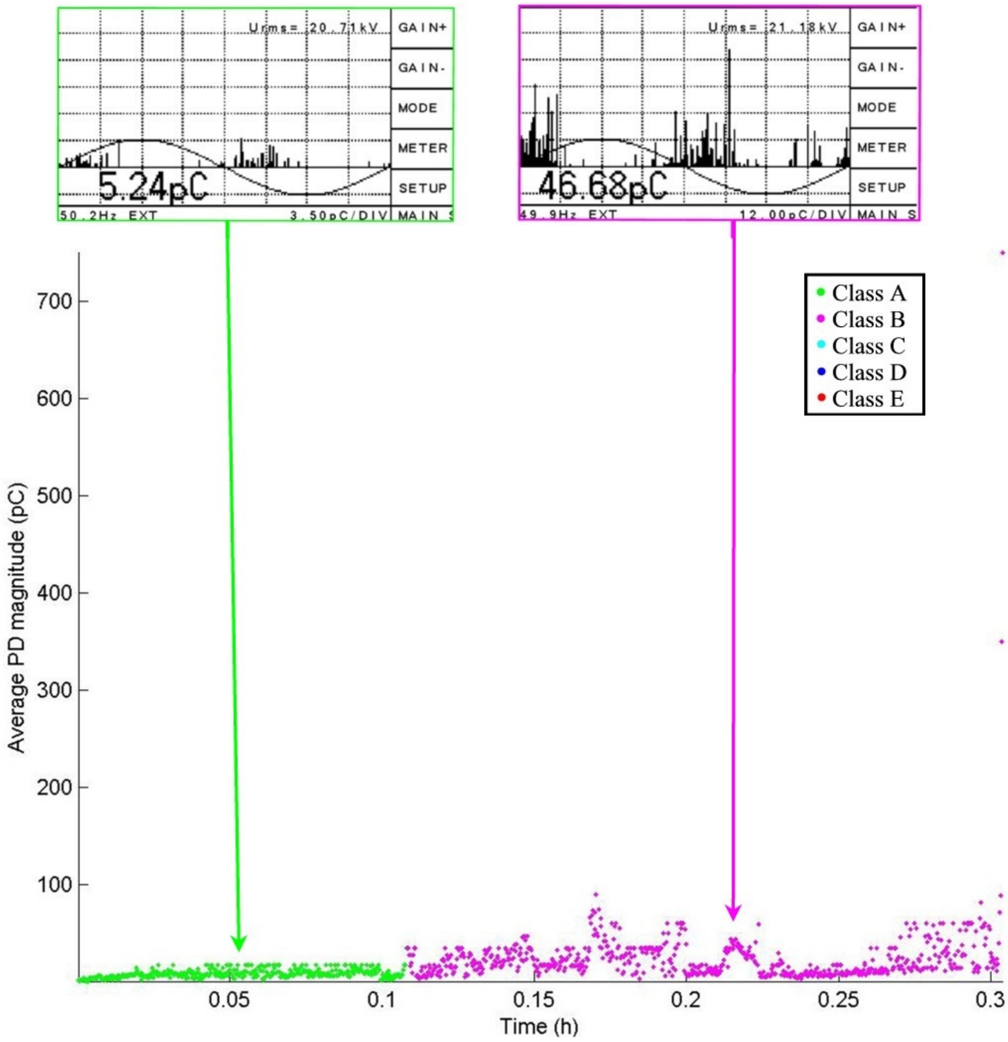

Figure 5.2: AL0.5-1 PD time evolution plot with PRPDPs.

- Class C:
  Class C is typified by a sudden and consistent drop in the Q_{p-avg}, however there is not a complete cessation of PD activity. This could indicate that the electrical tree tubules have started to carbonise. The

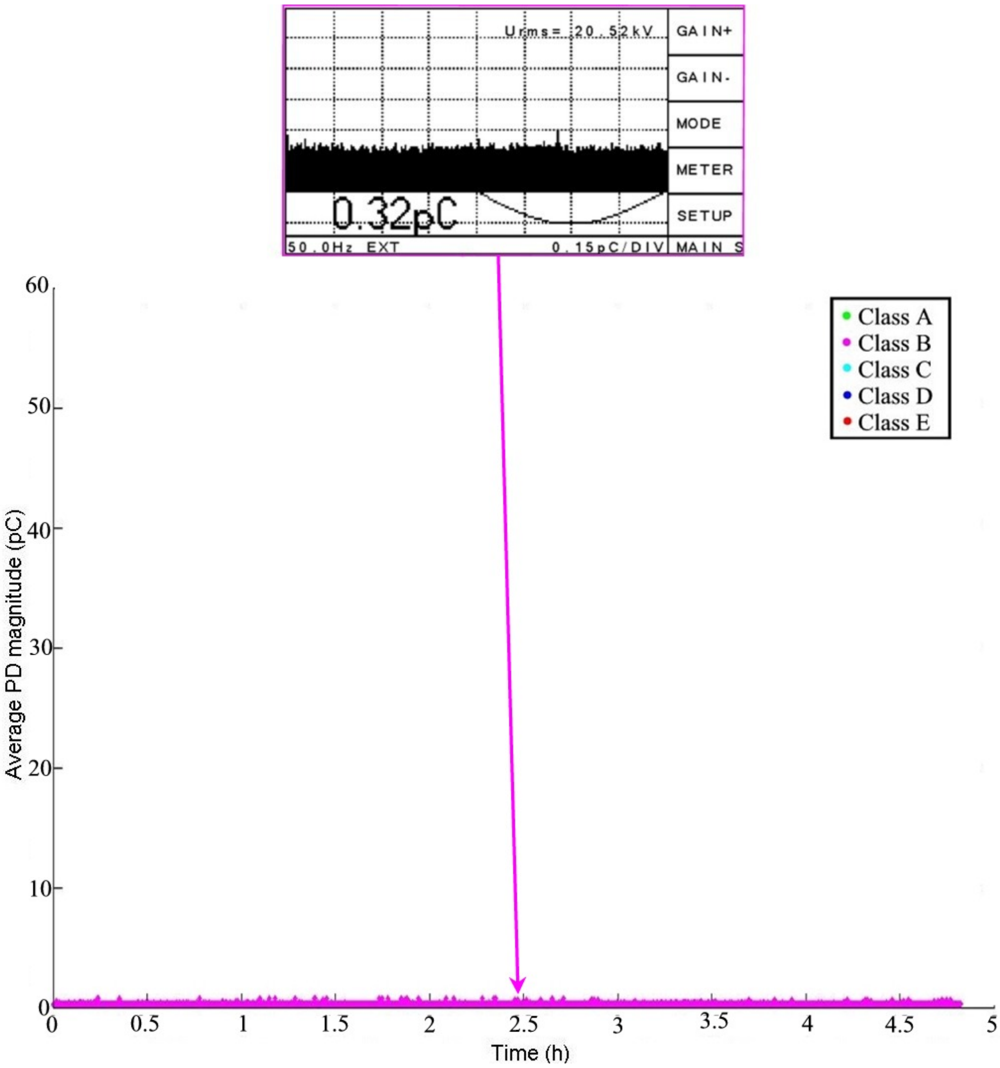

Figure 5.3: AL0.5-2 PD time evolution plot with PRPDPs.

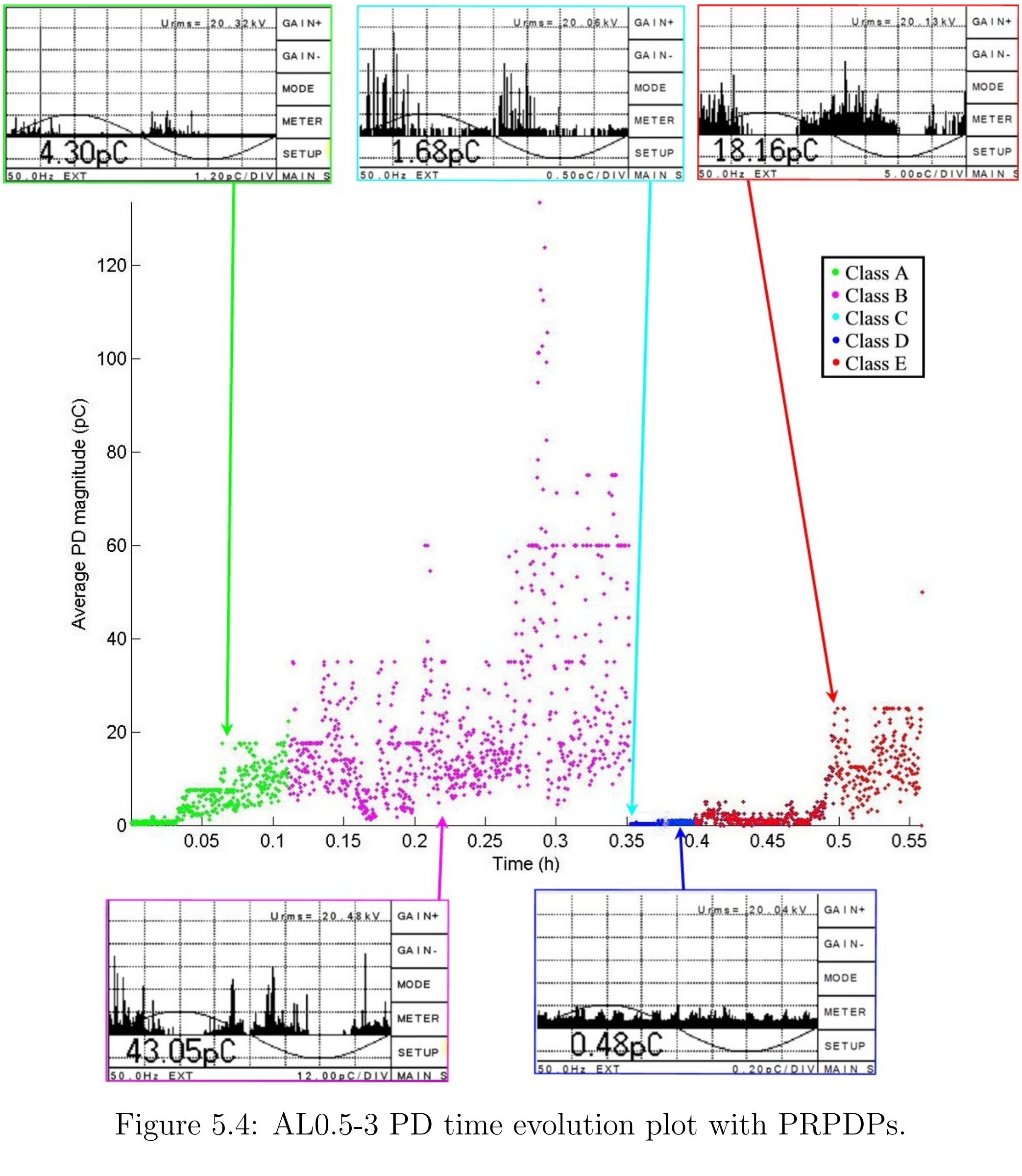

Figure 5.4: AL0.5-3 PD time evolution plot with PRPDPs.

carbonisation would cause the walls of the tubules to become conductive, not allowing charge to accumulate but rather dispersing it along the entire carbonised wall structure. The discharge area is effectively reduced, thereby reducing the Q_{p-avg} that can occur. Class C is not really visible in Figure 5.4, but the PRPDPs and the list of classes clearly display it. This class displays similar PRPDPs as seen in class B.

- Class D:
  Class D can be regarded as a complete cessation of PD activity greater than noise level in Figure 5.4. There may be some small, random spikes that occur inside this class, but they are isolated instances that do not greatly modify the overall trend of this class. It must be noted that PD activity could be occurring, but it would be masked in the 0.3 pC noise level. The cessation may indicate complete carbonisation of the tubules, resulting inner electric field in the tubules. A near zero electric field would cause a lack of PD activity, hampering further electrical tree propagation.

- Class E:
  A sudden resumption of PD activity occurs, heralding the beginning of the next class. Class E shows a similar pattern to class B in Figure 5.4 but clustering occurs around a lower Q_{p-avg}, indicating a prevalence of smaller PDs, and a wider variation in the Q_{p-avg}. These are not however, the main deviation from class B behaviour.

  Firstly, the resumption can be explained by propagation of the electrical tree tubules into the insulation. Three effects begin to dominate at this stage: the furthest carbonised tubule creates a new tip causing the electrostatic push-pull force; corrosive chemicals that are still present; and pressure increases. These three factors cause the initiation of a new electrical tree, allowing for PDs to resume.

  Analysing the PRPDPs in this class however reveals interesting patterns. The typical PRPDPs occur as expected but occasionally the

PRPDPs show behaviour similar to that of corona discharges as in Figure 5.4. This implies that not only are partial discharges occurring, but corona is occurring as well.

The presence of corona-like discharges is quite interesting as this would not be expected normally in internal discharges. As the nanoparticle and interface region would certainly have a different permittivity to the gas inside the electrical tree tubules, the nanoparticles may be acting as electric field enhancement points. These nanoparticles, due to their interfacial region, would protrude into the tubule and act as a rod electrode. Applying the Laplacian field enhancement model, the extremely small size of the rod tip (the nanoparticle plus interface radius) would result in extreme electric fields. This could cause localised breakdown of the gas inside the tubules, resulting in the corona PRPDPs.

Class C shows a significant reduction in its mean, even lower than class A's mean in this case. Class D also has a low mean but the general trend of this section is more important: class D appears flatter than class C. Finally, class E shows a large jump in its mean in comparison with class D, although not as great as class B. The smaller segments, comprising of classes C and D, show a much shorter duration than class B and E, but it remains to be seen if this is consistent. All these factors were important as they were used in the auto-classification algorithm. For brevity, any PRPDPs that display these additional classes beyond class A and B, will be referred to as an extended pattern. Any PRPDPs that can be classified into only class A and B will be referred to as typical patterns.

5.2.2 Al_2O_3 2 %wt

The 2 %wt samples in Figures 5.5 to 5.7 display two classes as with clean epoxy but one had more classes. As expected, class A and B occur again at the beginning of the pattern. Although class B shows distinctive clustering of data points towards a larger magnitude instead of apparent random scattering as in the clean samples. The second sample in Figure 5.6 shows the extra classes again, but two cycles are experienced.

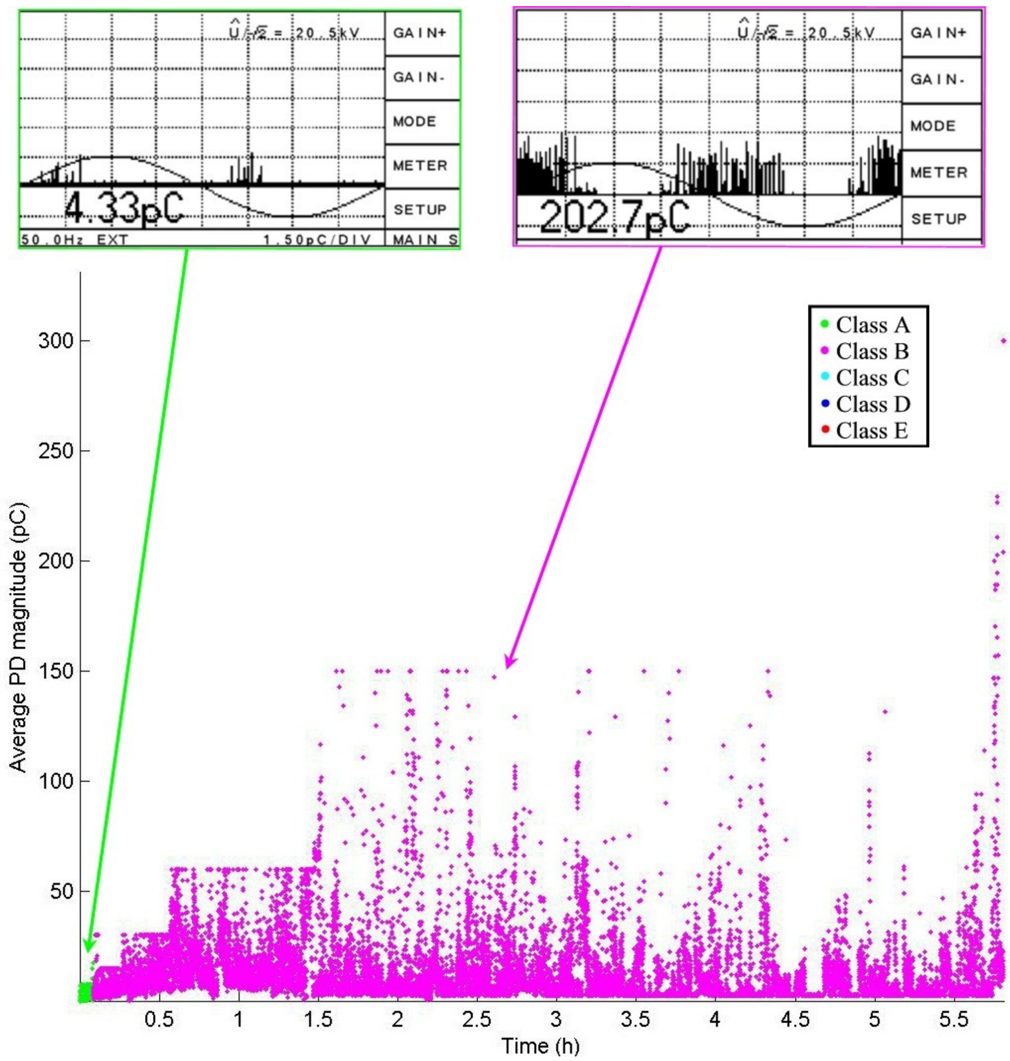

Figure 5.5: AL2-1 PD time evolution plot with PRPDPs.

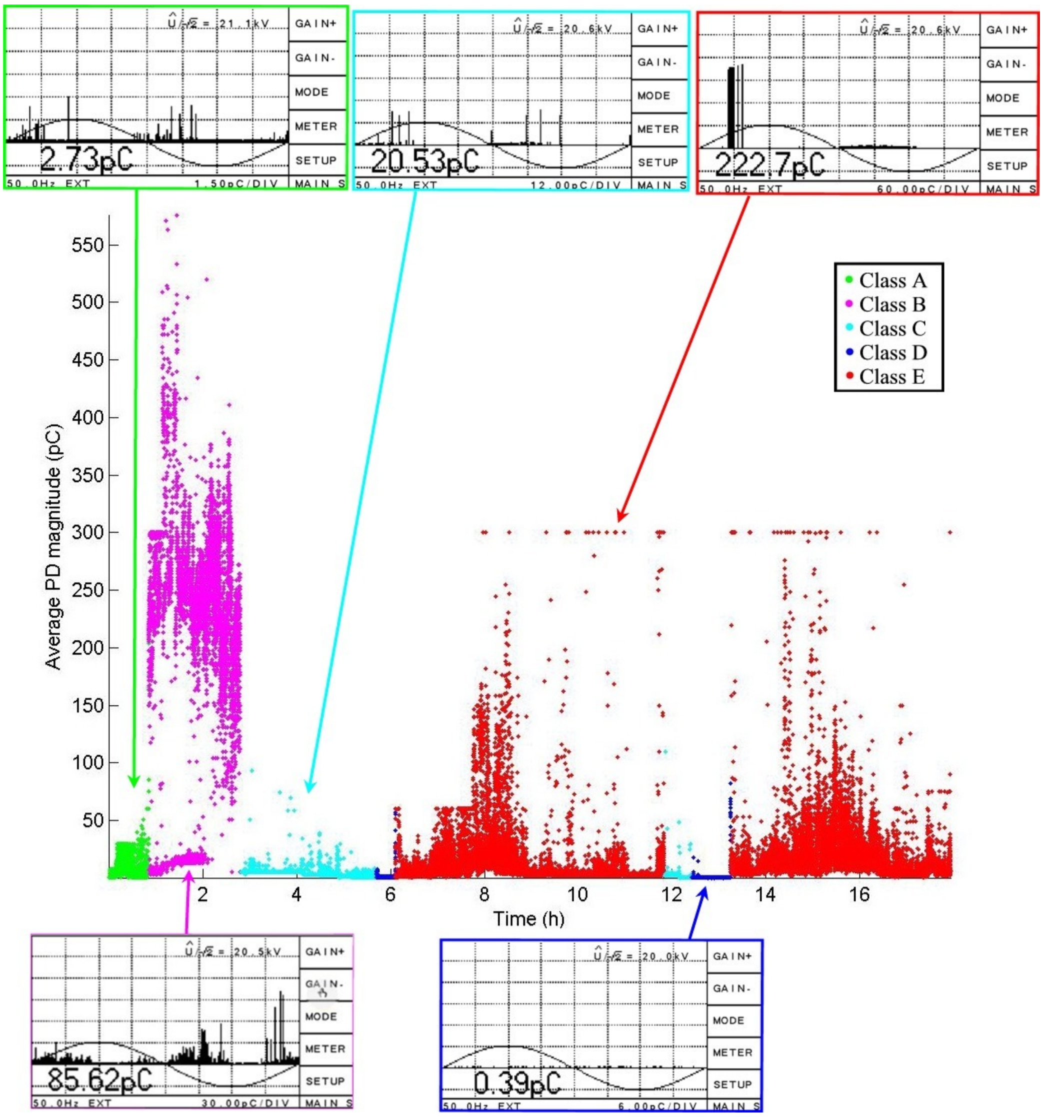

Figure 5.6: AL2-2 PD time evolution plot with PRPDPs.

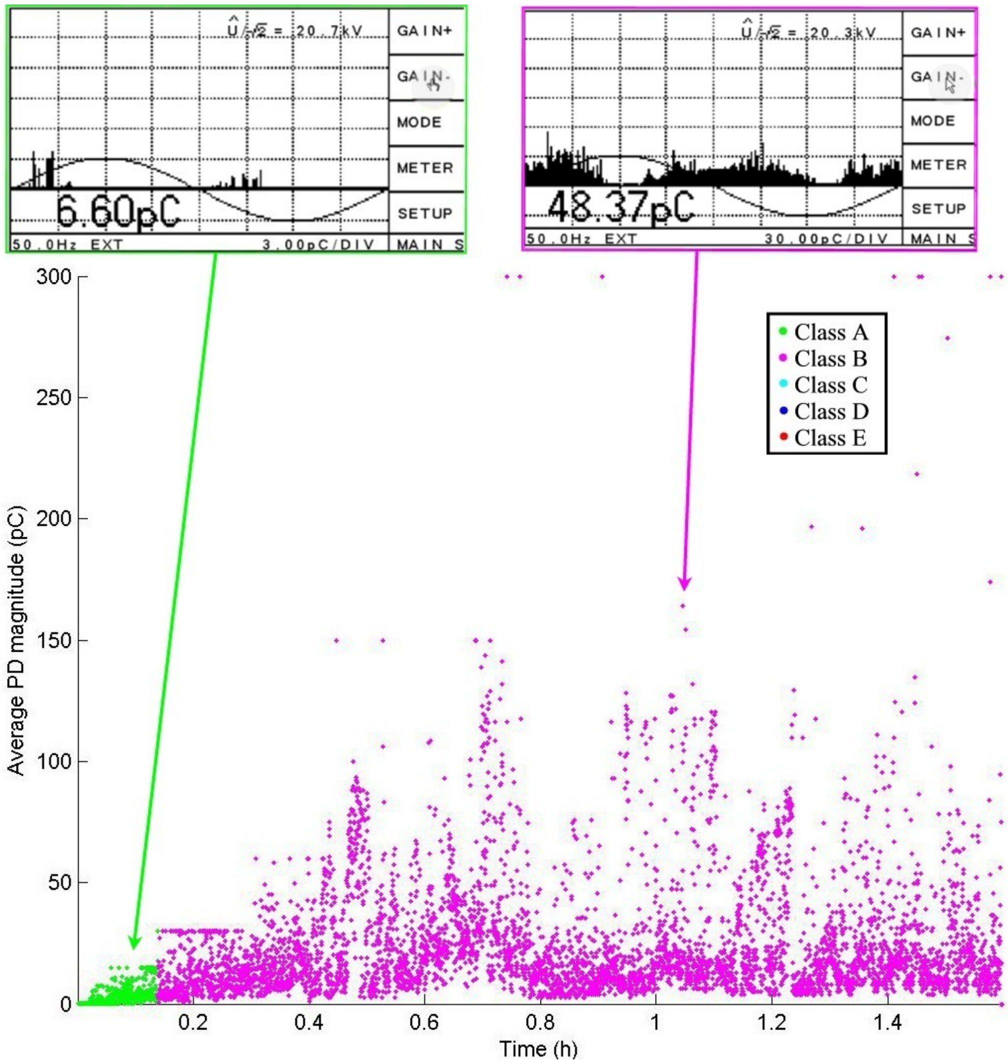

Figure 5.7: AL2-3 PD time evolution plot with PRPDPs.

As shown in Figure 5.6, classes C, D and E occur in more than one cycle before failure of the samples occurs. This may imply that classes C, D and E are not only new classes that may occur once, but may recur in multiple cycles. This cyclical behaviour would correlate to the above mechanisms occurring for each layer of nanoparticles being encountered. This idea is depicted further in Section 6.1.5 in the following chapter, with nanoparticles arrayed in shells extending radially from the inception point. Assuming that the nanoparticles are evenly dispersed throughout the epoxy, each shell would represent the next layer of nanoparticles that would be encountered by the electrical tree. From the proposed mechanisms above, each shell would represent one cycle of classes C, D and E as each layer of nanoparticles is encountered by propagating electrical tree tubules. This is a significant modification of behaviour even for just one sample. These samples were completely classified by the auto-classification system with no corrections being necessary.

The extended pattern shows similar class relationships except for two differences. Class B shows a significant clustering of data points at much higher Q_{p-avg} than seen in clean epoxy samples. Furthermore, the first class C that occurs has a much longer duration than the first class D. Lastly, the extended pattern displays a duration greater than the typical patterns by a minimum factor of 3.5. Again each class' PRPDPs correlate as expected from the class descriptions before.

5.2.3 Al_2O_3 5 %wt

Of the three samples, pictured in Figures 5.8, 5.9 and 5.10, the number of distinctive classes vary from one sample to another but a common feature is the initial classes A and B. Due to the extraordinarily flat behaviour of this pattern, the auto-classification program was not able to classify it correctly, requiring manual correction.

The relationships again remain consistent with respect to the means of Q_{p-avg} for each class. Each class lasts much longer but the relationships between classes C and D are again similar with both C and D being much

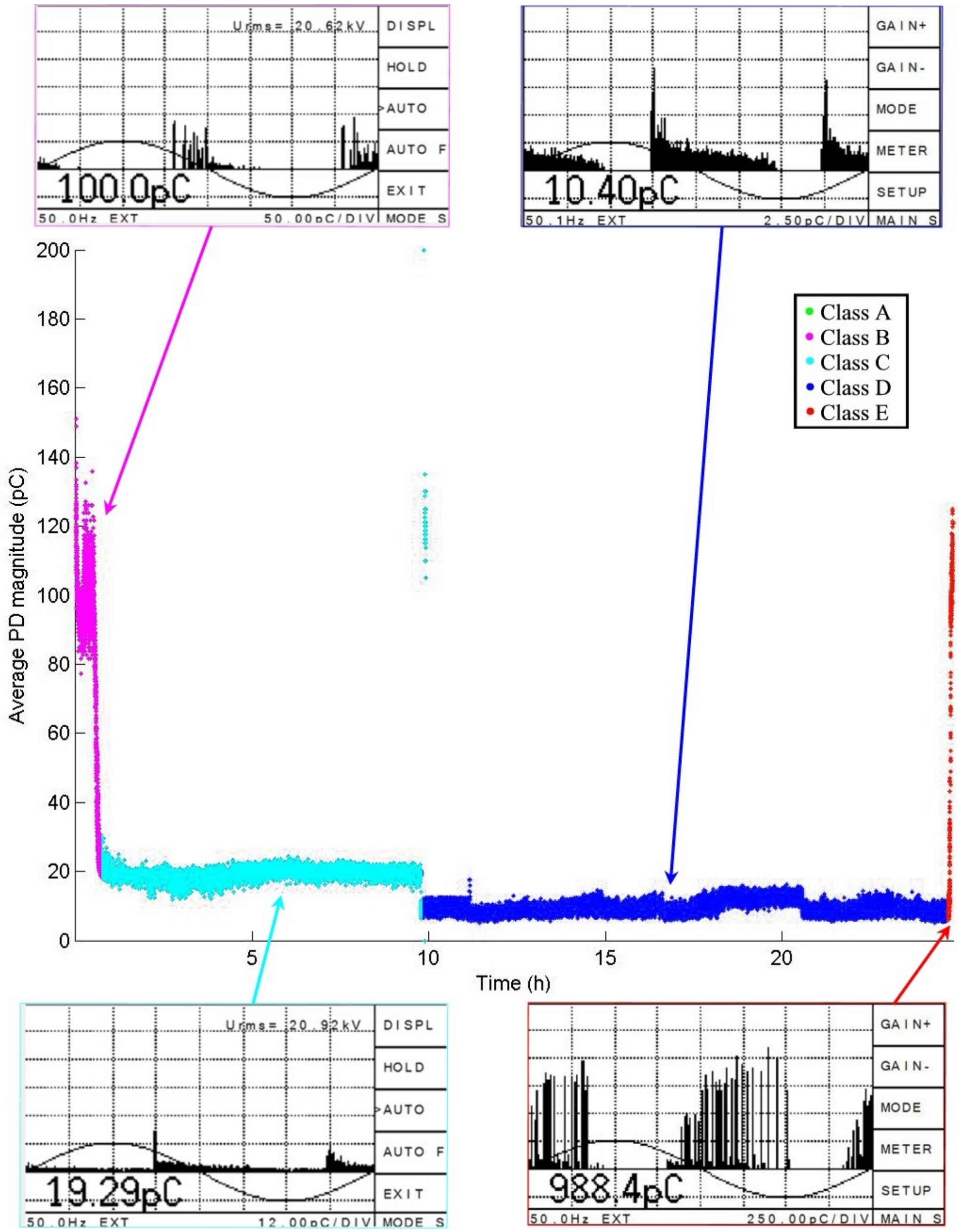

Figure 5.8: AL5-1 PD time evolution plot with PRPDPs

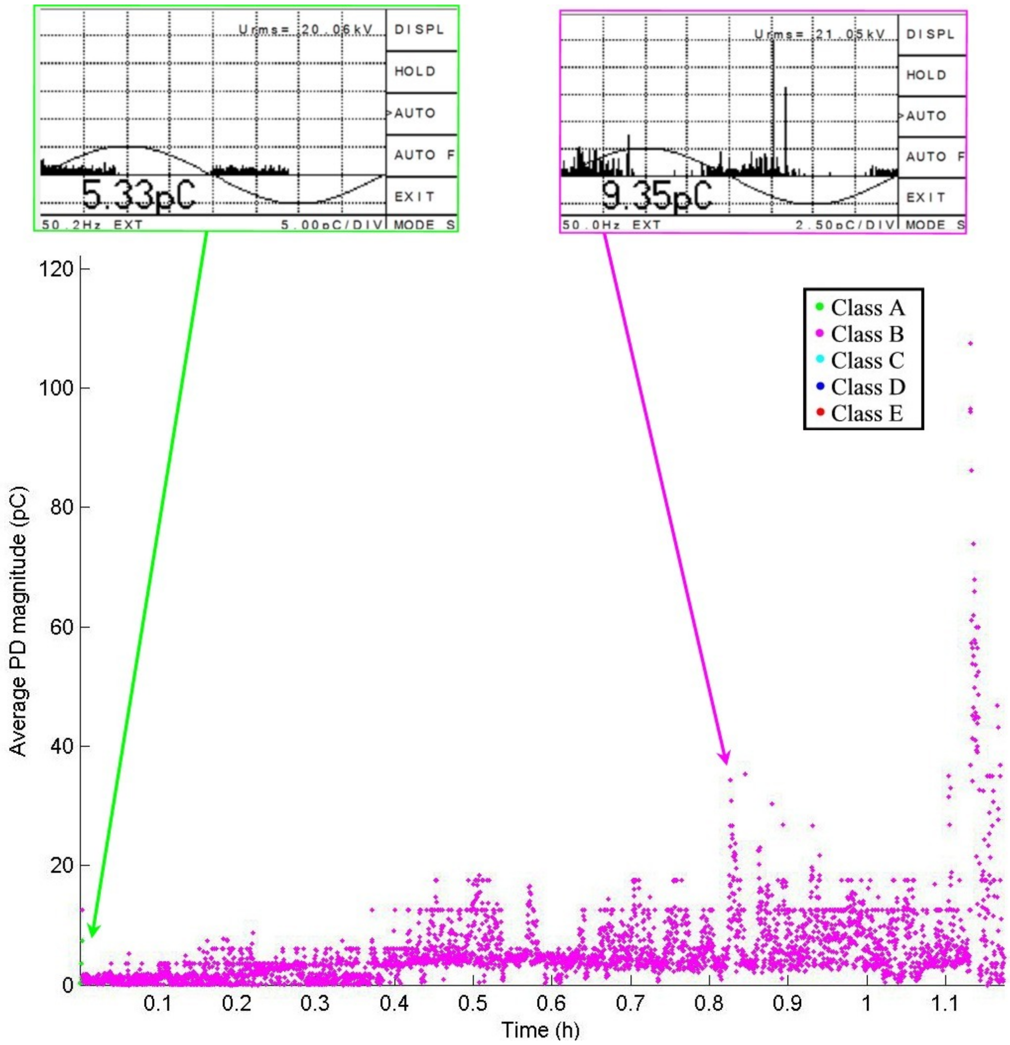

Figure 5.9: AL5-2 PD time evolution plot with PRPDPs

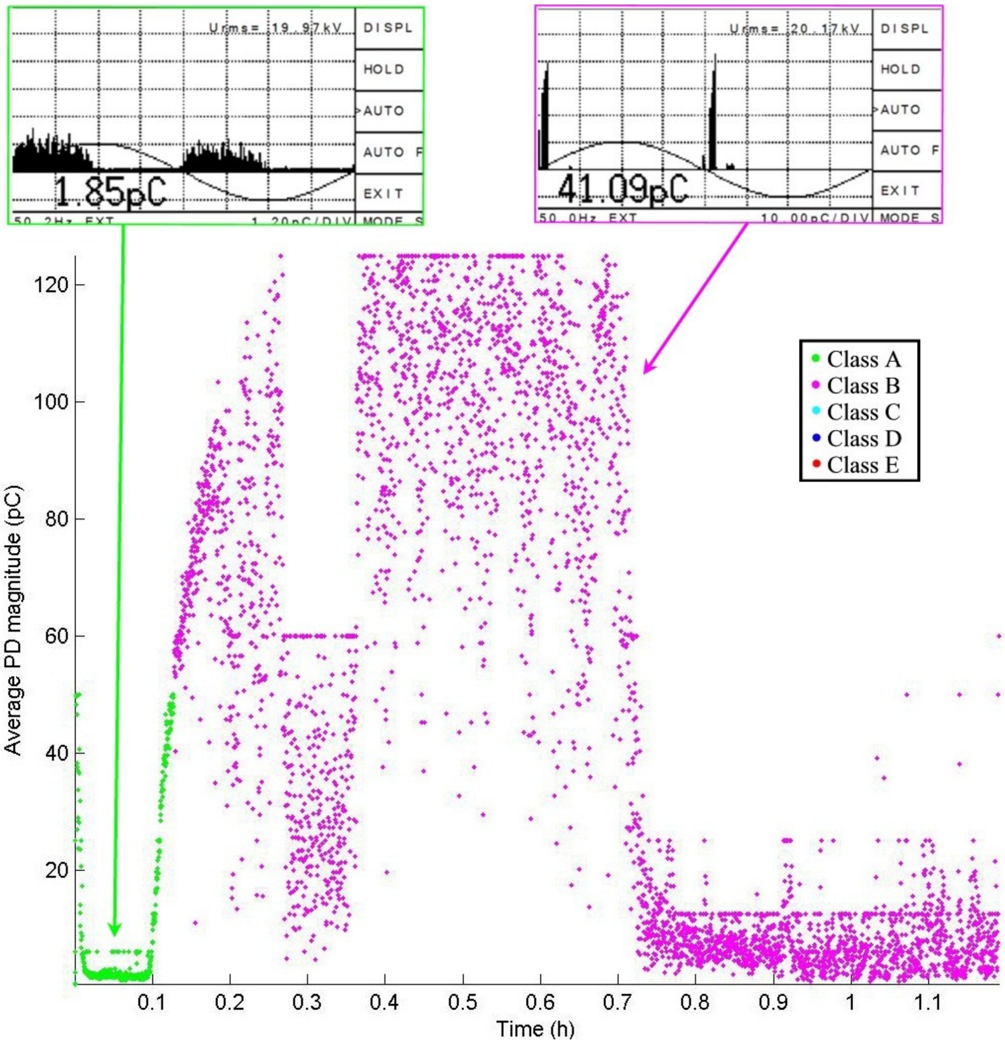

Figure 5.10: AL5-3 PD time evolution plot with PRPDPs

longer than classes B and E. The extended pattern of AL5-1 in Figure 5.8 shows a duration that is greater than the typical patterns by at least a factor of 20. Furthermore, the PRPDPs correlate with each class as expected.

5.2.4 Al_2O_3 Trends

A pattern is clear with most of Al_2O_3 samples in the relationship between the extended and typical patterns. The probability of there being more classes increases along with the loading level. Furthermore, the more distinct classes that occur, the higher the probability that the sample lasts longer. The relative increases in durations slowly increases from an approximate factor of 1 to a factor of 20. This implies the 5 %wt filler loading level would present the best results for extended patterns. The relationship between the durations of each class do not appear to be consistent however, pointing to some form of unpredictability inherent in the mechanisms.

5.3 MgO/Epoxy Samples

5.3.1 MgO 0.5 %wt

Of the three samples, only Figure 5.11, MG0.5-1, displays behaviour similar to clean epoxy patterns. The other two both show the same patterns as detected in the Al_2O_3 samples with classes A and B occurring with the addendum of a cycle of classes C, D and E. All of these PD time evolution plots were generated by the auto-classification with no modification by the author necessary.

The multiple class plots in Figures 5.12 and 5.13 again show the Q_{p-avg} relationships with clustering of class B data points at larger magnitudes and class C and class D showing the marked decreases. Class E again shows the corona-like PRPDPs with a mean on par with class B. Durations again remain similar but the class C and D segment is significantly longer than the class B. Given the previous class definitions and results, each class displays PRPDPs as expected. Figure 5.12 displays a duration 5 times longer than the unmodified pattern whilst Figure 5.13 modified pattern has a duration half the time of the unmodified plot.

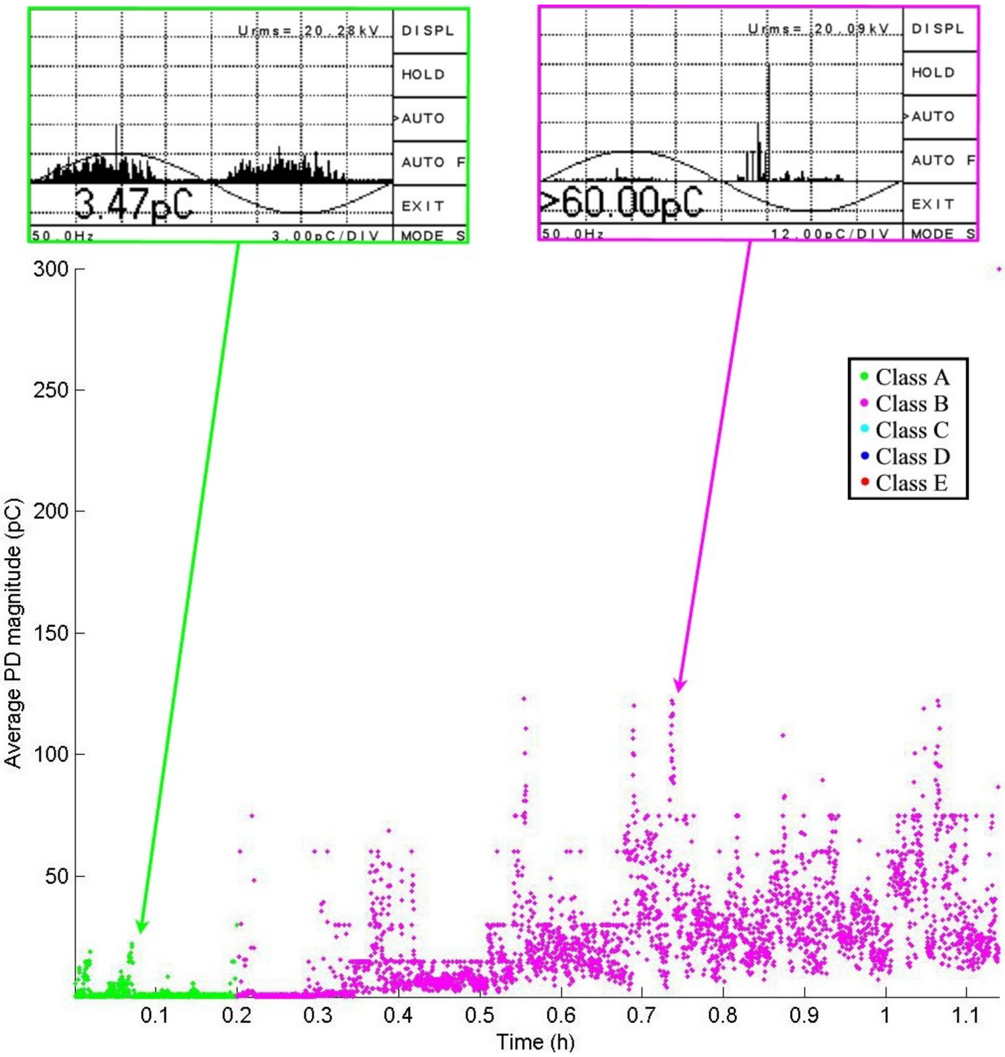

Figure 5.11: MG0.5-1 PD time evolution plot with PRPDPs.

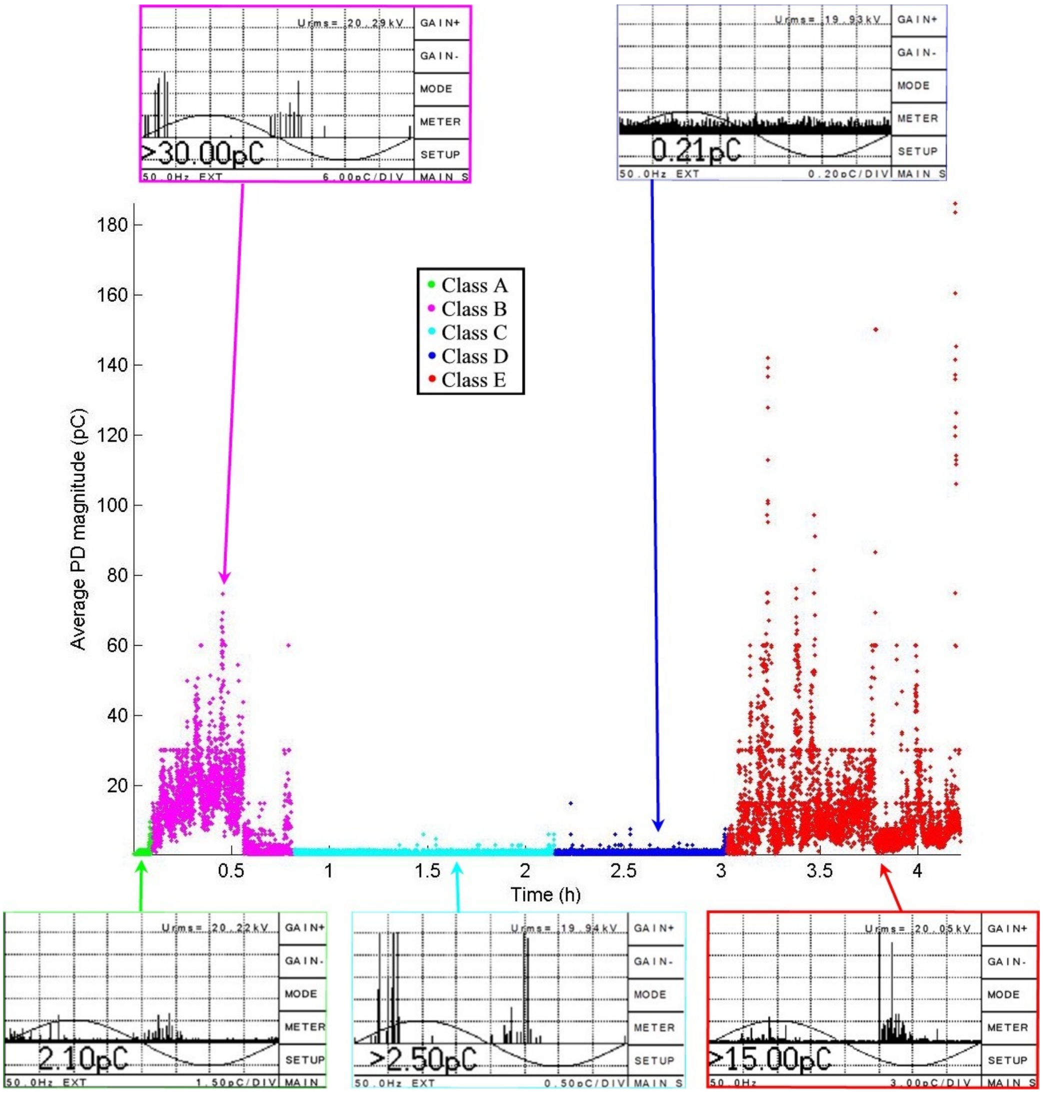

Figure 5.12: MG0.5-2 PD time evolution plot with PRPDPs.

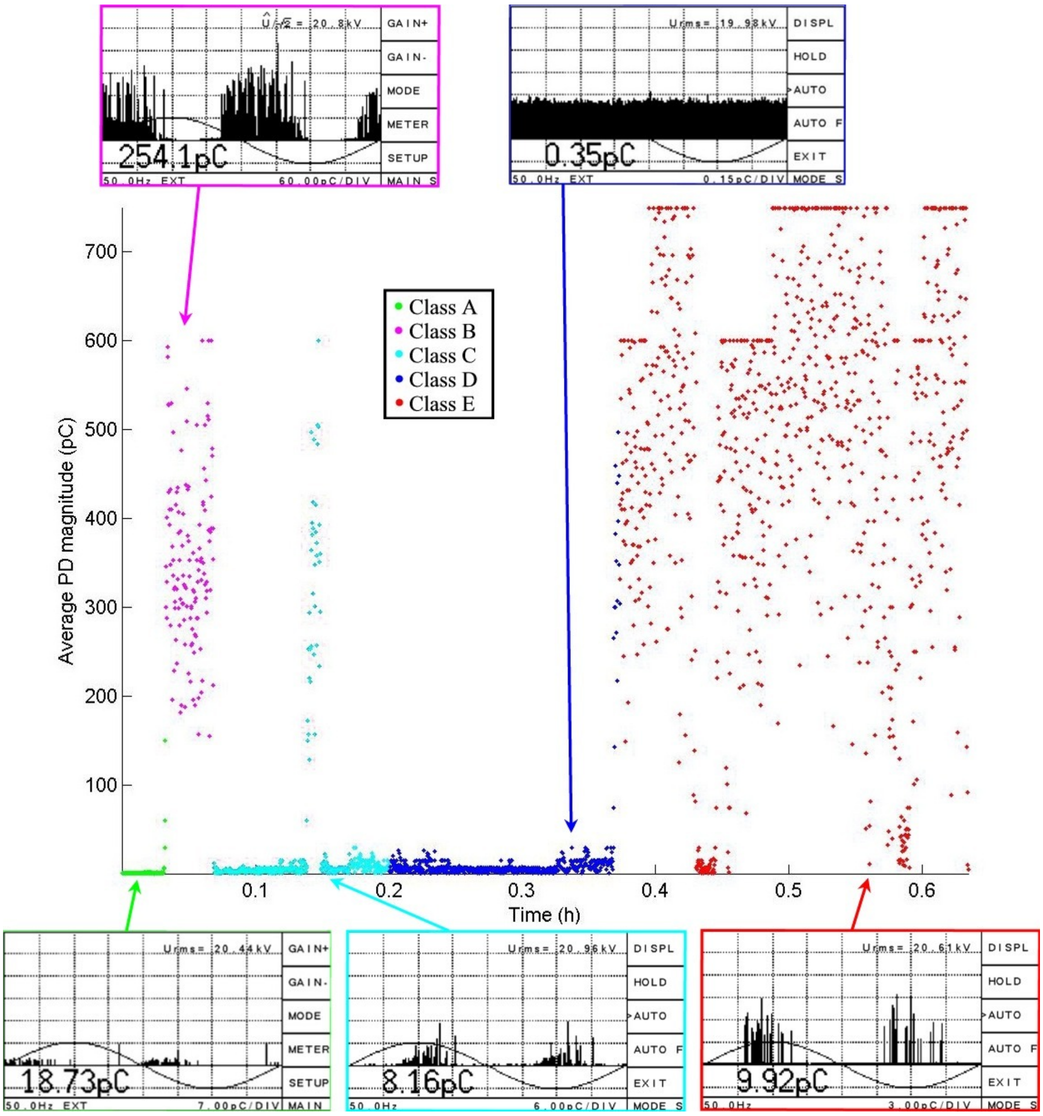

Figure 5.13: MG0.5-3 PD time evolution plot with PRPDPs.

5.3.2 MgO 2 %wt

Of the 2 %wt MgO samples' PD time evolution plots, only Figure 5.16 shows multiple classes. This has more than one cycle of class C, D and E with a duration at least 2 times longer than the patterns in Figures 5.14 and 5.15. The time relations for this plot are completely different compared with the Al_2O_3 samples. Furthermore these relationships are not consistent even within the plot. It should be noted that the one pattern, MG2-1 in Figure 5.14, shows clustering of the class B data points around higher magnitudes. The plot that displays the additional classes, Figure 5.16, required manual correction, but the other two were classified correctly by the auto-classification program.

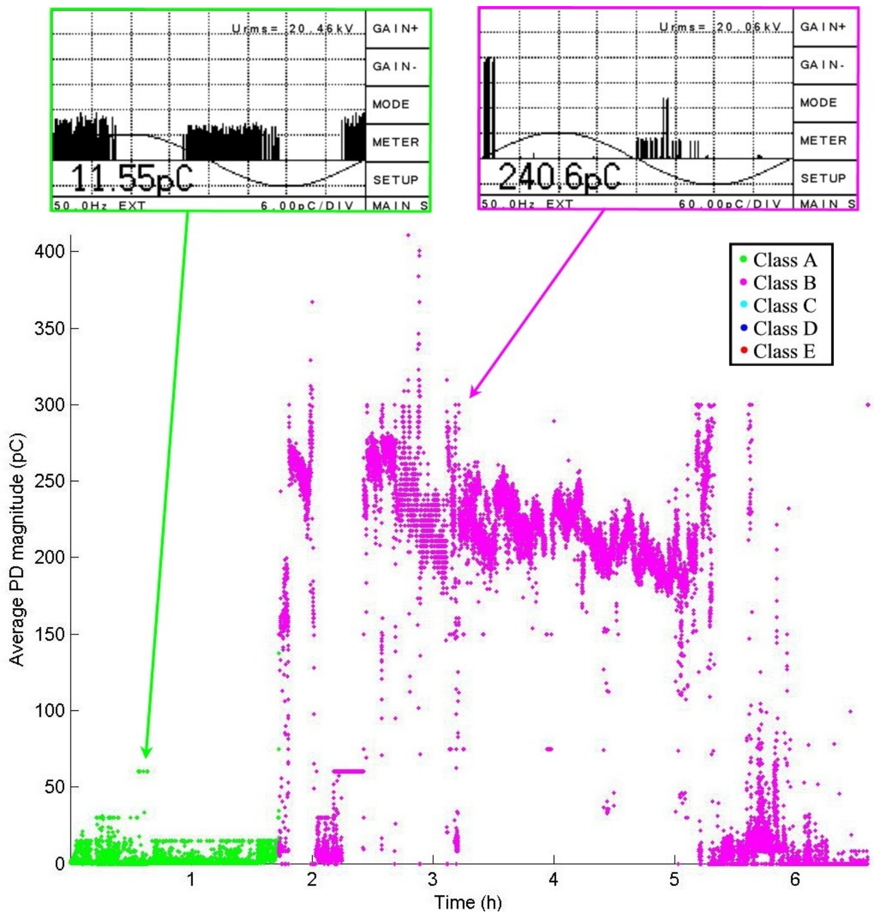

Figure 5.14: MG2-1 PD time evolution plot with PRPDPs.

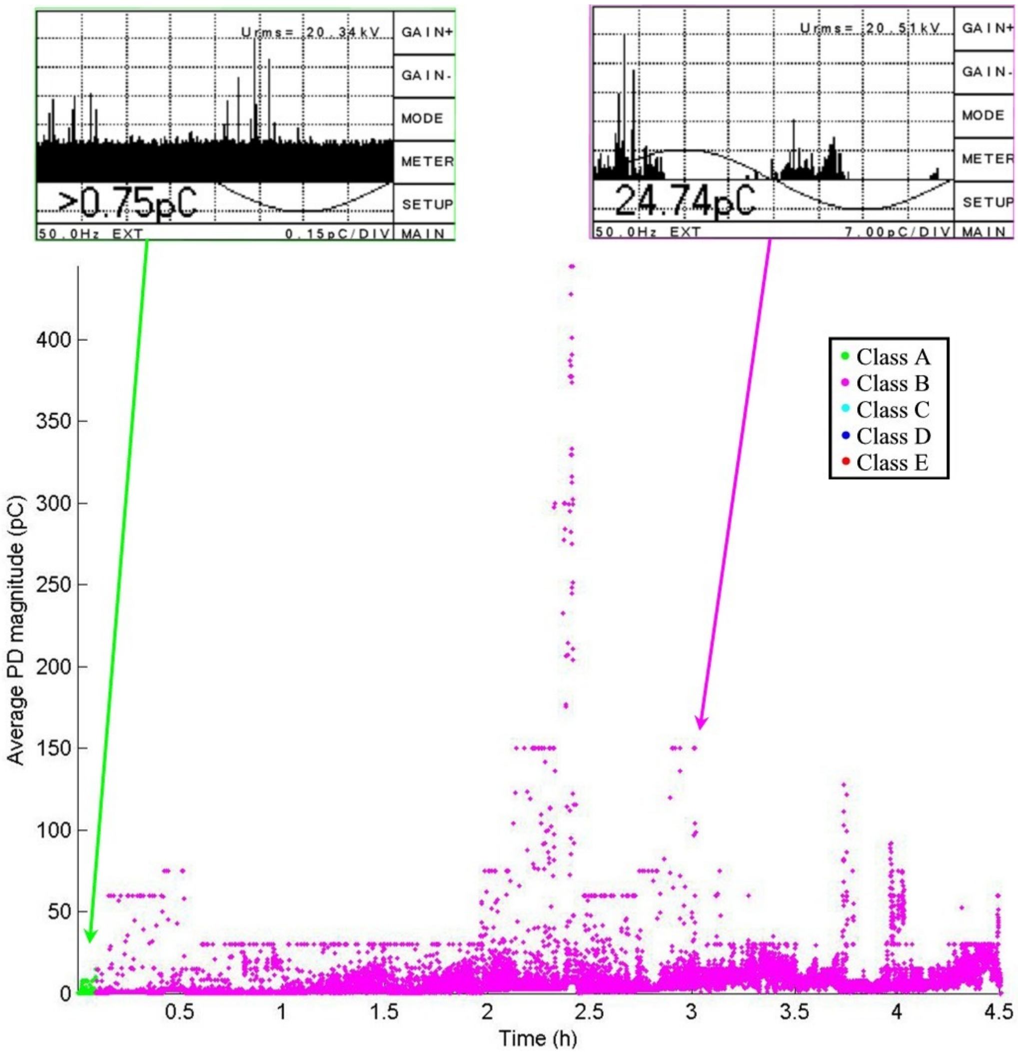

Figure 5.15: MG2-2 PD time evolution plot with PRPDPs.

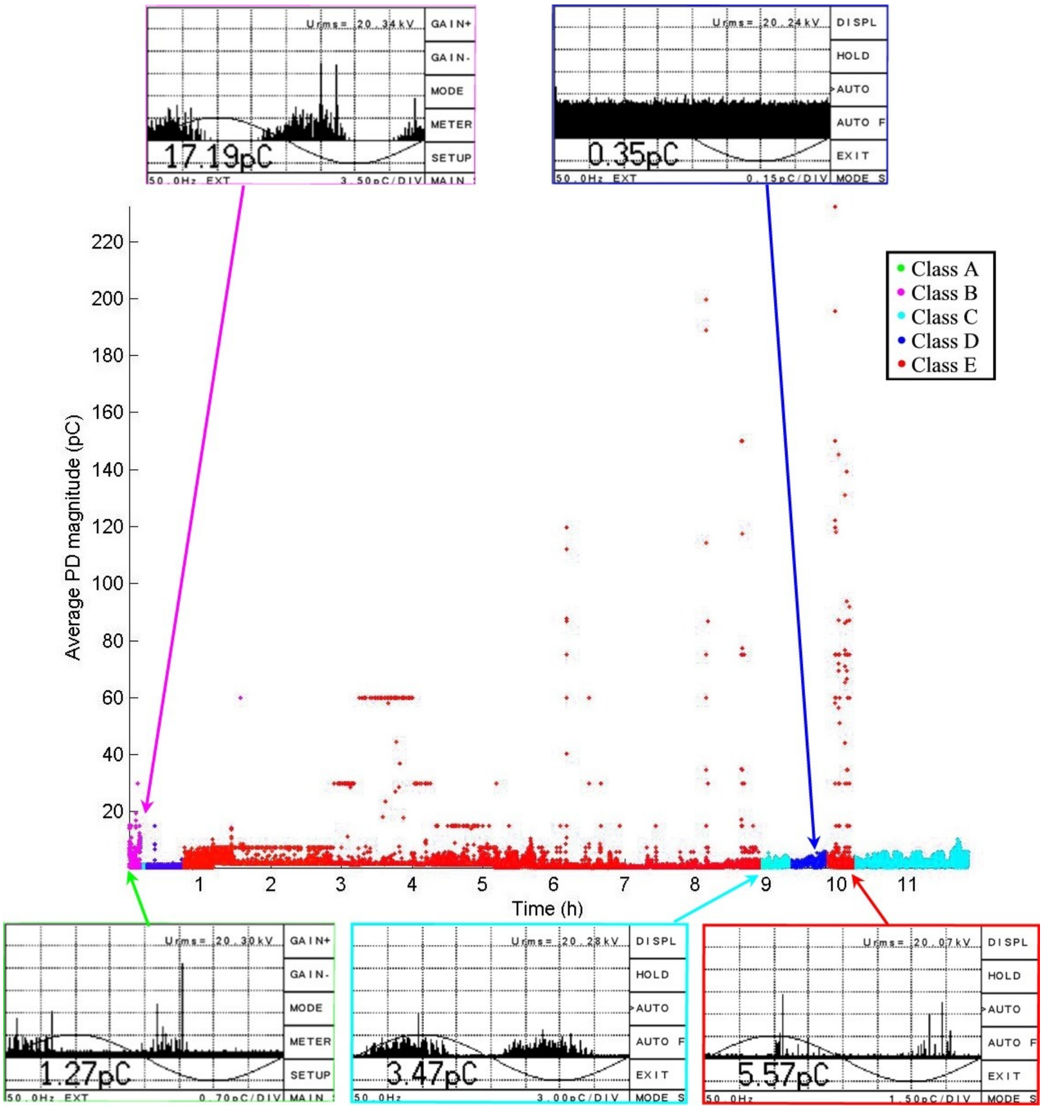

Figure 5.16: MG2-3 PD time evolution plot with PRPDPs.

5.3.3 MgO 5 %wt

All three MgO 5 %wt samples in Figures 5.17 to 5.19 display extended patterns but unfortunately the auto-classification program was not able to classify any of them without errors. This is most likely due to the large amount of PD magnitude spikes instead of groups of different clustering patterns. This displays a need to refine the pattern recognition capabilities of the auto-classification program. The PRPDPs however still remain consistent to each class. These samples show extreme increases in duration with one sample, Figure 5.18, lasting well over 10 days. These extreme durations highly compress the PD time evolution plots, causing difficulty in visually validation of the relationships seen in previous samples.

5.3.4 MgO Trends

MgO shows a marked improvement with each increase in filler loading level as well as increased consistency. The durations again increase with filler loading level with 5 %wt showing the most marked improvement. MgO tends to show impulse like behaviour in contrast to the broad clustering shown by the Al_2O_3 samples. This may be a factor influenced by the compression of the signals but even the samples that are not highly compressed show this impulse like behaviour.

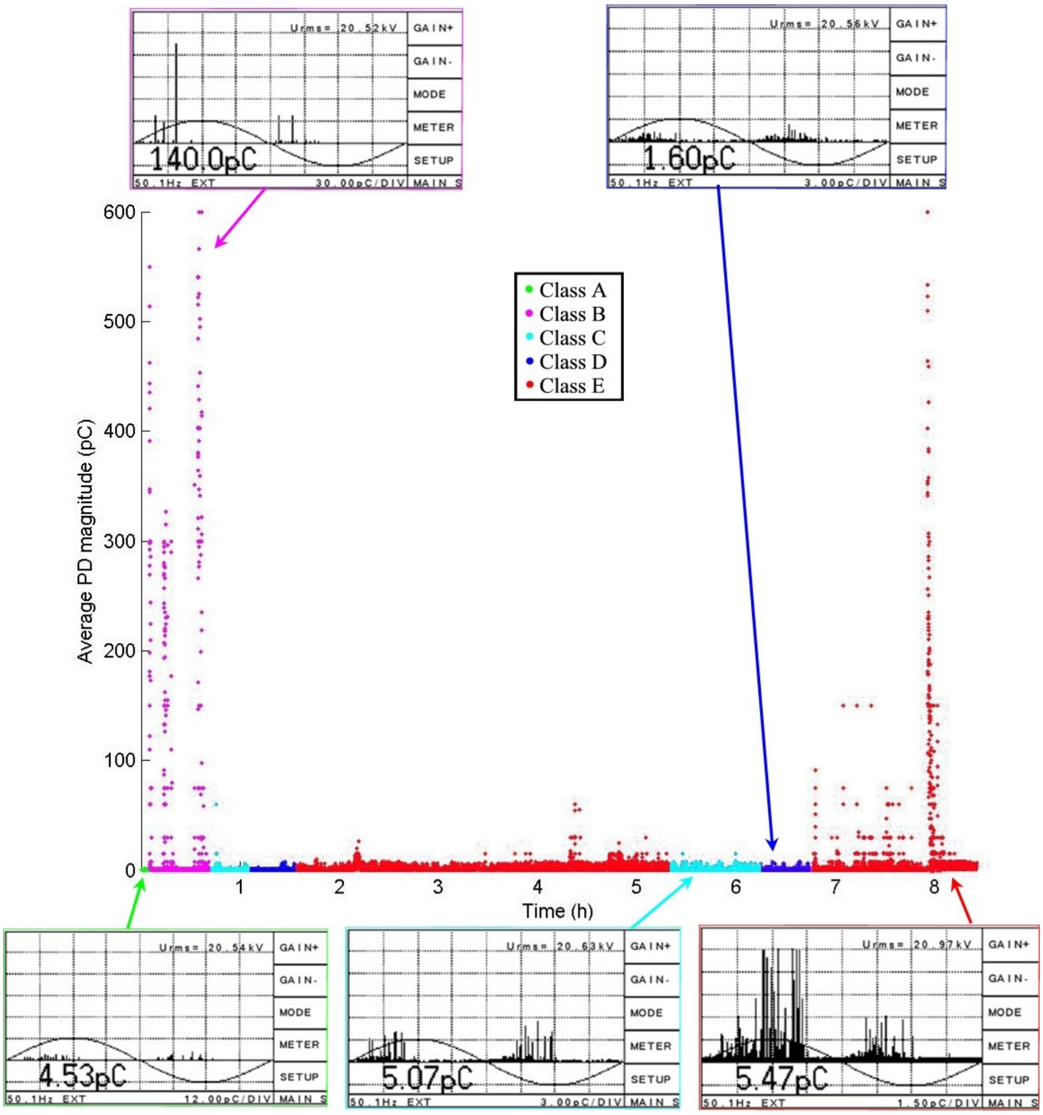

Figure 5.17: MG5-1 PD time evolution plot with PRPDPs.

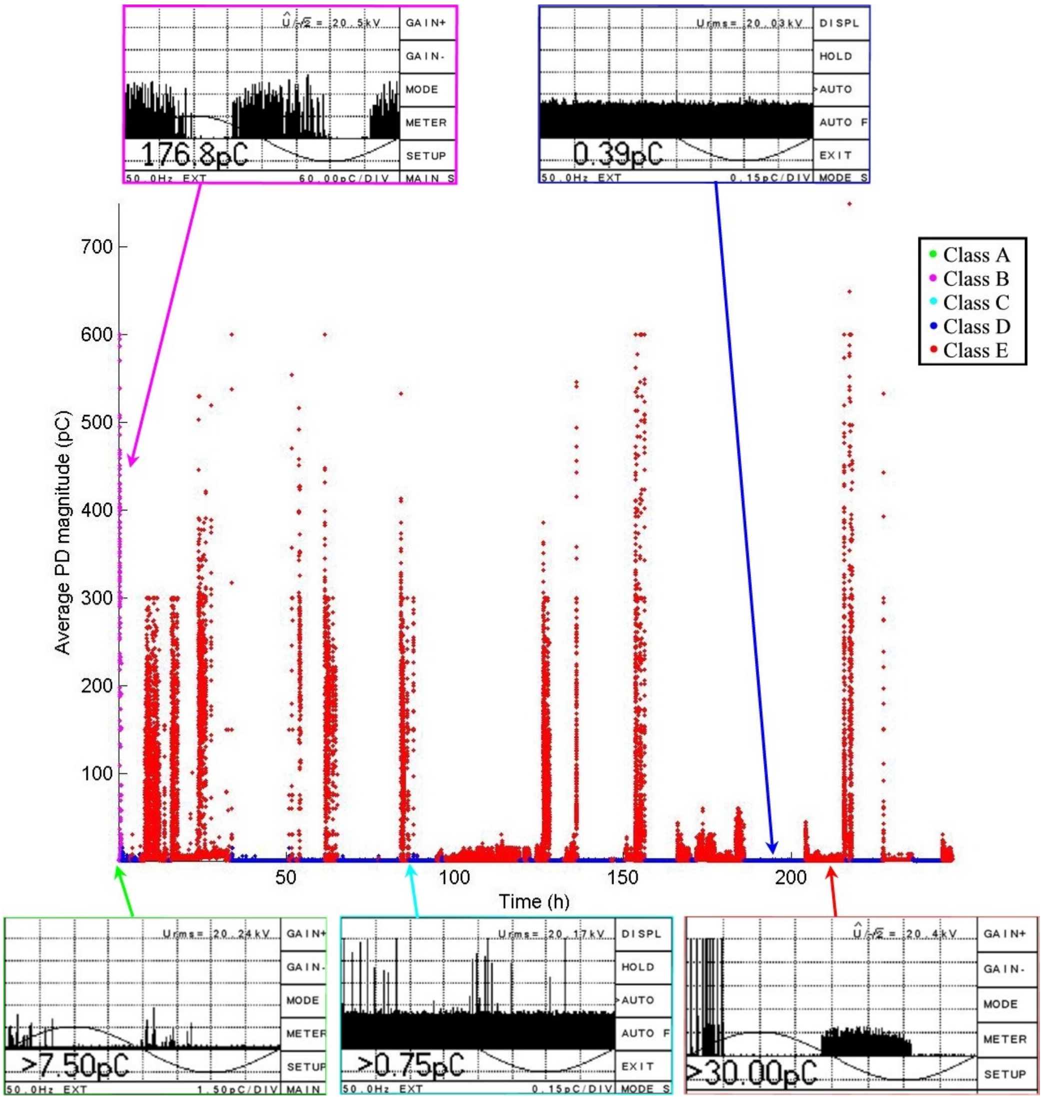

Figure 5.18: MG5-2 PD time evolution plot with PRPDPs.

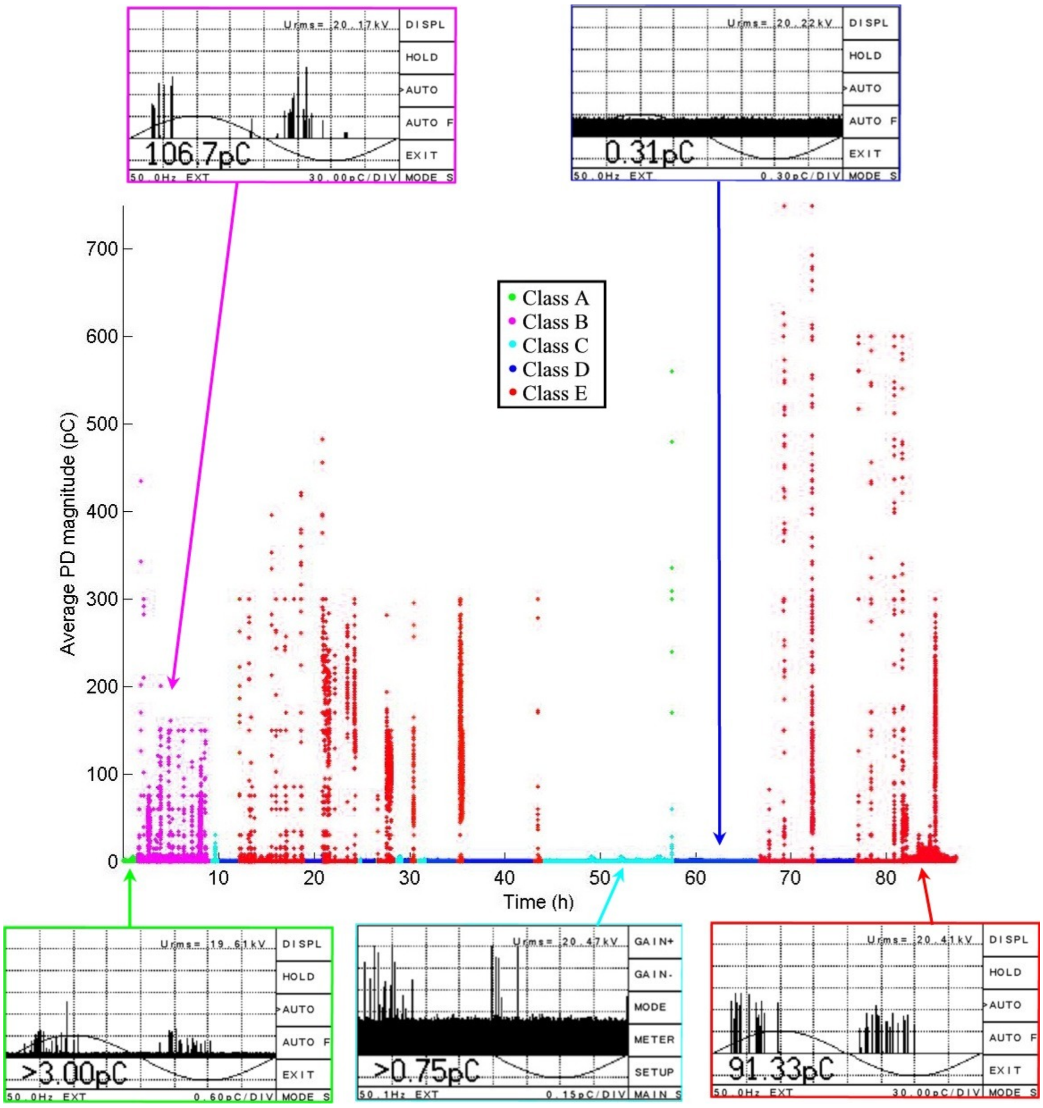

Figure 5.19: MG5-3 PD time evolution plot with PRPDPs.

5.4 Si_2O/Epoxy Samples

5.4.1 Si_2O 0.5 %wt

The 0.5 %wt Si_2O samples all display two PD class patterns similar to clean epoxy, as shown in Figures 5.20, 5.21 and 5.22. There is however, an oddity in SI0.5-3 (Figure 5.22) which shows an extended period of inactivity in the beginning that has been classified as Class A due to the auto-classification program's methodology. This is similar behaviour to what was seen in AL0.5-2, but SI0.5-3 shows standard behaviour after this period of inactivity. This may be due to the needle tip being in close proximity to a nanoparticle and its interface region. This would interfere with the bush tree formation and prevent any significant PDs occurring before a tree could form.

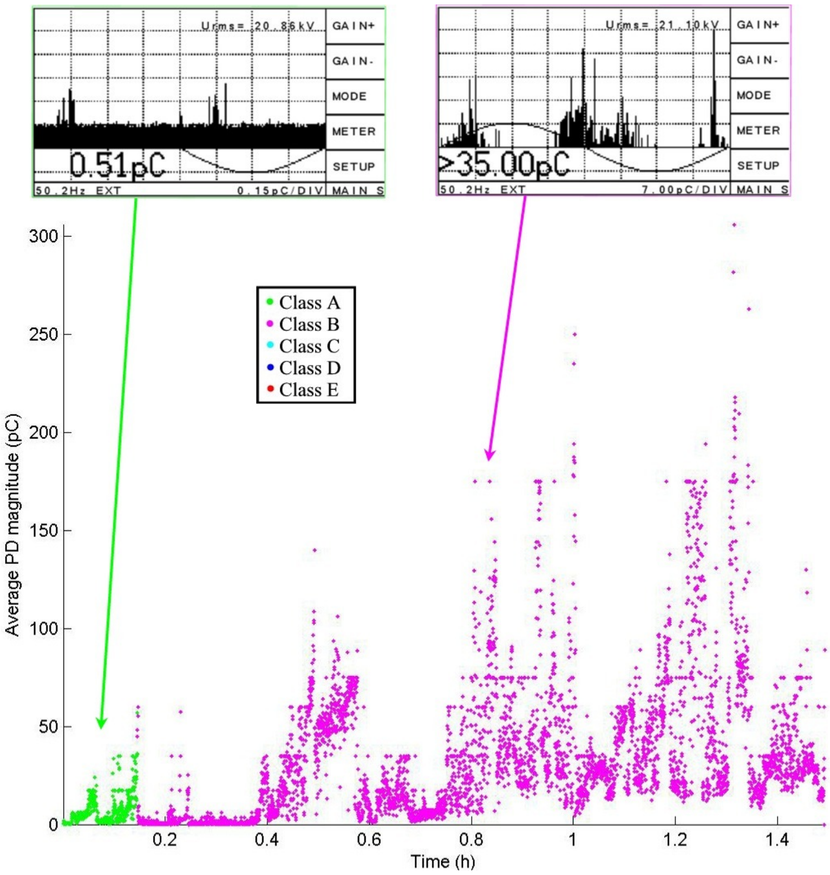

Figure 5.20: SI0.5-1 PD time evolution plot with PRPDPs.

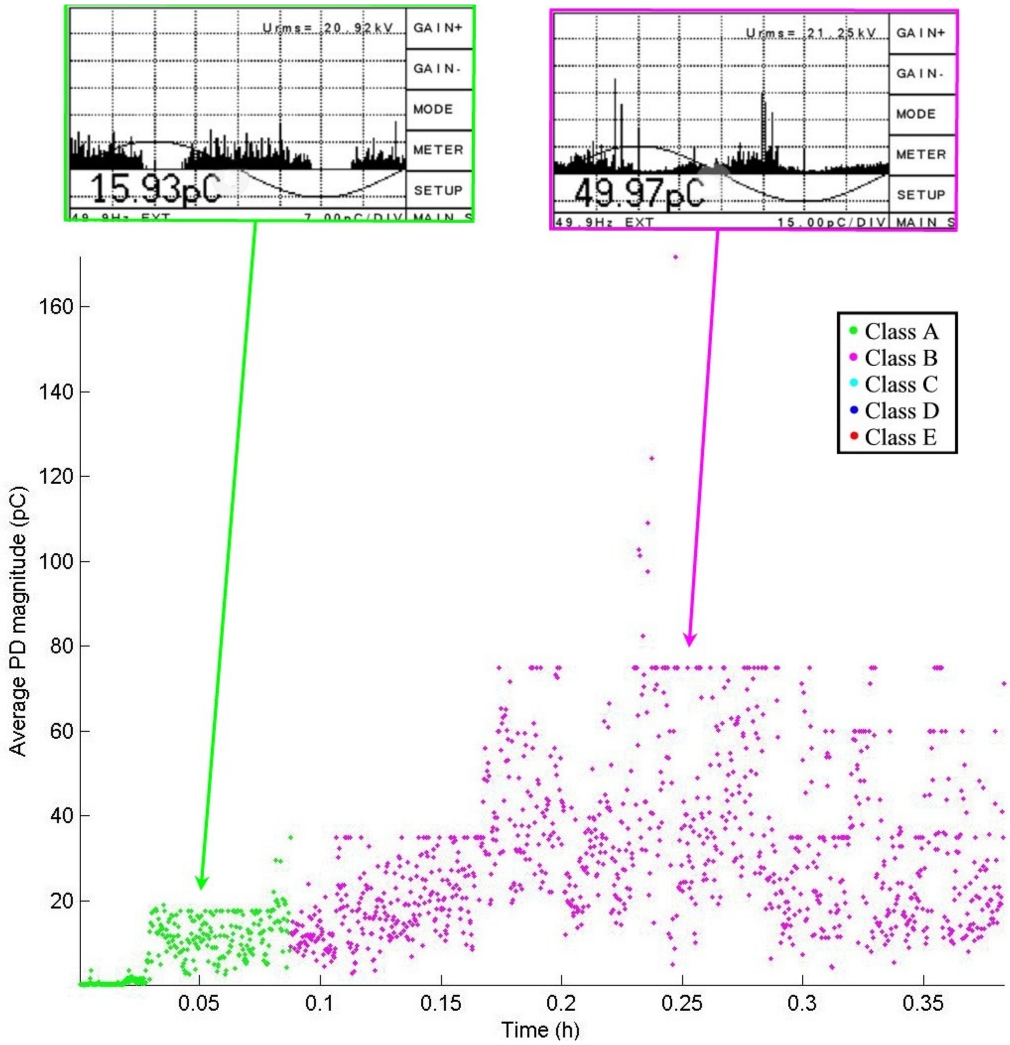

Figure 5.21: SI0.5-2 PD time evolution plot with PRPDPs.

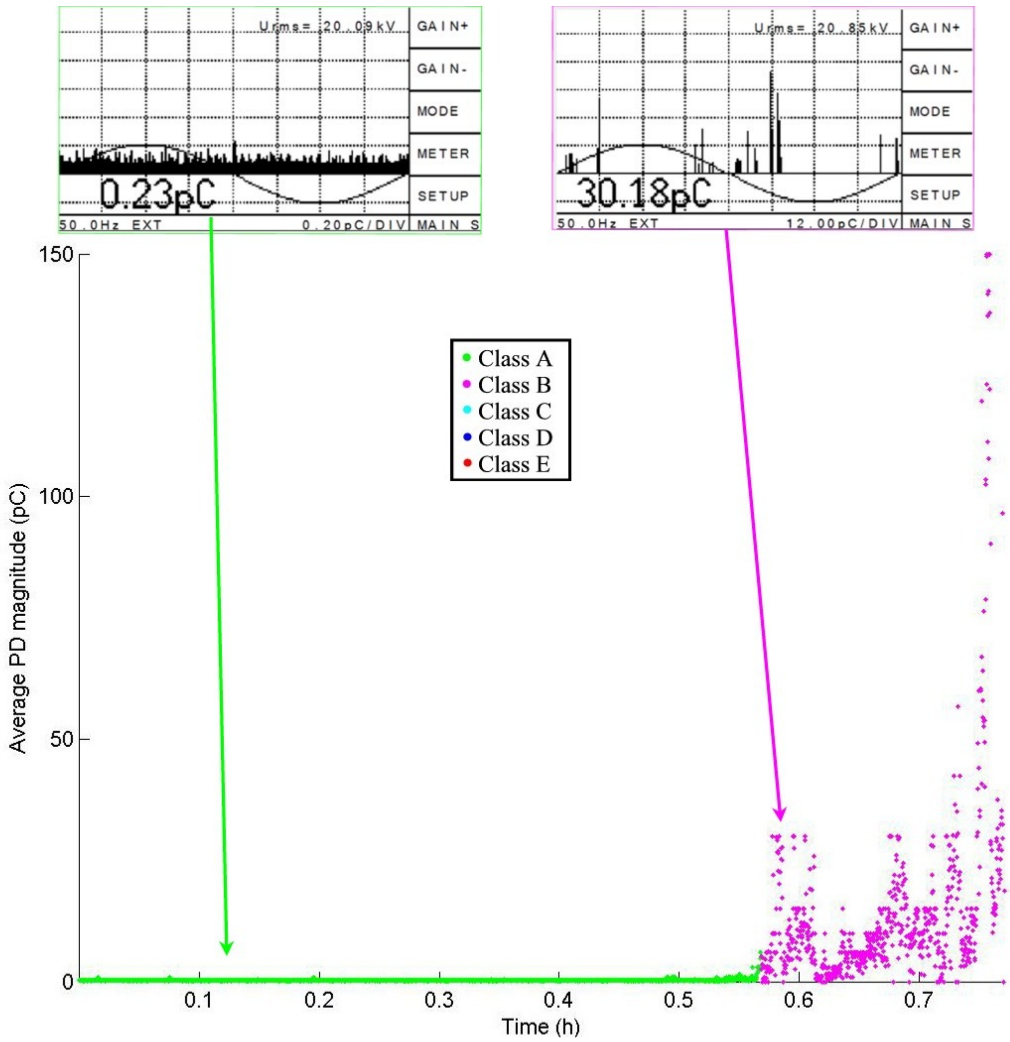

Figure 5.22: SI0.5-3 PD time evolution plot with PRPDPs.

5.4.2 Si_2O 2 %wt

For the 2 %wt Si_2O samples, Figures 5.23, 5.24 and 5.25, two display class A and B patterns with one sample displaying the additional classes that are typical for samples containing nanoparticles. Before discussing the extended pattern, the two samples appear to be displaying the exact same data. This is most likely due to some error in the experiment or recording process and implies one of these samples data must therefore be discarded. The one sample that displayed the extra classes, SI2-1 in Figure 5.25, however runs through two cycles of classes C, D and E before failure occurs after the standard class A and B events. Some correction of this sample signal was necessary due to a spurious split of the first class D and incorrect classification of the A and B classes as an E region. The relationships between the classes seem to be following similar patterns that the previous samples have shown, although class B shows significant clustering of the data points at very low Q_{p-avg}. One important aspect is the increase of time to failure by a factor of approximately 10.

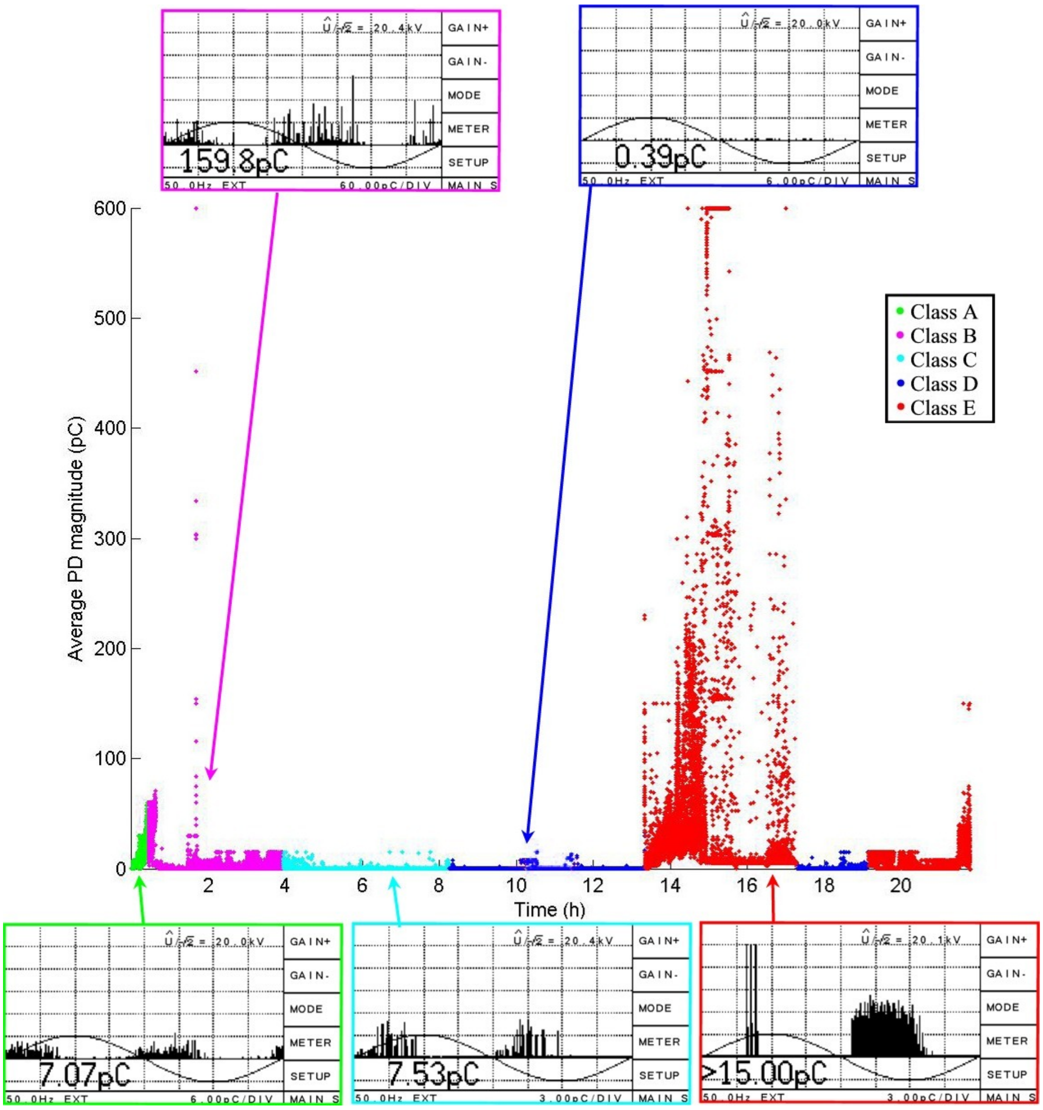

Figure 5.23: SI2-1 PD time evolution plot with PRPDPs.

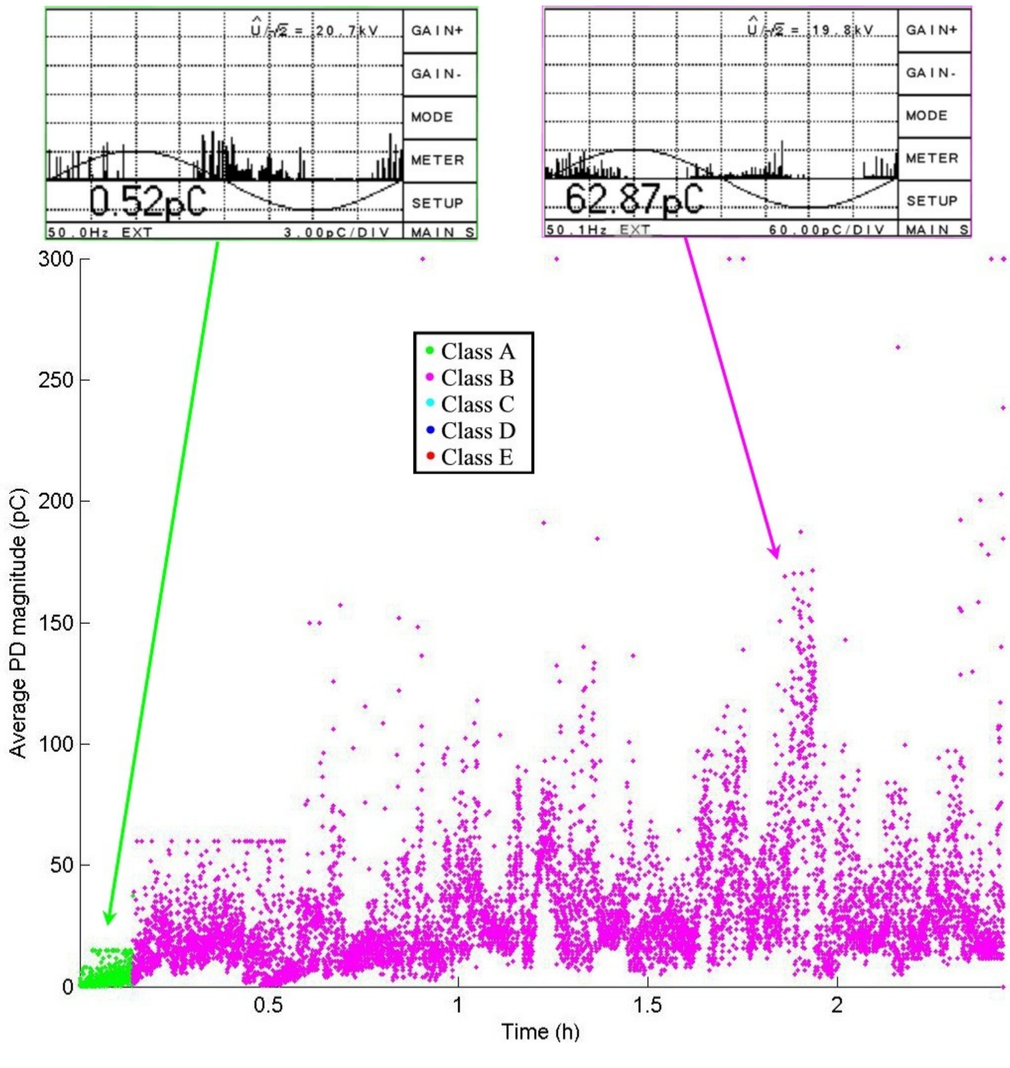

Figure 5.24: SI2-2 PD time evolution plot with PRPDPs.

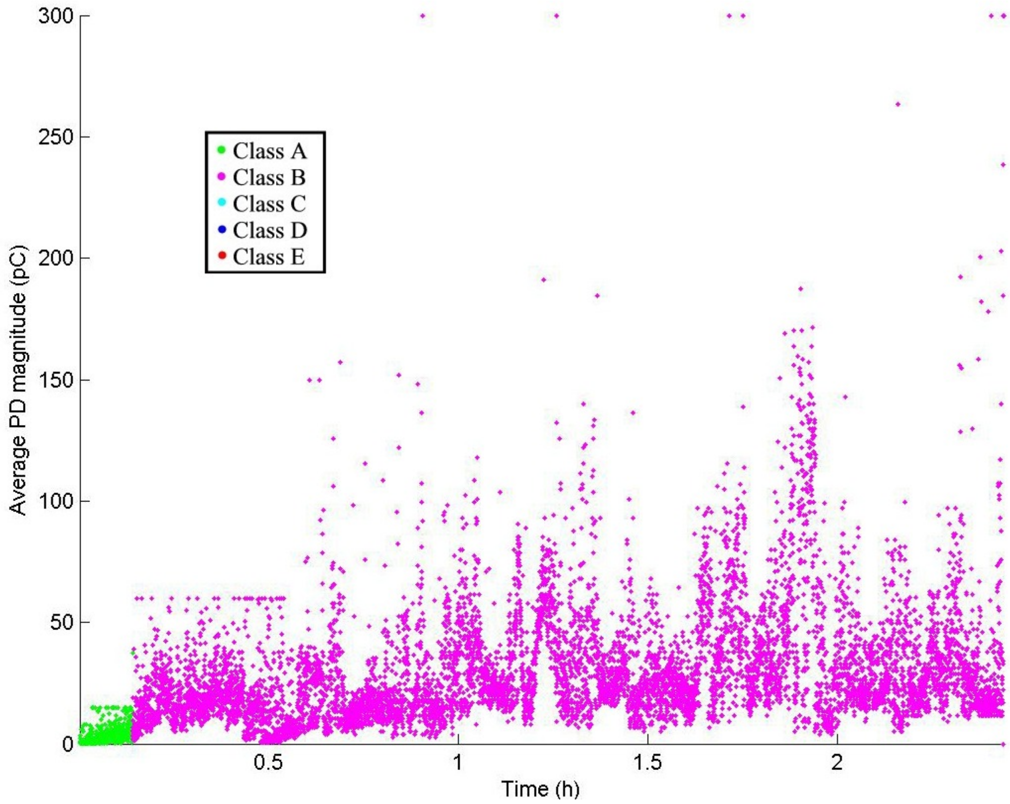

Figure 5.25: SI2-3 PD time evolution plot with PRPDPs.

5.4.3 Si_2O 5 %wt

This last group of samples has two samples with only two PD classes, Figures 5.27 and 5.28, but SI5-1 displays the characteristic additional classes as shown in Figure 5.26. SI5-1 required slight manual corrections such as reclassification of the last segment to E from an A and B segment. This was most likely incorrectly classified due to the length of this segment skewing the statistical measures used in the auto-classification program. The duration of these classes are again radically different from the others. The relationships between classes in terms of their means however do show similarity to the previous relationships. Furthermore, sample SI5-3 displays a similar pattern as SI0.5-3, with a relatively long period of minimal activity occurring before any appreciable PD activity is detected.

5.4.4 Si_2O Trends

Si_2O shows very similar trends as the Al_2O_3 and MgO filler materials but appears to have better suppression capabilities. By suppression, reference is made to the reduction of Q_{p-avg} detected for each sample. This is apparent in the samples where the quiet PD classes, C and D, appear to last for significant periods of time. Lastly, the improvement with filler loading level does not seem to show preference towards a specific filler loading level in terms of consistency. The time-to-failure does however still increase proportionally with filler loading level.

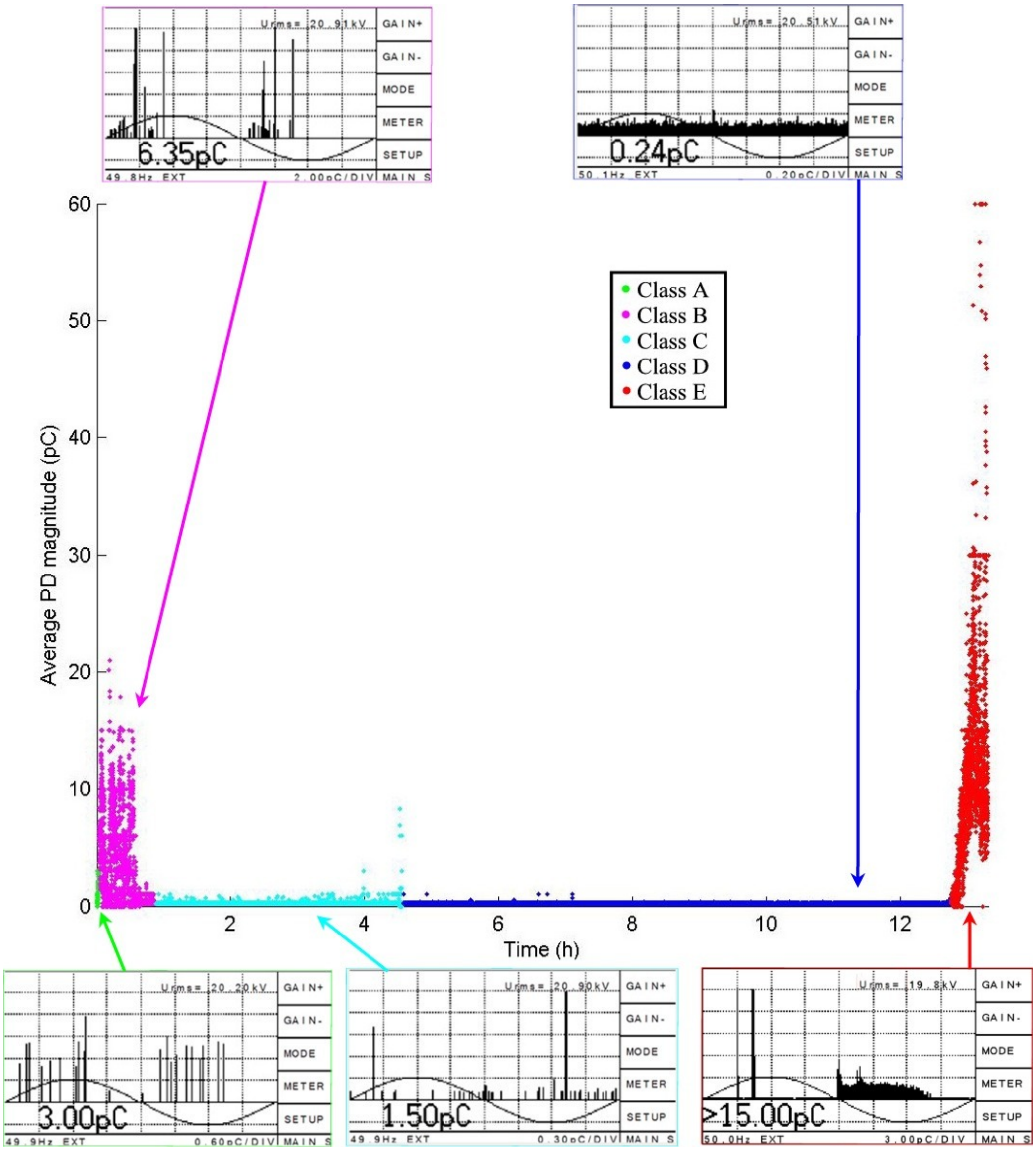

Figure 5.26: SI5-1 PD time evolution plot with PRPDPs.

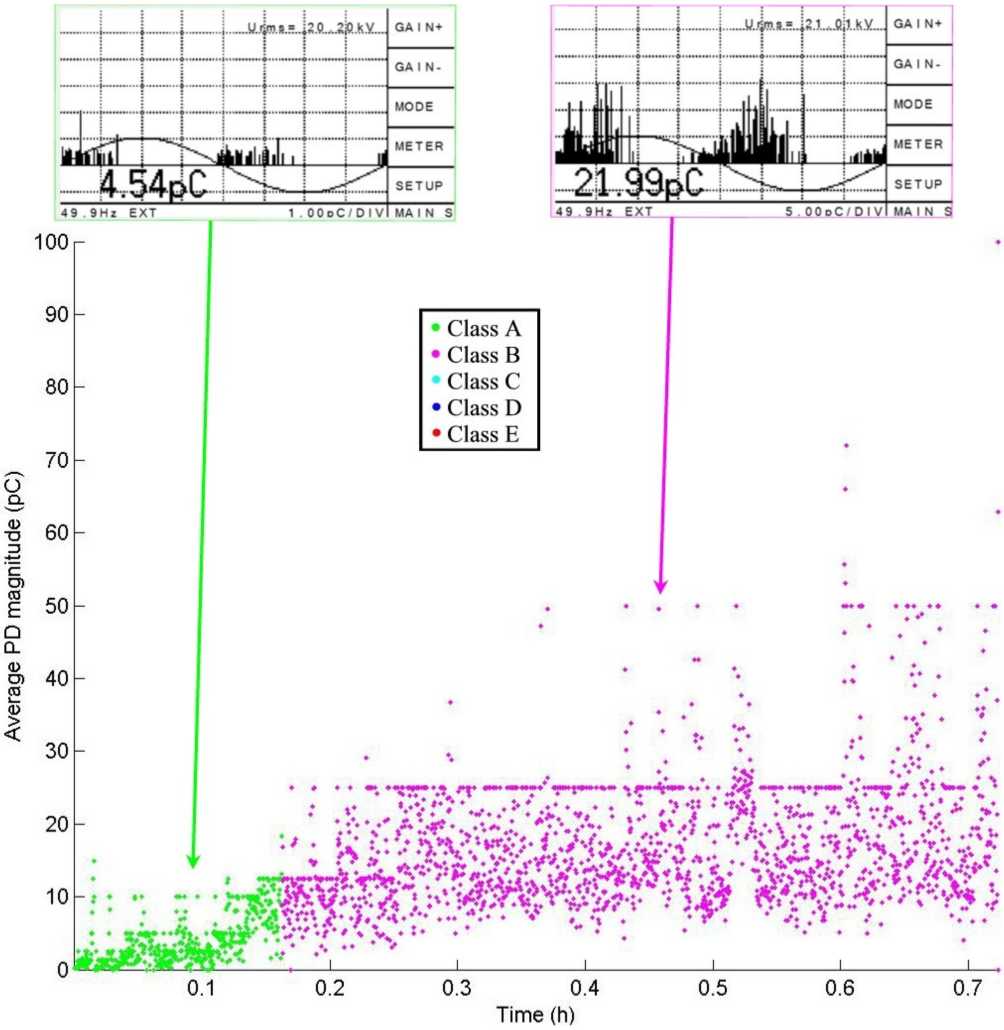

Figure 5.27: SI5-2 PD time evolution plot with PRPDPs.

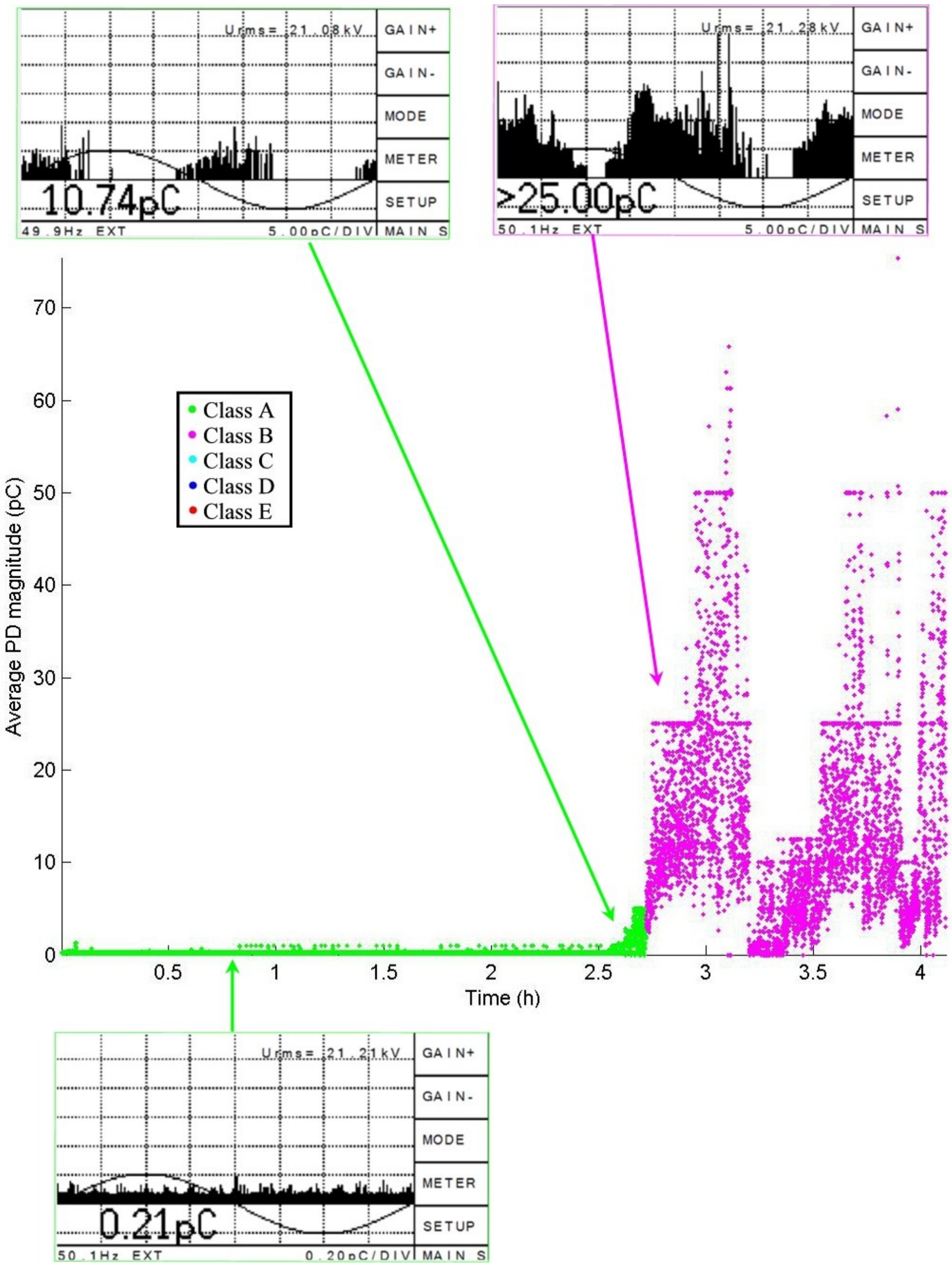

Figure 5.28: SI5-3 PD time evolution plot with PRPDPs.

5.5 Overall Comparison of the Trends

The results show that any sample displaying the additional classes C, D and E has a much longer time to failure than similar samples that did not. This implies that these additional classes are responsible for the increased longevity. Currently there is no concrete class duration values, but this may be found with more samples and may be dependent upon both the filler loading level and filler material type. The only definitive class is class A, which is always a small fraction of the duration of class B; this is to be expected however due to its definition.

The nanocomposite/epoxy samples appear to display two main differences from clean epoxy samples:

- The nanocomposite samples show an overall marked decrease in the PD magnitudes for the entire PD time evolution plot.
- Clean epoxy samples display class A and B only but the nanocomposite samples can exhibit additional classes C, D and E. Furthermore, more than one cycle of these additional classes can occur before final failure.

The reasons for only some of the samples displaying this behaviour will be discussed in detail in the next section, but agglomerations almost certainly play a part. This consistency did not show a necessary improvement with increasing filler loading level, except for MgO, where this was apparent. The reason behind the consistency for this specific material however is currently unknown and can only be speculated upon. This is most likely due to some difference in permittivity, but the reason this may have an effect will be elucidated upon in the next chapter. At this point it is difficult to say anything definitive about these classes in terms of exact, quantifiable values, but their occurrence is predictable and reproducible. Further testing may allow full quantization of these classes.

5.6 Summary

The results have shown marked extended patterns of the PD time evolution behaviour. Whilst there are small number of samples displaying these extensions, they show direct correlation to increase in time to failures and other distinct characteristics. Furthermore, the trends across both filler loading level and filler material are discussed allowing for contrast between filler materials and their filler loading levels. It is notable that MgO filler material gives the best results with higher consistency of samples and much greater time to failures than the other filler materials. The results detailed along with the suppositions about the mechanics can now be compiled into one cohesive model of behaviour that will explain the results.

Chapter 6

GENERALISED MODEL OF OBSERVED BEHAVIOUR

In the previous chapter, explanations were suggested for the Partial Discharge (PD) behaviours in each class of the PD evolution plot. This chapter suggests a model representing the physical mechanisms of treeing phenomena on nanocomposites.

From the results, analysis, interpretation and discussion in the previous chapter a pattern of the behaviour of nanocomposites can be deduced. If the Polymer Chain Alignment Model (PCAM) is assumed to be correct, there are a limited number of explanations for this behaviour. A model will help to predict the behaviours and allow for theoretical testing of different nanocomposites. This chapter serves to combine the observations and discussions from the previous chapters into one cohesive model description, along with detailed descriptions of the processes involved.

6.1 Basic Model

The basic model is primarily derived from the classification scheme devised in this dissertation, explaining the physical mechanisms that give rise to the different characteristics of each class.

6.1.1 Class A and B

Class A and B are the standard Partial Discharge (PD) time evolution behaviour in clean epoxy. Class A is typified by its approximately linear PD magnitude increase that can be attributed to the expansion of the initial bush tree. This is supported by the Phase Resolved Partial Discharge Patterns (PRPDPs) for this class which are typical for a bush electrical tree.

Class B starts once a branch tree has developed to form a combined electrical tree as illustrated in Figure 6.1b. This branch tree allows for a much greater range and size of the average PD magnitudes measured. The pattern is characterised by the presence of both big and small PD pulses. The PRPDPs for class B correlate to a PRPDP associated with branch electrical trees.

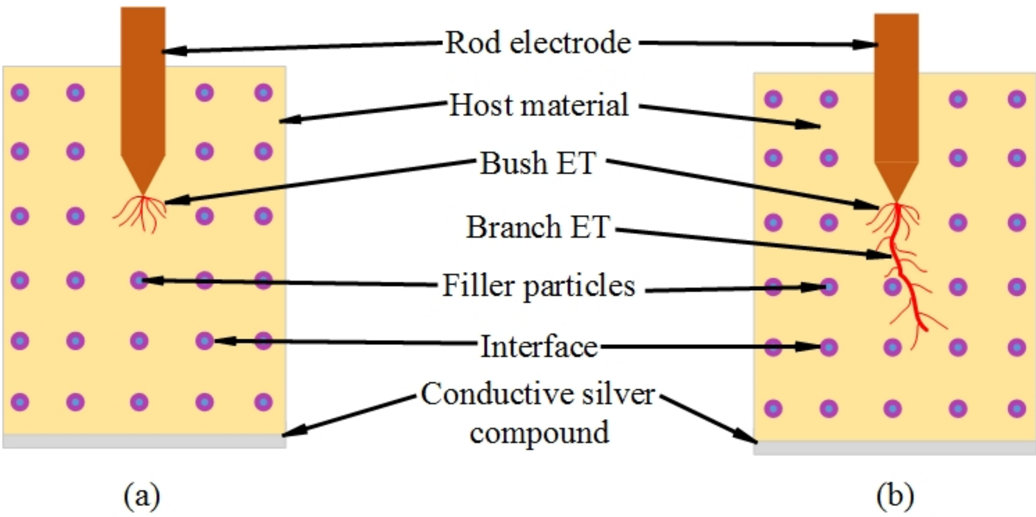

Figure 6.1: Model of class A and B behaviour.

In clean epoxy, classes A and B occur before experiencing failure. All nanocomposites start with a sequence of class A and B, but may exhibit further classes before failure. Classes A and B in nanocomposites do however differ from the clean epoxy classes. The PD magnitudes of a nanocomposite are significantly smaller than in clean epoxy. The difference in PD magnitude may occur due to the nanoparticles restricting both the longitudinal path of the microtubules and the width they can expand to.

6.1.2 Class C

Class C shows a sudden drop in average PD magnitude to only slightly above the noise level mask. This most likely arises due to partial carbonisation of the electrical tree tubules. It is proposed that at this point, the majority of tubules have encountered and terminated upon a nanoparticle and its interface region. Even though the electrical tree tubules' widths are in the order of micrometers and the nanoparticles (and its interface region) in nanometers, the expansion of the tubules will form a new rod-like extension as displayed in Figure 6.2. The tip of this expansion point is very small as it slowly breaks polymer chains, which can be blocked by the nanoparticle and its interface region.

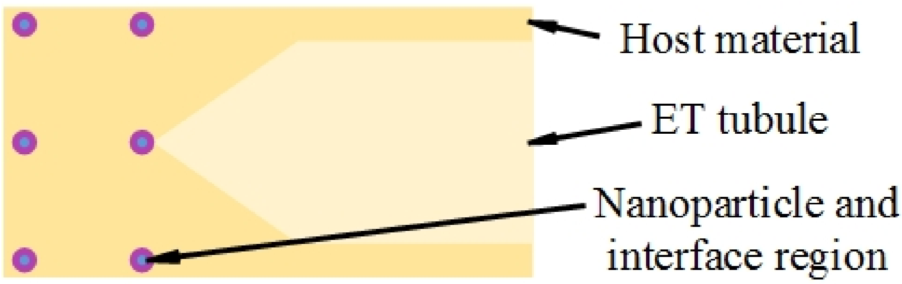

Figure 6.2: Display of the termination mechanic given the difference in dimensions.

This causes partial carbonisation of the older tubules, which inhibits the size of PDs in the tubule, as the carbonised walls do not accumulate charge but disperse it as illustrated in Figure 6.3. This limits the amount of surfaces that can accumulate charge and the distances between these surfaces, thereby reducing the size of the PD magnitudes.

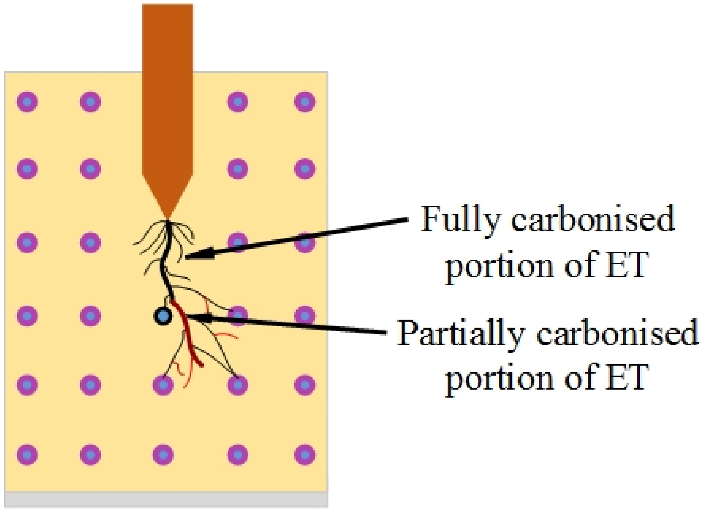

Figure 6.3: Model of the class C mechanics.

6.1.3 Class D

Class D displays a complete cessation of any PDs above the noise level mask, except for random and infrequent impulses. This implies that the tubules have either terminated on a nanoparticle and its associated interface region or have been completely carbonised as shown in Figure 6.4.

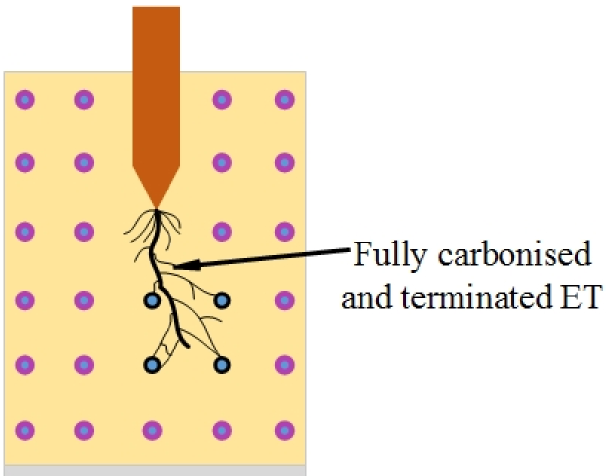

Figure 6.4: Model behind class D behaviour.

The nanoparticles and their associated interface region almost certainly have a different permittivity from the host material. This combined with the their small size means that at least some electric field stress enhancement would be experienced. The electric field stress enhancements would attract the electrical tree propagation towards the nanoparticles and its associated interface. This would increase the likelihood that the electrical tree tubules terminate on an interface region.

This implies that the small size combined with the slight electrical field stress may actually cause the filler material to act as a benefit. This would also explain the difference in consistency for the different filler materials, as the permittivity difference for the MgO samples may be just the right amount to allow this effect to be optimised. Whereas the other filler materials' permittivity difference may be either too low or too high to enjoy the same optimised benefit.

As the tubules are fully carbonised, the tree acts as a conductor, causing the tree and nanoparticle to act as a new electrode tip. This results in the effective electrode gap distance (d) decreasing and the tip radius (r) to become the size of the radius of the nanoparticle and its interface region. The electric field stress consequently increases and possibly attain the electric breakdown strength of the host material. This effect is displayed in Figure 6.5.

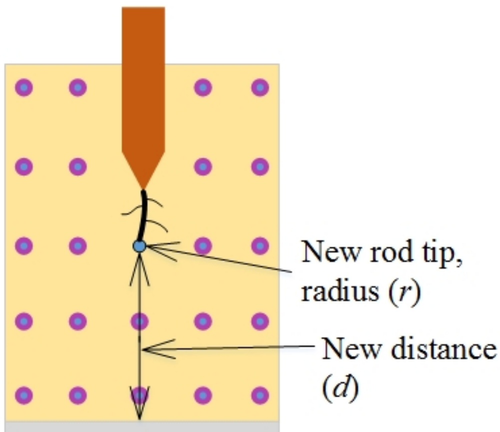

Figure 6.5: Change in the rod-plane model due to carbonisation.

6.1.4 Class E

After class D occurs, two effects begin to dominate: the PD side-effects and the extension of the rod electrode. The previous PDs will have evolved corrosive fluids that slowly degrade the host material, increase pressure and cause the crystallisation mechanism as discussed in Section 2.4. Furthermore, as the electrode has been extended due to the conductive carbonisation, an electrical tree initiation phase is entered, characterised by electroluminescnce and the push-pull forces damaging molecular bonds. An example of this new tree initation is shown in Figure 6.6. For this reason, class E shares many similarities with class A and B as this is essentially the initiation of a new tree, but a complication arises.

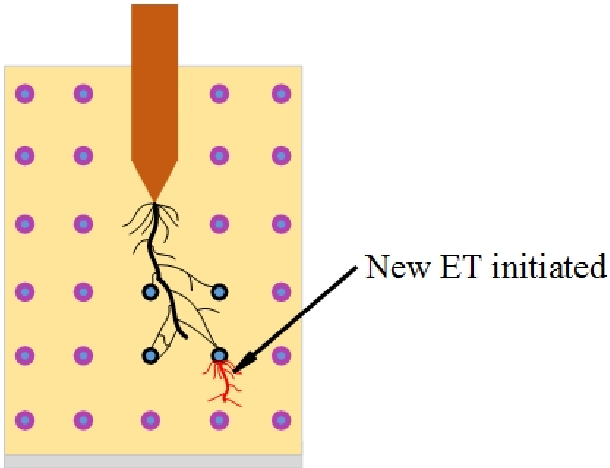

Figure 6.6: Model behind class E mechanics.

Once a new tree has been initiated, the previously encountered nanoparticles and their interface regions now protrude into the tubule as shown in the Figure 6.7 and 6.8.

These protrusions have been confirmed by Toshikatsu Tanaka in a series of TEM images presented in his paper [10]. An example of these images with the protrusions clearly visible is shown in Figure 6.8. These protrusions will have a different permittivity and thereby act as an electric field stress enhancement. If the opposite wall of the microtubule is approximated as a plane, Equation (2.1) can be used to analyse the problem. It can be assumed

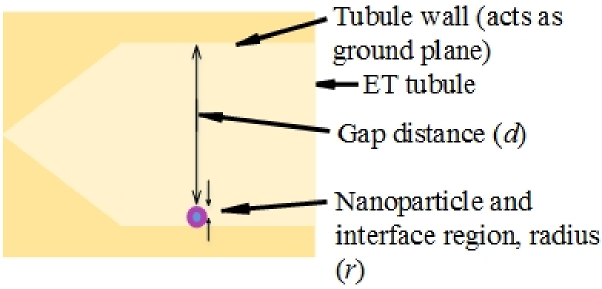

Figure 6.7: Model of the cause of corona behaviour in class E.

that r is smaller than d by at least a factor of 100 due to known measurements of nanoparticles and its interface region and microtubule. Approximating the geometry of a rod-plane configuration results in Equation (2.1) simplifying as follows:

$$
\begin{aligned}
E_{max} &= \frac{2V}{r\ln(1+\frac{4d}{r})} \\
&= \frac{2V}{100r\ln(1+\dfrac{4(100r)}{r})} \\
&= \frac{2V}{100r\ln(1+400)} \\
&\approx \frac{2V}{100r(6)} \\
&= \frac{2V}{600r} \\
&= \frac{V}{300r} \\
&= \frac{V}{300\alpha\times 10^{-7}} \\
&\approx \frac{(3\times 10^{4})V}{\alpha} kV/m
\end{aligned}
$$

Where V is the electrostatic charge difference (taken as kV in this example) and $r = \alpha\times 10^{-7}$ is the approximate size of the nanoparticle and interface region. As α is a factor with small variation, a maximum electric field approximately thirty thousand times greater than the E_{max} experienced by the needle-plane electrodes is formed around the interface region. At such a high electric field stress enhancement, breakdown of the gas inside the tubule, or corona, is inevitable. The difficulty with measuring corona occurring in the microtubules is that the PDs that occur simultaneously with the corona and will mask the PRPDP that would have indicated corona occurring. This makes it difficult for a human to detect an E class, much less a computer program.

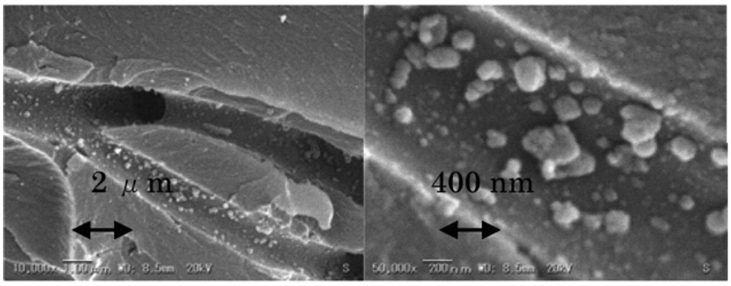

Figure 6.8: TEM image confirming protrusions in electrical tree tubules from Toshikatsu Tanaka's paper [10]. Used with permission from Toshikatsu Tanaka.

6.1.5 Cycles

The suggested reason behind the cyclical nature of C, D and E is attributed to layer encounters. With the above model of behaviour, only one layer of nanoparticles encountered is described. If Figure 6.9 is used, which does assume even dispersion, and assume the electrical tree propagation will have an overall radial growth pattern, the nanoparticles can be broken down into layers of hemispheres. Due to the electric field, the majority of encounters will be on a narrow vertical band between the electrodes. The electrical tree tubules will propagate through several layers of nanoparticles, each causing a cycle of classes C, D and E to occur. The electrical tree tubules may suffer another termination encounter on a further layer or may continue until failure. This would be highly probabilistic as it depends primarily on the electrical tree propagation pattern itself. This cycle of encounters will occur until the insulation material experiences failure.

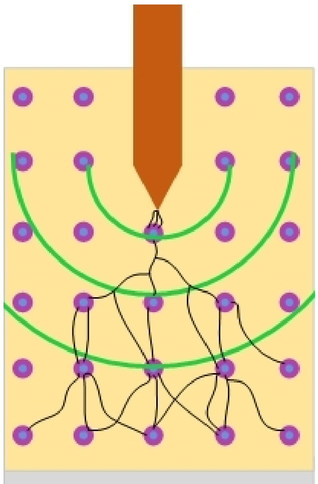

Figure 6.9: Model of the cause behind the cyclical nature of classes C, D and E.

6.2 Complications in the Model

As can be seen the model does not apply to all the nanocomposite samples, in fact the majority of the samples exhibit behaviour more akin to clean epoxy's pattern than the extended patterns. Furthermore, a rare few samples showed an initial dead zone.

6.2.1 Consistency

The extension of the sample PD time evolution patterns is not consistent due to factors that may include imperfect uniform dispersion of the nanoparticles. As described in the sample synthesis subsection, Subsection 4.2.2, it was noted that there is a probability of agglomerations remaining in the nanocomposite samples. These agglomerations imply that the nanoparticles may not be evenly distributed throughout the epoxy. This uneven distribution makes it far more likely that an electrical tree can form without encountering any nano-particles. As the interruption of electrical tree propagation by the nanoparticles is the fundamental reasoning behind the existence of additional of more electrical tree PD classes, these classes will not occur.

Agglomerations also display the biasing of electrical tree propagation paths, but as the particles are not evenly dispersed the likelihood of an encounter is much lower. This means that class C and D are much less likely to occur, which would account for the large number of samples that did not display this behaviour.

6.2.2 Dead zones

Two of the samples showed an initial dead zone before any appreciable activity was detected. This implies that an electrical tree took much longer to initiate. The delayed tree inception is probably due to the presence of a nanoparticle and its interface region close to the tip of the Ogura™ needle. A nanoparticle and its interface region close to the needle tip would interfere with the initiation phase of the electrical tree as the push-pull mechanism would be largely negated. This negation occurs because of the electron-hole recombination provided by the nanoparticle. The likelihood of this occurring is very low and is dependant upon the needle tip happening to be placed close to a nanoparticle and its interface region during synthesis.

6.3 Summary

The observed time evolution of electrical tree PD in nanocomposite epoxy can be explained using a suggested generalised model. The model is described in detail with both the mechanisms and supporting information presented. The previous chapters discussion is refined and compiled into a cohesive generalised model along with validations against the observed results. What is clear is that the particles do appear to retard the formation of an electrical tree, possibly due to the interface region and as a side-effect of the electrical stress they cause. Any model can be improved and refined by incorporating more information. The following chapter details the possible refinements that can be made to the model as well the other aspects of this research.

Chapter 7

FUTURE WORK

Given the previous chapters detailing the work in this dissertation, an important aspect is the future direction the research could and should take. This is detailed in three different ways: future work on the samples; the model; and the Auto-Classification program. This chapter details the directions of interest with regard to each of these aspects of the experimental work.

As this field of research is still in its infancy, the avenues for future work are numerous. The PD-based method of characterising electrical trees in nanocomposites has only been used recently. The specific possible directions in which the research can be taken further are explained below. First, the changes that can be made to investigate the variations in nanocomposites. Second, the changes that can be made to the analysis and modelling portions of the research are delineated.

7.1 Samples

There are several areas where the sample's can be expanded upon for further research. These changes will focus on evaluating the combination of factors for nanocompistes that will optimise the improvements exhibited by nanocomposites.

The filler types can be expanded beyond the MgO, Si_2O and Al_2O_3 filler materials used for this research. As there is no model that can relate the material to the its effects when used as a nanofiller, each material must be tested to ascertain its effects and optimal configuration. This also leads to experimenting with different filler loading levels. Most of the samples with extended patterns in this dissertation work showed increases with loading level. Experiments are necessary to find the improvements as a function of loading level.

A method to quantify the dispersion of the nanofiller is paramount to quality control. This would allow for better models as it will be able to remove the uncertainty regarding the agglomerations present in the test samples.

This work only regards the electrical property improvements around electrical treeing. This is not to imply that these are the only improvements as it is possible that the nanocomposite displays improved mechanical properties as well. A natural step forward is to try improving both a mechanical and an electrical property simultaneously.

7.2 Model and Auto-Classification

A model was presented in Chapter 6 that serves to explain the mechanisms behind the extended patterns. As with all models, this model can be refined further by incorporating more information. Including more samples results will provide this information and possibly cement several suppositions presented.

Similarly, the auto-classification program developed in this dissertation can be improved. The program is relatively simplistic in that it uses tolerances in combination with statistical parameters for the segmentation process. Whilst simplistic, it is still quite accurate, with very few corrections necessary as shown in Chapter 5. Future improvements can incorporate more complex pattern detection systems such as computational intelligence techniques. Computational intelligence techniques may be far more complicated than the current scheme, but this complexity has many advantages such as easily teaching new patterns, as well as more robust pattern recognition. This program warrants a large amount of attention as a more robust solution may also allow for easy classification of the current state of the electrical tree, and accurate information on the lifetime of the insulation may be extractable.

7.3 Summary

As this research is still in its infancy, the avenues of research are broad, with the preceding sections only detailing the primary areas of interest with respect to the research covered in this dissertation. Specifically, varying both the filler material and filler loading levels even further to allow for a greater level of comparison. There also exist possibilities in modifying more than one property simultaneously to be investigated. The model and Auto-Classification program will be refined further to help analyse future data and possibly extract further information. The possibilities for this technology are, at the least, promising and future research should yield increasingly interesting results.

Chapter 8

CONCLUSION

The work of this dissertation has shown that electrical trees in nanocomposites display a clearly modified behaviour. The consistency in the results has been discussed and future work would require more stringent manufacturing process quality control. Secondly, the monitoring of electrical trees through PD discharge detection techniques is not only viable, but useful. Using PD detection techniques also offers more information that was not previously available with other detection techniques. These results show promise for the future improvements that can be developed for current insulation technology.

This dissertation contributes to the current knowledge on nanocomposite insulation. The first and primary addition is the introduction of a new detection scheme, through the use of monitoring PD phenomena, that may allow the systematic tracking of the an electrical tree's progress through the nanocomposite insulator. This further allows for monitoring of the behaviour of the electrical tree through the patterns formed by the PD time evolution plot in combination with the corresponding PRPDPs. This has shown many surprising features that have contributed significantly to the formulation of a model that could describe the very foundational mechanisms that give nanocomposites their enhanced electrical properties. Future experimentation in this field is most likely to yield results that will change the frontiers in the electrical insulation knowledge domain.

REFERENCES

[1] R. Gibson. *Principles of composite material mechanics*. CRC Press, Taylor & Francis Group, 2012.

[2] L. A. Dissado. "Understanding Electrical Trees in Solids: From Experiment to Theory." *IEEE Transactions on Dielectrics and Electrical Insulation*, vol. 9, pp. 483–497, 2002.

[3] C. Nyamupangedengu, R. Kochetov, P. H. F. Morshuis, and J. J. Smit. "A Study of Electrical Tree Partial Discharges in Nanocomposite Epoxy." *2012 Annual Report Conference on Electrical Insulation and Dielectric Phenomena (CEIDP)*, vol. 1, pp. 912–915, 2012.

[4] "IEC 60270: High-voltage test techniques Partial discharge measurements."

[5] D. Z. Gang. *Study on Strategic Planning of Ultra-High Voltage Grid Development in China*. Ph.D. thesis, Shandong University, 2008.

[6] N. Mahatho, I. R. Jandrell, T. Govender, and N. Parus. "Ageing of Silicone Rubber Insulators Under High Voltage Direct Current: Results of Inclined Plane Testing and Materials Analysis." In *18th International Symposium on High Voltage Engineering*. 2013.

[7] E. H. Kerner. "The Electrical Conductivity of Composite Media." *Proceedings of the Physical Society Section B*, vol. 69, p. 802, 1956.

[8] T. Tanaka. "Nanodielectics: how does the presence of interfaces influence behaviour?" *International Journal of Enhanced Research in Science Technology & Engineering*, vol. 2, pp. 1–4, 2013.

[9] T. Tanaka. "Comprehensive understanding of treeing V-t characteristics of epoxy nanocomposites." In *Proceedings of the 17th International Symposium on High Voltage Engineering (ISH), Hannover, Germany*. 2011.

[10] T. Tanaka. "Mechanisms of crossover phenomenon in tree length vs. applied voltage characeteristics between base epoxy and its nanocomposites." In *18th International Symposium on High Voltage Engineering*. 2013.

[11] M. Brebu, C. Vasile, S. R. Antonie, M. Chiriac, M. Precup, J. Yang, and C. Roy. "Study of the natural ageing of PVC insulation for electrical cables." *Polymer Degradation and Stability*, vol. 67, pp. 209–221, 2000.

[12] J. Densley. "Ageing Mechanisms and Diagnostics for Power Cables – An Overview." *IEEE Electrical Insulation Magazine*, vol. 17, pp. 14–22, 2001.

[13] J. K. E. Kuffel, W. S. Zaengl. *High Voltage Engineering: Fundamentals*. Butterworth Heinemann, 2008.

[14] S. M. Tamboli, S. T. Mhaske, and D. D. Kale. "Crosslinked polyethylene." *Indian Journal of Chemical Technology*, vol. 11, pp. 853–864, 2004.

[15] S. V. Nikolajevic. "The behaviour of water in XLPE and EPR cables and its influence on the electric characteristics of insulation." *IEEE Transactions on Power Delivery*, vol. 14, pp. 39–45, 1999.

[16] R. J. Densley. "An investigation into the growth of electrical trees in XLPE cable insulation." *IEEE Transactions on Electrical Insulation*, vol. EI-14, pp. 148–158, 1979.

[17] M. Amin, M. Akbar, and S. Amin. "Hydrophobicity of Silicone Rubber used for outdoor insulation." *Review of Advanced Materials Science*, vol. 16, pp. 10–26, 2007.

[18] M. S. Bhatnagar. “Epoxy Resins (overview).” *The Polynmeric Materials Encyclopedia*, vol. 1, pp. 1–11, 1996.

[19] T. Andritsch. *Epoxy Based Nanocomposites for High Voltage DC Application - Synthesis, Dielectric Properties and Space Charge Dynamics*. Ph.D. thesis, Technical University of Delft, 2010.

[20] M. Danikas and T. Tanaka. “Nanocomposite A review of electrical treeing and breakdown.” *IEEE Electrical Insulation Magazine*, vol. 25, pp. 19–25, 2009.

[21] G. Droval, I. Aranberri, J. Ballestero, M. Verelst, and J. Dexpert-Ghys. “Synthesis and characterization of thermoplastic composites filled with gamma-boehmite for fire resistance.” *Fire and Materials*, vol. 35, pp. 491–504, 2011.

[22] P. P. Budenstein. “On the Mechanism of Dielectric Breakdown of Solids.” *IEEE Transactions on Electrical Insulation*, vol. EI-15, pp. 225–240, 1980.

[23] Y.-S. Cho, H.-K. Lee, M.-J. Shim, and S.-W. Kim. “Characteristics of Polymer Insulator Materials: Fractal Characteristics of Electrical Tree in DGEBA/MDA/nitrile System.” *Journal of Industrial and Engineering Chemistry*, vol. 6, pp. 13–18, 2000.

[24] L. Cisse, S. Bamji, and A. Bulinski. “Electric field calculations for needle-plane geometry and space charge in polyethylene.” *IEEE Transactions on Dielectrics and Electrical Insulation*, vol. 10, pp. 176–180, 2003.

[25] B. Florkowska, M. Florkowski, J. Roehrich, and P. Zydron. “Partial discharge mechanism a non-uniform electric field at highmechanism.” *IET Science, Measurement and Technology*, vol. 5, pp. 59–66, 2010.

[26] F. H. Kreuger. *Discharge Detection in High Voltage Equipment*. Temple Press Books Ltd., 1964.

[27] S. A. Boggs. "Partial discharge: overview and signal generation." *IEEE Electrical Insulation Magazine*, vol. 6, pp. 33–39, 1990.

[28] R. H. Cole. "Time Domain Reflectometry." *Annual Review of Physical Chemistry*, vol. 28, pp. 283–300, 1977.

[29] S. Singha and M. J. Thomas. "Permittivity and tan delta characeteristics of epoxy nanocomposites in the frequency range of 1 MHz - 1 Ghz." *IEEE Transactions on Dielectrics and Electrical Insulation*, vol. 15, pp. 2–11, 2008.

[30] N. Shimizu and C. Laurent. "Electrical tree initiation." *IEEE Transactions on Dielectrics and Electrical Insulation*, vol. 5, pp. 651–659, 1998.

[31] R. H. Friend, R. W. Gymer, A. B. Holmes, J. H. B. abd R. N. Marks, C. Taliani, D. D. C. Bradley, D. A. D. Santos, J. L. Brdas, M. Lglund, and W. R. Salaneck. "Electroluminescence in conjugated polymers." *Nature*, vol. 397, pp. 121–128, 1999.

[32] T. Tanaka. "Similarity between Treeing Lifetime and PD Resistance in Aging Mechanisms for Epoxy Nanocomposites." In *IEEE 9th Conference on the Properties and Applications of Dielectric Materials*, vol. 1, pp. 741–744. 2009.

[33] L. A. Dissado, S. J. Dodd, J. V. Champion, P. I. Williams, and J. M. Alison. "Propoagation of electrical tree structures in solid polymeric insulation." *IEEE Transactions on Dielectrics and Electrical Insulation*, vol. 4, pp. 259–279, 1997.

[34] M. F. Ashby. "Technology of the 1990s: Advanced materials and predictive design." *Philosophical Transactions of the Royal Society of London*, vol. A232, pp. 393–407, 1987.

[35] S. Raetzke and J. Kindersburger. "Role of the interphase on the resistance to high-voltage arcing, on tracking and erosion of silicone/SiO2 nanocomposites." *IEEE Transactions on Dielectrics and Electrical Insulation*, vol. 17, pp. 607–614, 2010.

[36] T. Lewis. “Interfaces are the dominant feature of dielectric at the nanometric level.” *IEEE Transactions on Dielectrics and Electrical Insulation*, vol. 11, pp. 739–753, 2004.

[37] J. Weidner, F. Pohlmann, P. Groppel, and T. Hildinger. “Nanotechnology in high voltage insulation systems for turbine generators first results.” In *XVII Internataional Symposium on High Voltage Engineering, Hannover Germany*. 2011.

[38] E. Ruckenstein and J. S. Park. “Hydrophilic-hydrophobic polymer composites.” *Journal of Polymer Science Part C: Polymer Letters*, vol. 26, pp. 529–236, 1988.

[39] S. Avanzino, R. Cheung, D. M. Erb, and R. Klein. “Composite insulation with a dielectric constant of less than 3 in a narrow space separating conductive lines.”, 1995.

[40] T. Tanaka, M. Kozako, N. Fuse, and Y. Ohki. “Proposal of a multi-core model for polymer nanocomposite dielectrics.” *IEEE Transactions on Dielectrics and Electrical Insulation*, vol. 12, pp. 669–681, 2005.

[41] J.-K. Kim and Y.-W. Mai. *Engineered Interfaces in Fiber Reinforced Composites*. Elsevier, 1998.

[42] Y. K. Godovsky. *Thermophysical properties of polymers*. Springer-Verlag Berlin, New York, 1992.

[43] R. Bartnkias and R. M. Eichhorn. *Engineering dielectrics volume 2a - electrical properties of solid insulation materials: molecular structure and electrical behaviour*. American Sociery for Testing and Materials, 1983.

[44] F. H. Kreuger. *Industrial High DC Voltage*. Delft University Press, 1995.

[45] H. Sirringhaus, P. J. Brown, R. H. Friend, M. M. Nielsen, K. Bechgaard, B. M. W. Langeveld-Voss, A. J. H. Spiering, R. A. J. Janssen, E. W.

Meijer, P. Herwig, and D. M. de Leeuw. “Two-diemensional charge tansport in self-organized, high mobility conjugated polymers.” *Nature*, vol. 401, pp. 685–688, 1999.

[46] P. Preetha and M. J. Thomas. “AC breakdown characteristics of epoxy alumina nanocomposites.” *2010 Annual Report Conference on Electrical Insualtion and Dielectric Phenomena*, vol. 1, pp. 1–4, 2010.

[47] “Ogura Industrial Jewel.” URL `http://www.ogura-indus.co.jp`.

[48] R. Kochetov. *Thermal and elcetrical properties of nanocomposites, including material processing*. Ph.D. thesis, Technical University of Delft, 2012.

[49] M. Frchette, M. Trudeau, H. D. Alamdari, and S. Boily. “Introductory remarks on Nanodielectrics.” *IEEE Transactions on Dielectrics and Electrical Insulation*, vol. 11, pp. 808–818, 2004.

[50] C. D. Green and A. S. Vaughan. “Polyethylene / montmorillonite nanocomposites: Effect of masterbatch composition and maleic anhydrite on ac electrical breakdown performance.” *International Conference on Solid Dielectrics*, vol. 1, pp. 364–367, 2007.

[51] A. Haque, M. Shamsuzzoha, F. Hussain, and D. Dean. “S2-Glass/Epoxy Polymer Nanocomposites: Manufacturing, Structures, Thermal and Mechanical Properties.” *Journal of Composite Materials*, vol. 37, pp. 1821–1837, 2003.

[52] F. Hussain, M. Hojjati, M. Okamoto, and R. E. Gorga. “Review article: Polymer-matrix Nanocomposites, Processing, Manufacturing, and Application: An Overview.” *Journal of Composite Materials*, vol. 40, pp. 1511–1575, 2006.

[53] “ICMcompact - Digital Partial Discharge Detector Brochure.” URL `http://www.pdix.com/index.php?eID=tx_nawsecuredl&u=0&file=fileadmin/user_upload/pdix/downloads/documents/`

Brochure_Pages/ICMcmp_broc_893.pdf&t=1405093243&hash=8183ac53a3248cf7e68cef12faf248bd5324aaf7.

[54] *ICMcompact User Manual Rev. e315*.

[55] I. ENOM. "Ammyy Admin - Free Zero-Config Remote Desktop Software.", January 2008. URL http://www.ammyy.com/en/.

[56] "Object Orientated Programming in MATLAB." URL http://www.mathworks.com/help/matlab/object-oriented-programming.html.

[57] M. Dawson. *Python Programming for the Absolute Beginner*. Course Technology, 2010.

[58] R. Bartnikas. "Partial Discharges: Their Mechanism, Detection and Measurement." *IEEE Transactions on Dielectrics and Electrical Insulation*, vol. 9, pp. 763–808, 2002.

[59] J. V. Champion and S. J. Dodd. "Systematic and reproducible partial discharge patterns during electrical tree growth in epoxy resin." *Journal of Physics D: Applied Physics*, vol. 29, p. 862, 1996.

[60] D. Cornish and C. Nyamupangedengu. "Electrical tree partial discharge characteristics in nanocomposites." In *18th Symposium on High Voltage Engineering*. 2013.

[61] E. Cuddihy. "A concept for the intrinsic dielectric strength of electrical insulation materials." *IEEE Transactions on Electrical Insulation*, vol. EI-22, pp. 573–589, 1987.

[62] H. Z. Ding and B. R. Varlow. "Effects of nano-fillers on electrical treeing in epoxy resin subjected to ac voltage." In *Annual Report Conference on Electrical Insulation and Dielectric Phenomena*. 2004.

[63] N. Fuse, Y. Ohki, M. Kozako, and T. Tanaka. "Possible Mechanisms of Superior Resistance of Polyamide Nanocomposites to Partial Discharges and Plasmas." *IEEE Transactions on Dielectrics and Electrical Insulation*, vol. 15, pp. 161–169, 2008.

[64] K. Ishimoto, E. Kanegae, Y. Ohki, T. Tanaka, Y. Seikiguchi, Y. Murata, and C. C. Reddy. "Superiority of Dielectric Properties of LDPE/MgO Nanocomposites over Microcomposites." *IEEE Transactions on Dielectrics and Electrical Insulation*, vol. 16, pp. 1735–1742, 2009.

[65] W. Jiandong, T. Izuka, K. Monden, and T. Tanaka. "Characteristics of Initial Trees of 30 to 60 μm Length in Epoxy/Silica Nanocomposite." *IEEE Transactions on Dielectrics and Electrical Insulation*, vol. 19, pp. 312–320, 2012.

[66] J. Katayama, N. Fuse, M. Kozako, T. Tanaka, and Y. Ohki. "Comparison of the Effects of Nanofiller Materials on the Dielectric Properties of Epoxy Nanocomposites." *2011 Annual Report Conference on Electrical Insualtion and Dielectric Phenomena*, vol. 1, pp. 318–321, 2011.

[67] J. Katayama, Y. Ohki, N. Fuse, and M. K. K. Tanaka. "Effects of Nanofiller Materials on the Dielectric Properties of Epoxy Nanocomposites." *IEEE Transactions on Dielectrics and Electrical Insulation*, vol. 20, pp. 157–165, 2013.

[68] R. Kochetov, T. Andritsch, U. Lafont, P. Morshuis, and J. Smit. "Electrical tree propogation time to breakdown for epoxy resin composites containing alumina and silica nanocparticles." In *18th Symposium on High Voltage Engineering*. 2013.

[69] M. Kozako, S. Yamano, R. Kido, Y. Ohk, M. Kohtoh, S. Okabe, and T. Tanaka. "Preparation and Preliminary Characteristic Evaluation of Epoxy/Alumina Nanocomposites." In *Proceedings of 2005 International Symposium on Electrical Insulating Materials*, vol. 1, pp. 231–234. 2005.

[70] T. Kusunose, T. Sekino, Y. H. Choa, and K. Niihara. "Fabrication and microstructure of silicon nitride/boron ntride nanocomposites." *Journal of the American Ceramic Society*, vol. 85, pp. 2678–2688, 2002.

[71] S. Raetzke, Y. Ohki, T. I. I. Kindersburger, and T. Tanaka. "Enhanced Performance of Tree Initiation V-t Characteristics of Epoxy/-Clay Nanocomposite in Comparison with Neat Epoxy Resin." *Annual*

Report Conference on Electrical Insulation and Dielectric Phenomena, vol. 1, pp. 528–531, 2008.

[72] C. C. Reddy and T. S. Ramu. "Polymer Nanocomposites as Insulation for HV DC Cables Investigations on the Thermal Breakdown." *IEEE Transactions on Dielectrics and Electrical Insulation*, vol. 15, pp. 221–227, 2008.

[73] G. C. Stone. "Partial Discharge. VII. Practical techniques for measuring PD in operating equipment." *IEEE Electrical Insulation Magazine*, vol. 7, pp. 9–19, 1991.

[74] T. Tanaka. "Buds for Treeing in Epoxy Nanocomposites and their Possible Interaction with Nano Fillers." In *10th IEEE International Conference on Solid Dielectrics*, vol. 1, pp. 1–4. 2010.

[75] T. Tanaka. "Dielectric Nanocomposites with Insulating Properties." *IEEE Transactions on Dielectrics and Electrical Insulation*, vol. 12, pp. 914–928, 2005.

[76] T. Tanaka. "Polymer Nanocomposites as Dielectrics and Electrical Insulation-perspectives for Processing Technologies, Material Characterization and Future Applications." *IEEE Transactions on Dielectrics and Electrical Insulation*, vol. 11, pp. 763–784, 2004.

[77] T. Tanaka. "Charge Transfer and Tree Initiation in Polyethylene Subjected to ac Voltage Stress." *IEEE Transactions on Electrical Insulation*, vol. 27, pp. 424–431, 1992.

[78] T. Tanaka, A. Bulinski, J. Castellon, M. Frchette, S. Gubanski, J. Kindersberger, G. Montanari, M. Hagao, P. Morshuis, Y. Tanaka, S. Plissou, A. Vaughan, Y. Ohki, C. Reed, S. Sutton, and S. Han. "Dielectric properties of XLPE/SiO_2 nanocomposites based on CIGRE WG D1.24 cooperative test results." *IEEE Transactions on Dielectrics and Electrical Insulation*, vol. 18, pp. 1484–1517, 2011.

[79] T. Tanaka and T. Iizuka. "Generic PD Resistance Characteristics of Polymer Nanocomposites." *2010 Annual Report Conference on Electrical Insualtion and Dielectric Phenomena*, vol. 1, pp. 1–4, 2010.

[80] T. Tanaka, Y. Mizutani, T. Imai, and N. Fuse. "Digest Report of Investigation Committee on Polymer Nanocomposites and their Applications as Dielectr ics and Electrical Insulation." *International Symposium on Electrical Insulating Materials*, vol. 1, p. i, 2008.

[81] W. Zhu, P. Bartos, and A. Porro. "Application of nanotechnology in construction." *Materials and Structures*, vol. 37, pp. 649–658, 2004.

[82] "IEEE 400-2001: IEEE Guide for Field Testing and Evaluation of the Insulation of Shielded Power Cable Systems."

Appendix A

AUTO-CLASSIFICATION MATLAB CODE

The data processing was a large portion of the work due to its complexity but this saved time overall as it allowed for many laborious operations to be done automatically. The data processing program was split into two sections: collation; and analysis (auto-classification). The M files containing the code for each section of code (described through flowcharts and UML Diagrams in Section 4.4) is given below.

A.1 Collation Program

The collation section of the program consists of three parts: the main script; a recursive search function; and a function to performs the data extraction and concatenates the data into a CSV file. The main script uses a recursive function to search through subdirectories until leaf-node directories are found. For each leaf-node the spreadsheet files are read and the relevant data (Q_{p-avg} and U_{RMS}) extracted. This data is then trimmed, using U_{RMS}, to exclude the data from the initiation phase and the data after failure has occurred. The final treated data is then written to a CSV file with the leaf-node directory name as the CSV filename.

collate.m

```
close all;

% request parent directory containing data from user
inputFolder = uigetdir;
outputFolder = 'analysis';

if( ~isequal(exist(outputFolder, 'dir'),7) )
    mkdir(outputFolder);
end

% recursively navigate directory structure
findLeaf( inputFolder, outputFolder);
```

findLeaf.m

```
function out = findLeaf(parent, outputFolder)

    % list directory contents
    list = dir(parent);

    leaf = true;

    % search through list
    for n=3:length(list)
        folder = [ parent, '\', list(n).name ];
        % if not a leaf node recurse
        if( isdir( folder ) )
            leaf = false;
            findLeaf(folder, outputFolder);
        end
    end

    % if a leaf extract data
    if( leaf )
        for n=3:length(list)
            writeData( parent, outputFolder );
        end
```

```
    end

end
```

writeData.m

```
function out = writeData(inputFolder, outputFolder)

% constants
qpMeanCol = 6;
VRMSCol = 11;
emptySpace = 3;
Vapp = 20;

out_time = 1;

% list directory contents
files = dir(inputFolder);

% tolerance for pruning of data
tolerance = 0.5;

data = [];
% for each file, read in Q_p-avg and voltage
for i=3:length(files)
   xls_data = xlsread( [inputFolder, '\', files(i).name] );
   data = [data; [ xls_data(1:end-emptySpace,VRMSCol), ...
        xls_data(1:end-emptySpace,qpMeanCol) ] ];
end
% define start of data and end of data using V_app and ...
    tolerance
% on the extracted voltage
begin_ind = find(data(:,out_time) > ...
    (1-tolerance)*Vapp,1,'first');
end_ind = find(data(begin_ind:end,out_time) <= ...
    (1-tolerance)*Vapp |...
    data(begin_ind:end,out_time) >= ...
        (1+tolerance)*Vapp,1,'first');
```

```

if( isempty(end_ind) )
    end_ind = length(data);
else
    end_ind = end_ind + begin_ind;
end

% define name using directory leaf node name
parent_dir =  strfind( inputFolder, '\' );

name = inputFolder(parent_dir(end)+1:end);

% write data to CSV file in output folder
data = data(begin_ind:end_ind,:);
data(:,out_time) = [1:length(data)]';
csvwrite([outputFolder, '\', name, '.csv'],data)
```

A.2 Analysis and Auto-Classification Program

The Auto-Classification is split into multiple M files due to the implementation of an OO system. The backbone of the system is the batch script which requests the directory containing the collated CSV files. These files are then iterated through, analysed, Auto-Classified and plotted. the auto-classification section operates by segmenting the PD signal data into multiple segments, based on whether they are considered large segments or small segments. These large and small segments are then further segmented with the use of tolerances and comparisons of overall PD signal means to segment means as well as trend data where necessary. The final portion consists of a call to a function, *editClassification* which implements a Graphical User Interface (GUI) which allows the user to easily modify portions of the auto-classified sample signals.

batch.m

```
close all;

```

```
% verify the user version of MATLAb can run this program ...
    correctly
if( verLessThan('matlab','7.12') )
    warning(['This program will not work for your version ...
        of MATLAB! ',
        'Version 7.12 (R2011a) or above is needed due to ...
            the use ',
        'polymorphism!']);
    exit(1);
end

% request CSV file directory from user
dataFolder = uigetdir(pwd);
outputFolder = 'figures';
if( dataFolder == 0 )
    status = 0;
    return;
end

% retrieve list of CSV files
files = dir([ dataFolder, '\', '*.csv']);

for n=1:length(files)

    % read data from CSV files
    file_name = [dataFolder, '\', files(n).name];
    data = csvread(file_name);

    % create Sample object using extracted from CSV
    sample_set(n) = Sample(files(n).name, data);
    fig1 = figure;

    % plot SAmple's data
    sample_set(n).plot();
    set(gcf,'Visible','off');
    print(fig1, '-djpeg', [outputFolder,'\', ...
        sample_set(n).sample_code,'.jpg']);

    close(fig1);
```

```
end


finished = false;

% GUI to modify Auto-Classification
% continuously ask if modifications must be made until No is selected
while( ~finished )
    finish = questdlg('Would you like to change any of the Sample plots?',...
        'Check figures', 'Yes', 'No', 'Yes');
    switch finish
        case 'Yes'
            sel_sample = editClassification(sample_set);
            if(sel_sample == 0 )
                break;
            end
            % replot modified sample data
            dim = [1280, 550];
            fig1 = figure('Position',[0 0 dim(1) dim(2)]);
            sel_sample.plot();
            set(gcf,'Visible','off');
            print(fig1, '-djpeg', [outputFolder,'\', ...
                sel_sample.sample_code,'.jpg']);
            close(fig1);
        case 'No'
            finished = true;
    end
end
```

editClassification.m

```
function sample = editClassification( sample_array)

options = {sample_array.sample_code};

ok = false;
```

```
% allow selection of specific sample
[selection,ok] = listdlg('PromptString','Select a sample ...
    to edit:',...
     'SelectionMode','single',...
     'ListString',options, 'ffs', 12);

if(~ok)
     sample = 0;
     return;
end

% return sample
sample = sample_array(selection);

[cum, sample_categories] = sample.getClasses();

for n=1:cum(end)
     cat_options{n} = sample_categories(n).getClassName();
end

% ask user which class they wish to edit
[cat_selection,ok] = listdlg('PromptString','Which class ...
    would you like to edit?',...
     'SelectionMode','single',...
     'ListString',cat_options, 'ffs', 12);

if(~ok)
     sample = 0;
     return;
end

% ask user what class they want to change it to
class_list = { 'A', 'B', 'C', 'D','EF' };

[new_class,ok] = listdlg('PromptString','What would you ...
    like to change that it to?',...
     'SelectionMode','single',...
     'ListString', cat_list, 'ffs', 12);
```

```
if(~ok)
    sample = 0;
    return;
end

% calculate indices of segments and classes in object members
segment_ind = find( cum >= cat_selection, 1, 'first' );

if( segment_ind > 1 )
    cat_ind = cat_selection - cum(segment_ind-1);
else
    cat_ind = cat_selection;
end

% change the class as user directed
sample.changeClass( segment_ind, cat_ind, ...
    cat_list{new_cat} );

end
```

The rest of the program is implemented through OO class M files.

Sample.m

```
% Sample Class
% Class to represent a sample for these experiments

classdef Sample < handle
% inherit from handle to allow pass by reference

    properties(SetAccess = 'public')
        filler_material;
        filler_level;
        sample_number;
        sample_signal;
        sample_code;
    end

```

```
    % constants specific to CSV format
    properties( Constant, GetAccess = 'private')
       t_col = 1;
       PD_col = 2;
    end

    % Map data structure to allow for parsing of name
    properties( Constant, GetAccess = 'private' )
        name_map = containers.Map(...
            { 'MG', 'SI', 'AL', 'CE' },...
            { 'MgO', 'SiO_2', 'Al_2O_3', 'Clean Epoxy'});
    end

    methods( Access = 'public' )

        % constructor
        function obj = Sample(file_name, data)
            if( nargin > 0 )
                obj.sample_code = file_name( 1:end-4 );
                obj.sample_signal =...
                    PDSignal( ...
                    data(:,obj.t_col)./...
                    SignalProperties.time_factor,...
                    data(:,obj.PD_col) );

                ind = find(obj.sample_code=='-',1,'first');
                obj.filler_material = ...
                   obj.name_map(obj.sample_code(1:2));
                obj.filler_level = ...
                   str2num(obj.sample_code(3:ind-1));
                obj.sample_number = ...
                   str2num(obj.sample_code(ind+1:end));
            end
        end

        % function to retrieve list of classes in sample data
        % to be used to modify auto-classification
        function [ cum, cat_list ] = getClasses( obj )
            signal = obj.sample_signal;
```

```
            [ cum, cat_list ] = signal.getClasses();
        end

        % function to change specific class
        % to be used to modify auto-classification
        function changeClass( obj, segment_ind, cat_ind, ...
            new_cat)
            signal = obj.sample_signal;
            signal.changeClass(segment_ind, cat_ind, new_cat);
        end

        % plot function that cascades down into Signal object
        % and controls axes
        function plot( obj )
            hold on;
            plot( obj.sample_signal );
            axis('tight');
            xlabel( 'Time (h)' );
            ylabel( 'Average PD magnitude (pC)' );
        end

    end

end
```

PDSignal.m

```
% PDSginal Class
% represents Pd signal data of sample

classdef PDSignal < handle
% inherit from handle to activate pass by reference ...
    capabilities
    properties(GetAccess = 'protected', SetAccess = ...
        'protected')
        props;
        segments;
        trend;
```

```
    end

    methods( Access = 'public' )

        % constructor
        function obj = PDSignal(x, y)

            obj.props = SignalProperties(x,y);

            windowsize = 100;

            obj.trend = ...
                tsmovavg(obj.props.dependent,'s',windowsize,1);
            % first windowsize samples will be NaN, fill ...
                in with placeholder
            obj.trend(1:windowsize-1) = obj.trend(windowsize);
            obj.segments = obj.createSegments();

        end

        % plot function which cascades into segments
        function plot(obj)
            for n=1:length(obj.segments)
                plot(obj.segments(n));
            end
        end

        % function to retrieve list of classes in segment data
        % to be used to modify auto-classification
        function [ cum, cat_list ] = getClasses( obj )

            cat_list = 0;
              cum = 0;
            for n =1:length(obj.segments)
                [ num, temp ] = obj.segments(n).getClasses();
                if( n > 1 )
                    cum(n) = num+cum(n-1);
                    cat_list = [cat_list, temp];
                else
```

```
                    cum(n) = num;
                    cat_list = temp;
                end

            end

        end

        % function to change specific class
        % to be used to modify auto-classification
        function changeClass(obj, segment_ind, cat_ind, ...
            new_cat)
            edit_segment = obj.segments(segment_ind);
            edit_segment.changeClass( cat_ind, new_cat );
        end

    end

    methods( Access = 'protected' )

        % function to partially segment signal data
        function obj_array = createSegments( obj )

            y_max = obj.props.maximum;

            %tolerance to use for segmentation
            tolerance = 0.3*obj.props.mu;
            % find indices outside tolerance
            outside_tolerance = abs(obj.trend) > tolerance;
            out_tol_inds = find(outside_tolerance);
            % find lengths of inside tolerance regions
            runs = diff(out_tol_inds);

            % if none outside tolerance automatically a ...
                PDLargeSegment
            if( isempty(out_tol_inds) )
                obj_array = PDLargeSegment( ...
                    obj.props.independent,...
                    obj.props.dependent, obj.trend, y_max, ...
```

```
                        true );
                return;
            else
                last_out_tol = out_tol_inds(end);
            end

            x_max = length(obj.props.independent);

            last_run = x_max-last_out_tol;

            if( last_run ~= 0 )
                runs = [runs ; last_run ];
            end

            % minimum time a PDsmallSegment can have
            if( x_max <= 1*SignalProperties.time_factor )
                min_time = 0.1;
            elseif( x_max <= ...
                5*SignalProperties.time_factor )
                min_time = 0.3;
            else
                min_time = 1;
            end

            % use this to find segments of PDsmallSegments and
            % ignore small regions that are part of ...
                PDLargeSegments
            min_time = min_time.*SignalProperties.time_factor;

            inds = find(runs > min_time);

            if( isempty(inds) )
                obj_array = PDLargeSegment( ...
                    obj.props.independent,...
                    obj.props.dependent, obj.trend, y_max, ...
                        true );
                return;
            end

```

```
        segment_inds = [ 1 ];

        % otherwise find start points of segments
        small_sections = ...
           zeros(size(obj.props.independent));
        for n=1:length(inds)
            p1 = out_tol_inds(inds(n));
            if( inds(n) ~= length(out_tol_inds) )
                p2 = out_tol_inds(inds(n)+1);
                small_sections(p1:p2) = 1;
                segment_inds = [ segment_inds; ...
                   out_tol_inds(inds(n));...
                out_tol_inds(inds(n)+1) ];
            end
        end

        segment_inds = [ segment_inds; ...
           length(obj.props.dependent)+1 ];

        % create PDSegment object for each segment
        for n=1:length(segment_inds)-1
            p1 = segment_inds(n);
            p2 = segment_inds(n+1)-1;
            if( small_sections( round((p1+p2)/2)) )
                obj_array(n) =...
                    PDSmallSegment( ...
                       obj.props.independent(p1:p2),...
                    obj.props.dependent(p1:p2),...
                    obj.trend(p1:p2), y_max );
            else
                obj_array(n) =...
                    PDLargeSegment( ...
                       obj.props.independent(p1:p2),...
                    obj.props.dependent(p1:p2),...
                    obj.trend(p1:p2), y_max );
            end


        end
```

```
            end

        end

end
```

SignalProperties.m

```
% SignalProperties Class
% Class made to be a data member that encompasses
% all data members that comprise of a signal in general

classdef SignalProperties

    properties(GetAccess = 'public', SetAccess = 'protected')
        mu;
        sigma;
        maximum;
        independent;
        dependent;
    end

   % constant data members specific to this experiment
    properties( Constant, GetAccess = 'public' )
        time_factor = 3600;
        noise_level = 0.3;
    end

    methods( Access = 'public' )
        % constructor
        function obj = SignalProperties(x, y)
            if( nargin > 0 )
                    obj.independent = x;
                    obj.dependent = y;
                    obj.mu = mean( obj.dependent );
                    obj.sigma = std( obj.dependent );
                    obj.maximum = max( obj.dependent );
            end
```

```
        end

    end

end
```

PDSegment.m

```
% Abstract Superclass PDSegment
% allows for polymorphic arrays of PDSegments

classdef PDSegment < matlab.mixin.Heterogeneous & handle
% inherit from handle for pass by reference capability
% inherit from matlab.mixin.Heterogeneous to activate ...
    polymorphism

    properties( GetAccess = 'protected', SetAccess = ...
        'protected')
        props;
        trend;
        limit;
        classes;
    end

    methods( Access = 'public' )
        % constructor
        function obj = PDSegment(x, y, y_trend, y_max)
                        if( nargin == 0 )
                def = 0;
                obj.props = SignalProperties( def, def );
                obj.trend = def;
                obj.limit = def;
            else
                obj.props = SignalProperties( x, y );
                obj.trend = y_trend;
                obj.limit = y_max;
            end

```

```
        end

        % function to retrieve list of classes in segment data
        % to be used to modify auto-classification
        function [ num, cat_list ] = getClasses( obj )

            num = length( obj.classes );
            cat_list = obj.classes;

        end

        % function to change specific class
        % to be used to modify auto-classification
        function changeClass( obj, cat_ind, new_cat )
            edit_cat = obj.classes(cat_ind);
            edit_cat.classification = new_cat;
        end

    end

    methods( Abstract )
        %must provide a plot and futher segmentation functions
        plot( obj )
        createClasses( obj )
    end

end
```

PDLargeSegment.m

```
% Subclass PDLargeSegment
% allows specific segmentation method

classdef PDLargeSegment < PDSegment
% inherit from abstract class PDSegment for polymorphism

    properties( GetAccess = 'private', SetAccess = 'private')
        % boolean that defines if this segment is the only
```

```
        % segment for this signal
        is_only;
    end

    methods( Access = 'public' )


        function obj = PDLargeSegment(x, y, y_trend, ...
            y_max, only)
            if( nargin == 0 )
                def = 0;
                args{1} = def;
                args{2} = def;
                args{3} = def;
                args{4} = def;
            else
                args{1} = x;
                args{2} = y;
                args{3} = y_trend;
                args{4} = y_max;
            end

            % call superclass constructor
            obj = obj@PDSegment(args{:});
            if( nargin == 5 )
                obj.is_only = only;
            end
            obj.classes = obj.createClasses();

        end

        % plot function that cascades into classes
        function plot( obj )
            for i=1:length(obj.classes)
                plot(obj.classes(i))
            end
        end

        function obj_array = createClasses( obj )
```

```

            % if the entire signal, it must be a class A ...
                and B
            if( obj.is_only )
                obj_array = obj.segmentAB();
            % otherwise check if conditions are met to be ...
                considered
            % a class E segment
            elseif( obj.props.mu < 0.1*obj.props.maximum &...
                    obj.props.sigma > obj.props.mu)

                obj_array = PDClass( obj.props.independent,...
                    obj.props.dependent, 'E', obj.limit );
            % otherwise must be a class A and B segment
            else
                obj_array = obj.segmentAB();
            end

        end

    end

    methods( Access = 'private' )

        function obj_array = segmentAB( obj )
            % tolerance for segmentation
            tolerance = 1.25*obj.props.mu;
            p1 = find( obj.props.dependent > tolerance, 1, ...
                'first' );

            two_part = true;

            % no indices outside tolerance must be a class B
            if( isempty(p1) )
                p1 = length( obj.props.dependent );
                two_part = false;
            end

            % create class A segment
```

```
            obj_array(1) = PDClass( ... obj.props.independent(1:p1),...
                obj.props.dependent(1:p1), 'A', ... obj.limit );

            % if indices outside tolerance create class B ... segment
            if( two_part )
                obj_array(2) = PDClass( ... obj.props.independent(p1+1:end),...
                obj.props.dependent(p1+1:end), 'B', ... obj.limit );
            end

        end
    end

end
```

PDSmallSegment.m

```
% Subclass PDSmallSegment
% allows specific segmentation method

classdef PDSmallSegment < PDSegment
% inherit from abstract class PDSegment for polymorphism

    methods( Access = 'public' )

       % constructor
        function obj = PDSmallSegment(x, y, y_trend, y_max)
            if( nargin == 0 )
                def = 0;
                args{1} = def;
                args{2} = def;
                args{3} = def;
                args{4} = def;
            else
```

```
                args{1} = x;
                args{2} = y;
                args{3} = y_trend;
                args{4} = y_max;
            end

            % call superclass constructor
            obj = obj@PDSegment(args{:});
            obj.classes = obj.createClasses(y_trend, y_max);
        end

        % plot function that cascades into classes
        function plot( obj )
            for i=1:length(obj.classes)
                plot(obj.classes(i))
            end
        end

        % final segmentation function
        function obj_array = createClasses( obj, y_trend, ...
           y_max )

            % tolerance for segmentation
            tolerance = 2.5*min(y_trend);

            % find indices outside tolerance and calculate ...
               lengths
            % of regions inside tolerance
            outside_tolerance = y_trend > tolerance;
            out_tol_inds = find(outside_tolerance);
            runs = diff(out_tol_inds);

            % if not outside tolerance, classify as D
            if( isempty(out_tol_inds) )
                obj_array = PDClass( obj.props.independent,...
                    obj.props.dependent,'D', y_max);
                return;
            end

```

```
            last_run = ... length(obj.props.independent)-out_tol_inds(end);

            if( last_run ~= 0 )
                runs = [runs ; last_run ];
            end

            % find lengths of inside tolerance regions above
            % a certain value
            len = length(obj.props.independent);

            last_run_ind = find( runs > 0.1*len, 1, 'last');

            next_last_ind = find( runs(1:last_run_ind-1) > ... 0.1*len, 1, 'last');

            % define start points of each class
            p1 = out_tol_inds(next_last_ind);
            if( isempty(p1) )
                p1 = 1;
            end
            p2 = out_tol_inds(last_run_ind);
            p3 = len;


            if( max(y_trend(p1:p3)) < 2*obj.props.mu )
                start_ind = p1;
            else
                start_ind = p2;
            end
            end_ind = p3;

            % create PDclass object for each segment
            obj_array(1) = PDClass( ...
                obj.props.independent(1:start_ind-1),...
                obj.props.dependent(1:start_ind-1),...
                'C', y_max);
            obj_array(2) = PDClass( ...
                obj.props.independent(start_ind:end_ind),...
```

```
                    obj.props.dependent(start_ind:end_ind),...
                    'D', y_max);
            end
        end

end
```

PDClass.m

```
% PDClass Class
% represents classes that segments of the signal
% is classified into

classdef PDClass < handle
% inherit from handle to allow pass by reference

    properties( GetAccess = 'public', SetAccess = 'public' )
        props;
        classification;
        line_height;
    end

    % Map structure to allow plotting of different classes
    % in different colours
    properties( Constant )
        colour_map = containers.Map(...
            { 'A', 'B', 'C', 'D', 'E' },...
            { 'green', 'magenta',  'cyan', 'blue', 'red'});
    end

    methods( Access = 'public' )
        % constructor
        function obj = PDClass(x, y, class, y_max)
            obj.props = SignalProperties(x, y);
            obj.classification = class;
            obj.line_height = y_max;
        end

```

```
        function plot(obj)
            % plot x vs. y data with colour dependent upon ...
                category
            plot( obj.props.independent, ...
                obj.props.dependent, ...
                 [ obj.colour_map(obj.classification),'.'] )
        end

        % get function for class name
        function cat_letter = getClassName( obj )
            cat_letter = obj.classification;
        end

    end

end
```

Appendix B

SAUPEC 2013 PUBLICATION

A paper covering the basic concepts and complications that arise from electrical treeing was published in SAUPEC 2013 conference proceedings and is presented in this appendix. This paper formed some of the base research needed to complete this dissertation.

AN OVERVIEW OF THE ELECTRICAL TREEING PHENOMENA IN SOLID DIELECTRICS

Darryn R. Cornish and Cuthbert Nyamupangadengu

School of Electrical & Information Engineering, University of the Witwatersrand, Johannesburg, Private Bag 3, Wits 2050, Johannesburg South Africa, E-mail: darryn.cornish@students.wits.ac.za

Abstract: Electrical treeing is an insulation degradation phenomenon that is caused by enhanced electric field induced localised breakdown of insulation at molecular level. Once initiated, trees quickly progress to complete failure. In high voltage insulation engineering, it is therefore essential to understand and design for insulation endurance to degradation through treeing. A good understanding of treeing mechanisms is required and this has sustained research in the treeing phenomenon for many years. There is now a general agreement on how trees initiate propagate and eventually cause complete insulation failure. Tree detection and classification techniques have also been developed. Research in treeing phenomenon is ongoing worldwide in response to the need for keeping pace with increasing demands of quality in the electric power industry.

Keywords: Electrical trees, insulation, Partial Discharges, insulation defects, insulation failure

1. INTRODUCTION

Electrical trees are gas filled micro-tubes that develop in regions of localised high electric field in solid insulation [1]. The micro-tubes are tree shaped – hence the name, electrical trees. An example of an electrical tree is as shown in Figure 1. Once initiated, the trees progressively propagate in the electrode gap and eventually bridge the insulation. Electrical treeing is an insulation degradation phenomenon that characterises the final phase of most failure modes of insulation.

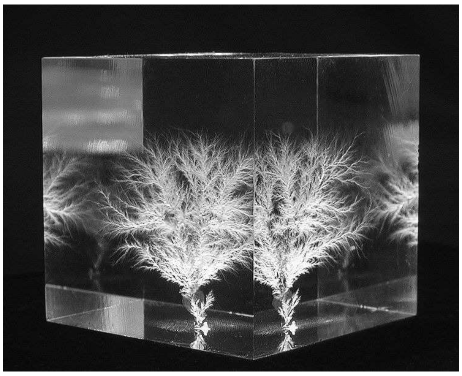

Figure 1: An electrical tree grown in a cube of Polymethyl Methacrylate (PMMA) [2]

Metallic protrusions into the insulation along the electrical/insulation interface, embedded particles in the insulation and water trees initiate electrical trees in insulation under high electric field conditions. Severely aged partial discharge defects also initiate electrical trees in the final phase of progression to complete insulation failure.

In the design and development of high voltage equipment, the knowledge of endurance capabilities of the insulation is essential. In that regard there has been sustained efforts in research to understand the electrical treeing phenomenon in solid electrical insulation.

This paper presents a review of various key aspects in treeing knowledge accumulated thus far. A significant body of knowledge on electrical treeing has been built up through many years of research and field experience. There is however need to continue research on treeing mechanisms in insulation especially in view of the need to keep up to speed with contemporary power system performance requirement.

2. ELECTRICAL TREEING MECHANISMS

Localised stress enhancement is a precondition for tree inception. Depending on the type of insulation defect causing the stress enhancement, different types of electrical trees occur. Typical insulation defects that initiate electrical trees are as illustrated in Figure 2 [3]. Once initiated electrical trees progressively propagate from the point of initiation until the insulation is completely bridged. The trees will eventually cause a complete short circuit.

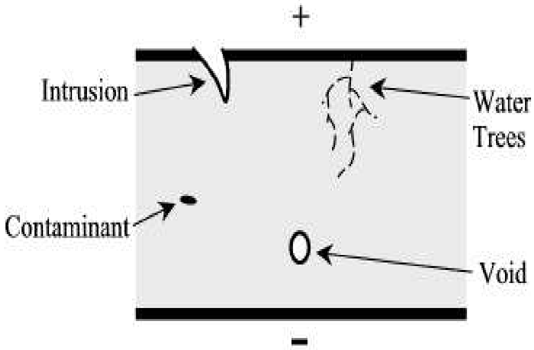

Figure 2: Illustration of the causes of electrical treeing

2.1 Tree inception mechanism

The electric field strength around a stress enhancement body or feature can be orders of magnitude bigger than that in the host insulation. For a needle-plane electrode configuration (simulating a conductive protrusion into the insulation), the maximum Laplacian electric field strength at the needle tip is given by equation 1 [4].

$$E_{\max} = \frac{2V}{r\ln\left(1+\frac{4d}{r}\right)} \qquad (1)$$

Where;

V is the applied voltage [kV_{rms}],

r is the needle tip radius [μm],

d is the gap between the needle tip and grounded plane electrode [mm].

As an example, for an insulation gap of 3 mm, defect tip of 5 μm and voltage across the electrode of 20 kV, the maximum field strength at the needle tip would be about 1 000 kV/mm compared to the background field strength of 6.7 kV/mm. At such high electric field, electrons that may be present in the insulation gain energy and accelerate towards or away from the needle tip depending on the polarity of the electric field as illustrated in Figure 3. The highly energetic electrons, having extracted energy from the field, bombard the insulation molecules and impart energy. This damages the molecular structure by weakening the links between the molecules [5]. The process may result in molecular bond scission creating microchannels in the insulation. The phenomenon also emits optical energy known as electroluminescence [5].

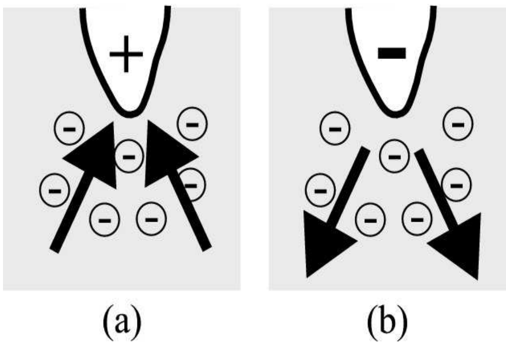

Figure 3: The electron motion for intrusion with overall (a) positive charge and (b) negative charge

If the voltage across the electrodes is alternating, electric charge is repeatedly injected and extracted increasing the damage susceptibility of the molecular structure. This damage explains why some materials, such as Cross-Linked Polyethylene (XLPE), are especially susceptible to treeing. XLPE's dielectric strength is in its cross-linked molecular bonds. Damage to these cross-links will literally weaken the molecular structure.

2.2 Propagation stage

Once a tree has been initiated, gas molecules migrate into the micro-tubules. Partial discharges (PDs) are initiated in these microtubes. The PDs are micro gas explosions and the energy from this activity further erodes the microchannel surface consequently widening and elongating the tree channels. The wider and longer channels support bigger PDs. The increase in PD activity feeds into further propagation, forming a reinforcement cycle until the final failure stage is reached [1].

The manner in which the tree propagates into the insulation is both deterministic and probabilistic. Consequently researchers have used combinations of deterministic and probabilistic techniques to simulate the propagation of electrical trees in insulation [6-8].

2.3 Failure stage

Once the tree has spread far enough into the insulation, complete breakdown is guaranteed. It is however noted that some researchers have observed the trees completely bridging the insulation but complete failure not occurring immediately [9], and this is attributed to the probabilistic behaviour of the treeing mechanisms. Similarly some cases only require the trees to reach a certain threshold length beyond which complete short circuit failure will occur. In any case however, once a tree has started to form, eventual failure is guaranteed and is generally not far into the future and in some cases, as little as 1 hour. The time to failure duration is primarily dependent upon the stress, insulation material and distance between conductors.

3. ELECTRICAL TREE TYPES

Among many ways of classifying electrical trees by types, the most common classification is by shape. The treeing pattern is a function of the type of defect initiating the trees, the electric field strength, type of the insulation and type of the voltage across the electrodes.

Bush trees: Bush trees are very similar in shape to their namesakes. The micro-tubules form multiple exits from the geometrical stress enhancement body, instead of one focused root. A bush tree is characterised by a multitude of short micro-tubules clustered around the stress enhanced region as illustrated in Figure 4a. Bush trees commonly occur under relatively high electric field strength [1]. The partial discharge signals associated with bush tree types are characterised by dominant relatively small pulse magnitude.

Branched trees: Branched trees are almost the opposite of bush trees. They comprise of both short and long branches extending into the insulation from the point of initiation. The PDs associated with branched electrical trees comprise of both big and small discharge magnitudes. Conditions conducive to the growth of branched electrical trees include relatively low electric field strength.

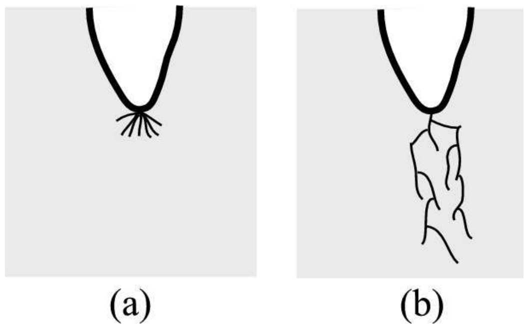

Figure 4: Micro-patterns of (a) bush and (b) branched trees

Bush-Branch trees: There are cases where the tree growth conditions favour both bush and branched trees such that the resulting tree shape is a combination of bush and branch trees and is therefore named bush-branch tree type as illustrated in Figure 5.

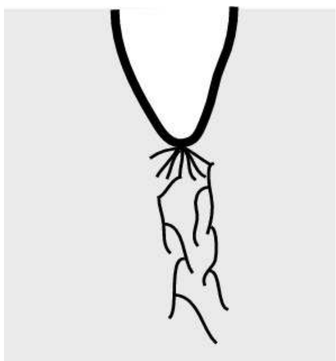

Figure 5: Combination of bush and branched trees

Bowtie trees: Bowtie trees generally form around a solid contaminant embedded in the insulation. The trees initiate and progress towards both electrodes as illustrated in Figure 6.

Electrical treeing mechanisms emit optical and electromagnetic energy. Detection and analysis of the emitted energy gives information about the treeing process. PD detection techniques are used to detect the electromagnetic energy in electrical trees [1]. Electrical treeing PD signals are however typically small such that detection is only feasible under laboratory conditions and mostly impossible in field conditions. An example of tree PD phase-resolved pattern detected by the authors in epoxy resin is showed below in figure 7.

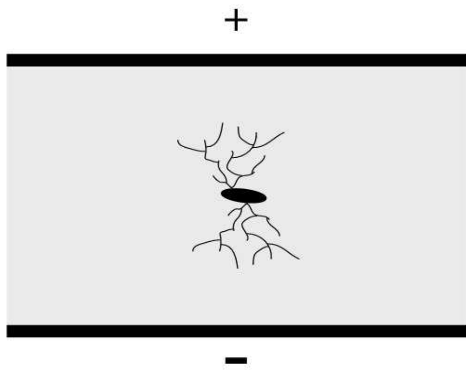

Figure 6: A bowtie tree initiated due to a contaminant

4. ELECTRICAL TREE DETECTION

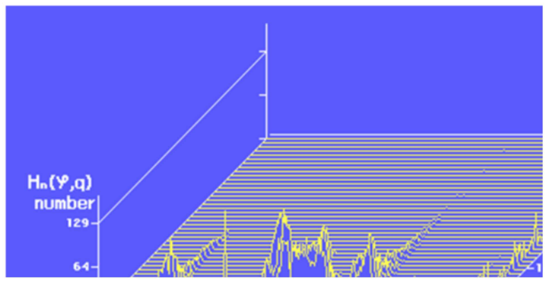

Figure 7: A three dimensional PD phase-resolved pattern of electrical trees in an epoxy resin needle to plane electrode setup.

Partial discharge signals in electrical trees are typically erratic in repetition and magnitude and this is due to physiochemical processes associated with PD mechanisms. The PD activity alternatively extinguish for some period and reignite cyclically as the tree evolve from inception to complete failure. Figure 8 shows an example of tree partial discharge magnitude variations over the tree life from inception to complete failure. In the Figure, it is evident that the PD magnitude initially started at about 20 pC and progressively decreased to complete extinction in 2 hours. It remained extinct for the next 5 hours after which it reignited but with an average magnitude of 2 pC for 7 hours. In the last 6 hours of the tree life the PD magnitude reached a magnitude of 140 pC before complete failure. The insulation in this case was a nanocomposite epoxy (AlO_3/epoxy) [10].

In addition to optical and PD detection, photographic techniques are also widely used to record electrical trees. An example of an electrical tree grown in Perspex by the authors is shown in Figure 9. Various image processing techniques such as fractal dimensions are used to extract useful information from tree images. A major shortfall with photographic imaging techniques of tree detection is in that the insulation has to be transparent. In that regard, recently, some researchers at the University of Manchester reported promising results on the development of an x-ray based tree imaging technique that can 'see trees' through non-transparent insulation [11].

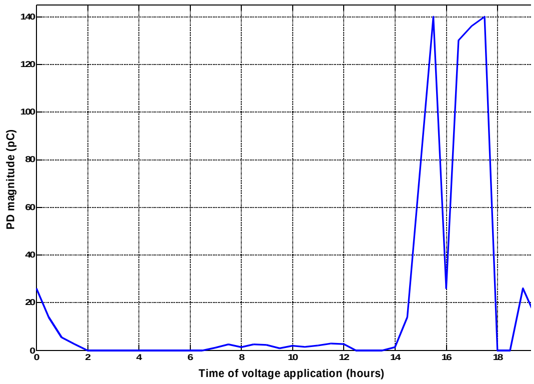

Figure 8: An example of electrical tree PD magnitude variations over the whole tree life [10].

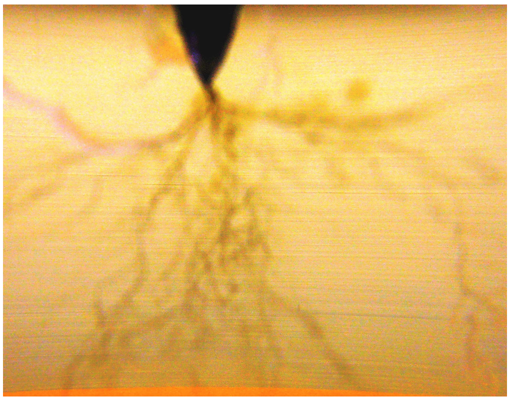

Figure 9: A microscopic photographic image of an electrical tree grown in Perspex.

5. THE FUTURE IN ELECTRICAL TREE RESEARCH

It is now generally agreed that contemporary and future research trends in the electric power industry are largely dictated by the need to use higher voltages, miniaturisation of equipment, more stringent reliability requirements and cost effectiveness [12]. Since electrical treeing endurance is a key insulation performance parameter, the phenomenon has to be well understood as a prerequisite for designing and developing electrical insulation that meets the increasing performance demand of modern power systems. Consequently electrical tree endurance performance in existing insulation designs are being continuously studied with the aim of devising performance improvement. Furthermore where new insulation is being developed such as nanocomposite electrical insulation, electrical tree studies have become an important tool in the research and development of the insulation [13].

6. CONCLUSION

While significant knowledge on electrical treeing phenomenon has been generated through research worldwide, the ever increasing quality demands in the power industry entail further research in the treeing phenomenon. In development of new insulation such as nanocomposites, electrical treeing research is further motivated.

7. ACKNOWLEDGMENT

The authors would like to acknowledge with gratitude Eskom for their support of the High Voltage Engineering Research Group through TESP. They would also like to express gratitude to the Department of Trade and Industry (DTI) for THRIP funding and to thank the National Research Foundation (NRF) for direct funding of the research group.

8. REFERENCES

[1] L. A. Dissado, "Understanding Electrical Trees in Solids: From Experiment to Theory", *IEEE Transactions on Dielectrics and Electrical Insulation*, Vol. 9, No. 4, pp. 483-497, August 2002.

[2] Bert Hickman, "A 3D Electrical tree image" http://en.wikipedia.org/wiki/File:ElectricalTree1.jpg last accessed 4 December 2012

[3] F. H. Kreuger, Partial discharge detection in high-voltage equipment. London: Butterworths, 1989.

[4] L. Cisse, S.S. Bamji and A.T. Bulinski, "Electric field calculations for needle-plane geometry and space charge in polyethylene", *IEEE Transactions on Dielectrics and Electrical Insulation*, Vol. 10, No. 1, 2003

[5] T. Tanaka, "Charge Transfer and Tree Initiation in Polyethylene Subjected to ac Voltage Stress", *IEEE Transactions on Electrical Insulation*, Vol. 27, No. 3, pp. 424-431, June 1992.

[6] K. Wu, Y. Suzuoi and H. Xie, "Model for partial discharges associated with treeing breakdown: I. PDs in tree channels", *Journal of Physics D: Applied Physics*, Vol. 33, No. 10, pp. 1197-1201, 2000.

[7] K. Wu, Y. Suzuoi and H. Xie, "Model for partial discharges associated with treeing breakdown: II. Tree growth affected by PDs", *Journal of Physics D: Applied Physics*, Vol. 33, No. 10, pp. 1202-1208, 2000.

[8] K. Wu, Y. Suzuoi and H. Xie, “Model for partial discharges associated with treeing breakdown: III. PD extinction and re-growth of tree”, *Journal of Physics D: Applied Physics*, Vol. 33, No. 10, pp. 1209-1218, 2000.

[9] T. Tanaka, “Comprehensive understanding of treeing V-t characteristics of epoxy nanocomposites”, *Proceedings of the 17th International Symposium on High Voltage Engineering (ISH)*, paper No. E-008, Hannover, Germany, 2011.

[10] C. Nyamupangedengu, R. Kochetov, P. H. F. Morshuis and J. J. Smit: “A Study of Electrical Tree Partial Discharges in Nanocomposite Epoxy”, *IEEE Conference On Electrical Insulation and Dielectric Phenomena*, Delta Centre-Ville Montréal, pp. 912-915, October 2012.

[11] R. Schurch, S. M. Rowland, R. S. Bradley and P. J. Withers: “A Novel Approach for Imaging of Electrical Trees”, *IEEE Conference on Electrical Insulation and Dielectric Phenomena*, Delta Centre-Ville Montréal, pp. 593-604, October 2012.

[12] H Okubo, Enhancement of electrical insulation performance in power equipment based on dielectric material properties”, *IEEE Transactions on Dielectrics and Electrical Insulation*, Vol. 19, No. 3. pp733-754, 2012.

[13] M.G. Danikas and T. Tanaka, “Nanocomposite – A review of electrical treeing and breakdown”, *IEEE Electrical Insulation Magazine*, Vol. 25, No. 4, pp. 19-25, 2009.

Appendix C

ISH 2013 PUBLICATION

A paper that analysed the results from similar experimentation on 2 %wt MgO, Si_2O and Al_2O_3 was published in ISH 2013 conference proceedings and is presented in this appendix. This paper also presented the first case of the detection methodology and the classes that were extracted from the data.

ELECTRICAL TREE PARTIAL DISCHARGE CHARACTERISTICS IN EPOXY NANOCOMPOSITES

D. R. Cornish[1*] and C. Nyamupangadengu[1]
[1]School of Electrical & Information Engineering, University of the Witwatersrand, Johannesburg, Private Bag 3, Wits 2050, Johannesburg, South Africa
*Email: darryn.cornish@students.wits.ac.za

Abstract: The behaviour of electrical trees in 2 %wt SiO_2 and Al_2O_3 nano-composite epoxy from inception to total failure was studied using PD detection techniques. It was observed that the PD signals were characterised by distinct groups of small and uniformly sized PD pulses as well as significantly bigger and random pulses. The combination of these types of PD pulses that represent bush and branch tree types respectively changed distinctly as the treeing process progressed from inception to total breakdown. Postulations of the observed behaviour are presented and confirm the understanding that nano-particles influence the behaviour of electrical trees in nano-composites.

1. INTRODUCTION

Nano-composite electrical insulation is set to be the new generation technology in electrical insulation [1]. Knowledge in nano-composite insulation however is still immature and this is testimony to the worldwide high level research activity in various aspects of nano-composite electrical insulation technology [2]. To date, significant strides have been achieved in characterising, optimising and developing various types of nano-filled electrical insulation. It has been reported that in some industrial applications, nano-composite insulation usage in electrical equipment is on the verge of being commercialised [3]. It is anticipated that use of nano-composite insulation results in better technical, environmental and economic performance of equipment.

Among other essential electrical insulation characteristics, endurance to electrical treeing degradation phenomena is a key performance criterion of insulation. In this regard, whilst electrical treeing phenomena in conventional insulation is reasonably well understood [4], knowledge on electrical treeing mechanisms in nano-composites is still in its infancy [5]. Furthermore treeing studies on various nano-composite insulations have been done through photographic imaging of the electrical trees as they grow from inception through propagation phases to total failure. Useful knowledge has been built up through such treeing study methodologies but is only limited to transparent insulation. When transparent insulation (such as some type of clean epoxy and polyethylene) is filled with nano-particles, the resultant insulation can be non-transparent and this can make it difficult to study treeing phenomena in the insulation using photographic techniques. Partial discharge (PD) detection of electrical trees has an advantage over other tree detection methods in that the insulation doesn't need to be transparent. PD technology therefore becomes effective in studying electrical trees.

This paper presents noticeable features in the PD signal behaviour as electrical trees in 2 %wt SiO_2 and Al_2O_3 nano-composite epoxy grow from inception to complete breakdown.

2. THE EXPERIMENTAL WORK

2.1 Sample preparation

The test samples used in this work were prepared at the Technical University of Delft (TU Delft) in the Netherlands. The procedures that were followed in the nano-particles' surface conditioning, dispersion into the host epoxy (Huntsman™ type CY231 with hardener type HY925), and curing are detailed in reference [6]. In essence, precautions were taken to ensure that the nano-fillers were uniformly dispersed in the epoxy. Transmission Electron Microscope (TEM) images were analysed to confirm uniform dispersion of the nano-fillers. The test samples comprised of 5 μm tip radius Ogura™ needle cast in epoxy to form a needle–plane electrode configuration with an insulation gap of 3 mm between the needle tip and grounded flat plane. To ensure good contact with the grounded plane electrode the bottom surface of the test sample was painted with conductive silver paint. More information on the test samples is depicted in Figure 1.

2.2 Test configuration

The standard PD measurement set up in accordance with the IEC60270 was used in measuring tree partial discharges generated in the needle-plane electrode test samples as shown in Figure 2.

The test sample was immersed in insulating oil to avoid flashover and spurious discharges. The coupling of the needle to the high voltage source was carefully designed to prevent corona and other unwanted discharges in the test voltage range. The supply voltage was gradually

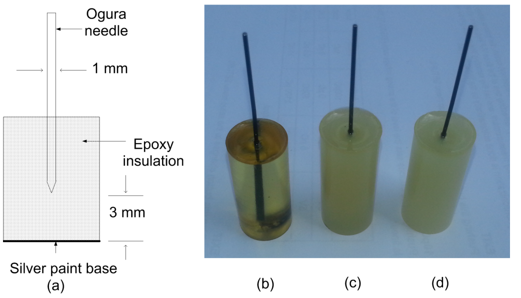

Figure 1 : Sample schematic (a) and examples of the test samples; (b) clean epoxy, (c) SiO_2 and (d) Al_2O_3,

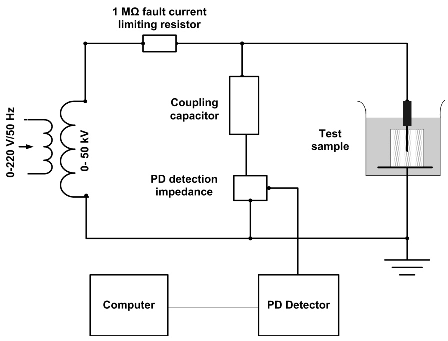

Figure 2 : The electrical tree PD detection configuration

raised until PD signals were detected above the background noise level; about 0.3 pC in the screened high voltage laboratory environment. The partial discharge signals were continuously logged every second using the Power Diagnostics ICMcompact^{TM} PD detection instrument. PD quantities such as mean (Q_{avg}), maximum (Q_{max}) and minimum (Q_{min}) magnitudes in every second were continuously logged. Furthermore the corresponding PD Phase Resolved Pattern (PDPRP) images were continuously recorded as a video from inception to total breakdown. Three samples each of 2 %wt Si_2O_3 and AlO_2 were tested. For comparison purposes, similar measurements were performed on a clean epoxy sample.

3. RESULTS AND DISCUSSION

In the nano-composite samples the average PD inception voltage was 16 kV compared to 11 kV in the clean epoxy. Examples of typical scatter plots of the average PD magnitudes over the entire tree life are shown in Figure 5 and 6. The scatter map of the treeing PD magnitudes can be divided into distinct categories as follows:

Category A: The discharges start relatively small, uniformly sized and gradually grow in magnitude and quantity. This category lasts for about an hour. Typical PDPRP in this category is as shown in Figure 3.

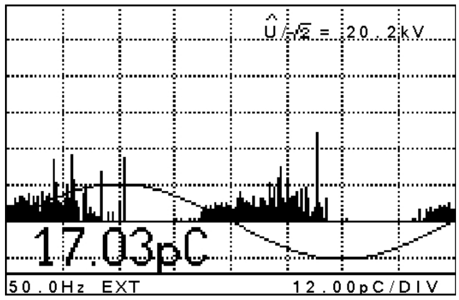

Figure 3 : PDPRP plot of a Category A PD pattern

It is suggested that the corresponding trees in Category A are mainly bush tree type initiated around the needle tip. The trees comprise of short branches thus supporting small PD discharges. The small branches however gradually grow in length and quantity and exhibit gradually increasing PD activity as shown in Figure 3.

Category B: After about an hour into tree growth since initial inception much bigger and erratic PD pulses occur together with much smaller and more uniformly sized pulses. The corresponding typical PDPRP is shown in Figure 4. This category lasts in the order of 2 hours. It is suggested that in this phase of tree development, the tree comprises of many short tunnels as well as much longer tunnels (bush/branch tree type) where small and large PD occur respectively.

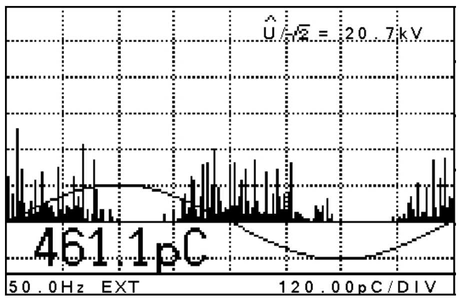

Figure 4 : PDPRP plot of a Category B PD pattern

Category C: The big PD pulses eventually disappear and the PD signals are mainly dominated by the smaller PD types that further diminish in number. In this phase of tree propagation, it is suggested that the nano-particles block progression of tree tunnels. Pressure changes and chemical PD by-products cause drop in electric field strength in the trees, thereby inhibiting PD activity. Typical PDPRP in Category C is as shown in Figure 7.

Category D: The PD restraining conditions get worse such that PD activity completely ceases for a couple of hours. An example of the PDPRP in Category D is as

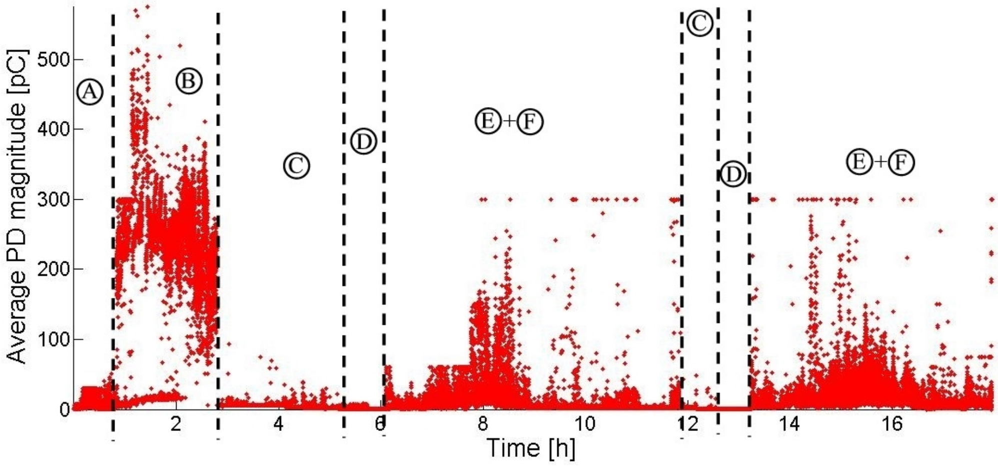

Figure 5 : Time evolution plot of 2 %wt Al_2O_3 epoxy sample

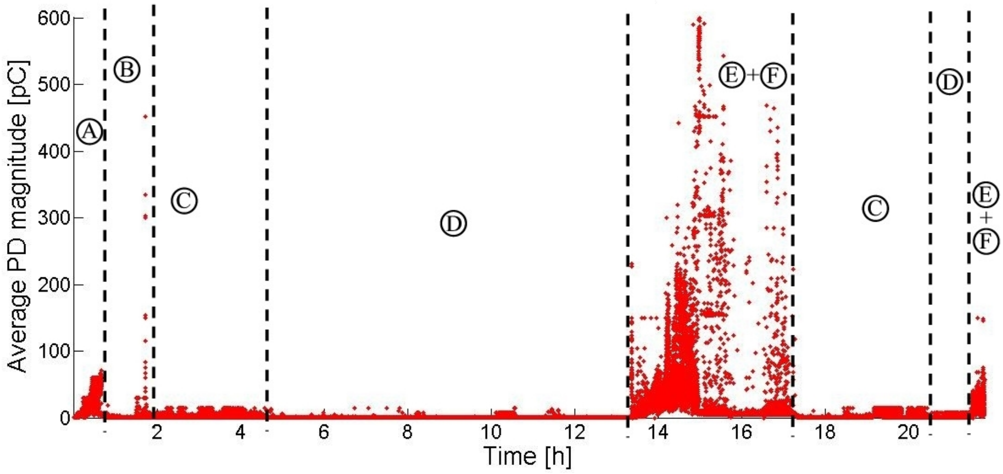

Figure 6 : Time evolution plot of 2 %wt SiO_2 epoxy sample

shown in Figure 8.

Category E: After a period of absolute or quasi-'quietness', the partial discharge activity resumes. This time however the discharges are characterised by random big pulses in the positive half cycle and uniformly sized smaller pulses in the negative half cycle of the AC supply voltage as depicted in Figure 9. The Category E partial discharges can be termed 'corona-like'.

It is postulated that one of the reasons of PD extinction in Category D is because the tree branches would have encountered blockages due to nano-particles stationed in their growth paths.The blocked channels are further short circuited by conductive liquid PD by-products. The needles therefore effectively become extended to the tips of the blocked tree tunnels. Due to electric field enhancement around the micro-tunnel tips, new treeing activity develops. The air-filled new micro-tunnels

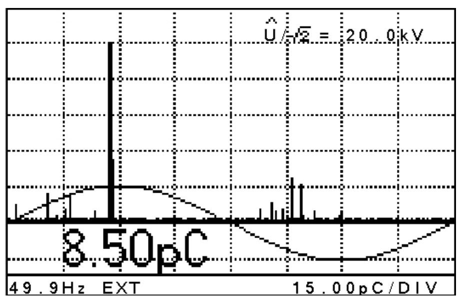

Figure 7 : PDPRP plot of a Category C PD pattern

and the carbonised old tunnels effectively form needle–plane electrode systems that give the 'corona-like' PD pulses as observed. Unlike in open air, the corona-like PD pulses are shifted away from the supply voltage

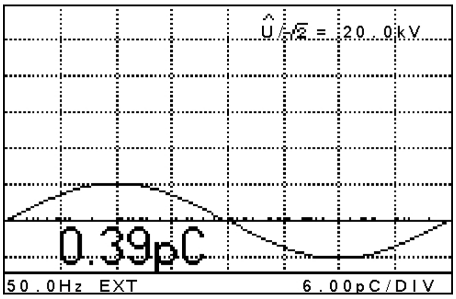

Figure 8 : PDPRP plot of a Category D PD pattern

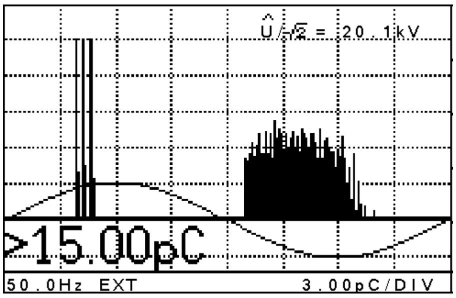

Figure 9 : PDPRP plot of a Category E PD pattern

positive and negative crests and this is due to the effect of charge retaining walls of the tree tunnels. The observed behaviour of PD in this phase of tree propagation suggests a model of PD in nano-composites as illustrated in Figure 10 [7]. The model however needs to be further confirmed through non-PD based measurements and observations of the treeing phenomenon in nano-composites.

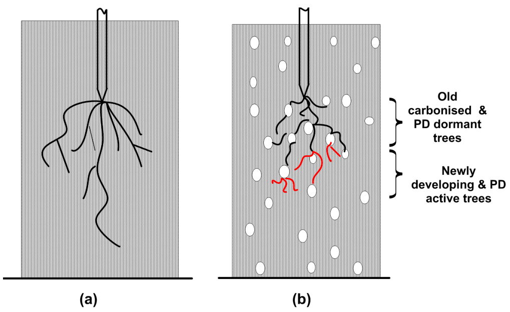

Figure 10 : Electrical tree growth models in (a) clean epoxy and (b) nanocomposite epoxy illustrating the blocking effect of nano-particles [7]

Category F: The micro-tubules giving 'corona-like' PD grow further into bush/branch trees that generate small and big PD pulses as in Category B. This phase can last a couple of hours in which the sample can fail. If the sample does not fail soon enough, the tree process can repeat the transitions back into Category C-D-E and repeat until total breakdown.

In clean epoxy only tree growth categories A and B exist as shown in Figure 11. Similarly where a nano-composite test sample failed much earlier than expected, the PD magnitude map looked similar to that of clean epoxy as depicted in Figure 12.

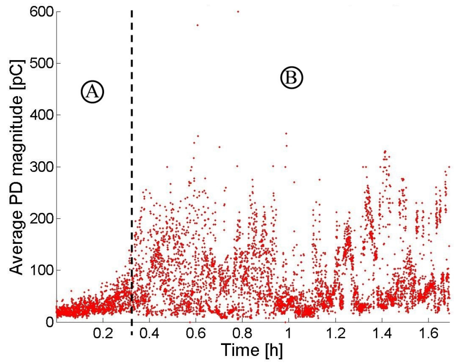

Figure 11 : Time evolution plot of clean epoxy sample

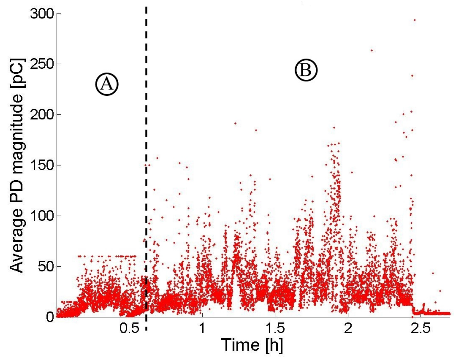

Figure 12 : Time evolution plot of 2 %wt SiO_2 epoxy sample that failed prematurely

Furthermore, the nano-composite, whilst being similar, shows a slight bias towards the low magnitude PDs. This could be attributed to the statistical nature of the treeing mechanisms and/or low level doping causing only a slight effect on the PD time evolution pattern. Experiments with different doping levels are necessary to confirm this postulate and may offer further insight into the modelling of electrical trees.

4. FUTURE WORK

The future work seeks to be both a confirmation and extension of these results. The authors are currently procuring the resources necessary to manufacture nano-composite insulation materials. These resources range from nano-particles (in different shapes and sizes), Ogura treeing needles and host insulation. Further the manufacture process will be such that there will be uniform dispersion of the nano-particles. Variation of nano-filler doping levels is also of extreme interest as well as the use of other types of nano-particles.

Good nano-composite manufacturing capabilities also offer the possibility of experimenting with the known effects of nano-particle doping applied to insulation to try produce unique combinations of properties. This includes the manufacture of fire-proof dielectrics with strong insulation properties. The mechanical and chemical disciplines have already found numerous advantages from nano-particle doping thereby generating excitement about the possibilities for their electrical properties.

With regard to electrical treeing, it would be interesting to extend the work reported in this paper into studying and correlating the treeing PD evolution trends using other methods of studying tree progression mechanisms - such as x-ray imaging of the trees [8].

5. CONCLUSION

Electrical tree partial discharges in nano-composite epoxy show distinct behavioural changes as the trees progress from inception to total breakdown. Partial discharge detection has a potential of being a useful means of characterising tree mechanisms in nano-composite insulation. Further research is necessary to expand and solidify these results, however the results as they stand show promise in extending the understanding of electrical treeing as a phenomena.

ACKNOWLEDGEMENTS

Professor J.J. Smit and his team at Technical University of Delft in the Netherlands, where the test samples where manufactured, are gratefully acknowledged. Sincere gratitude is extended to the Carnegie Corporation of New York for financial support that enabled the research collaboration with Technical University of Delft. In South Africa, Eskom and the National Research Foundation (NRF) are gratefully acknowledged for their continued support of the high voltage engineering research work at the University of the Witwatersrand, Johannesburg.

REFERENCES

[1] M. Frchette, M. Trudeau, H. D. Alamdari, and S. Boily. "Introductory remarks on Nanodielectrics." *IEEE Transactions on Dielectrics and Electrical Insulation*, vol. 11, pp. 808–818, 2004.

[2] T. Tanaka, A. Bulinski, J. Castellon, M. Frchette, S. Gubanski, J. Kindersberger, G. Montanari, M. Hagao, P. Morshuis, Y. Tanaka, S. Plissou, A. Vaughan, Y. Ohki, C. Reed, S. Sutton, and S. Han. "Dielectric properties of XLPE/SiO_2 nanocomposites based on CIGRE WG D1.24 cooperative test results." *IEEE Transactions on Dielectrics and Electrical Insulation*, vol. 18, pp. 1484–1517, 2011.

[3] J. Weidner, F. Pohlmann, P. Groppel, and T. Hildinger. "Nanotechnology in high voltage insulation systems for turbine generatorsfirst results." In *XVII Internataional Symposium on High Voltage Engineering, Hannover Germany*. 2011.

[4] L. A. Dissado. "Understanding Electrical Trees in Solids: From Experiment to Theory." *IEEE Transactions on Dielectrics and Electrical Insulation*, vol. 9, pp. 483–497, 2002.

[5] M. Danikas and T. Tanaka. "Nanocomposite A review of electrical treeing and breakdown." *IEEE Electrical Insulation Magazine*, vol. 25, pp. 19–25, 2009.

[6] C. Nyamupangedengu, R. Kochetov, P. H. F. Morshuis, and J. J. Smit. "A Study of Electrical Tree Partial Discharges in Nanocomposite Epoxy." *2012 Annual Report Conference on Electrical Insulation and Dielectric Phenomena (CEIDP)*, vol. 1, pp. 912–915, 2012.

[7] T. Tanaka. "Comprehensive understanding of treeing V-t characteristics of epoxy nanocomposites." In *Proceedings of the 17th International Symposium on High Voltage Engineering (ISH), Hannover, Germany*. 2011.

[8] R. Schurch, S. Rowland, R. Bradley, and P. Withers. "A novel approach for imaging of electrical trees." *Annual Report Conference on Electrical Insulation and Dielectric Phenomena (CEIDP)*, pp. 593–596, 2012.

Appendix D

SAUPEC 2014 PUBLICATION

A paper that analysed the results from similar experimentation on 0.5 %wt, 2 %wt and 5 %wt MgO was published in SAUPEC 2014 conference proceedings and is presented in this appendix. This paper also further expanded upon the model and classification scheme that was developed in the previous paper.

CHARACTERISING ELECTRICAL TREES IN MGO/EPOXY NANOCOMPOSITE INSULATION THROUGH PD MEASUREMENTS

D. R. Cornish* and C. Nyamupangadengu*

*School of Electrical & Information Engineering, University of the Witwatersrand, Johannesburg, Private Bag 3, Wits 2050, Johannesburg, South Africa

Abstract: Nanocomposite insulation provides a new possibility for enhancing the quality of of conventional insulations. This is desirable as most solid insulation is vulnerable to the phenomenon of electrical treeing. Any technology that can retard electrical trees would be beneficial. The effect on electrical teeing of varying levels of MgO nanofiller in an epoxy host material is tested using PD detection techniques. From the results of the experiments, a model is proposed that to add value to the recent models in the literature. Furthermore the data is analysed in an attempt to detect trends between filler levels, which can be tested on other nanofiller materials.

Key words: Nanocomposite, Electrical Tree, Partial Discharge, MgO Epoxy

1. INTRODUCTION

With the advent of solid insulation material, many of the biggest problems in cable insulation were solved: mainly with regards to ease of repair, weight and flexibility concerns. Susceptibility to electrical treeing is however still a problem. This has caused a concerted push in research concerning nanocomposite insulations which is currently occurring throughout the world. The success of first microcomposite materials and nanocomposite technology in construction materials have shown promising possibilities in material properties modification [1]. A major focus for the research community is electrical treeing: either its eradication or at least significant reduction in effects through nanocomposite technology. Nanocomposite insulation technology is however still in its infancy, with the actual electrical treeing mechanism still not fully understood [2]. Furthermore multiple nanoparticle materials are under investigation. Nanocomposite research also serves as a platform to re-evaluate the electrical tree models with a view towards conformation of both conventional insulation and the newer nanocomposite insulation. in that regard, an investigation into the effects seen with differing nanofiller levels of MgO in a host epoxy resin has been undertaken. This is done through electrical tree characterisation using Partial Discharge (PD) time evolution graphs and Phase Resolved PD Patterns (PRPDPs). This information is then analysed for trend data and a model for the time evolution of the electrical tree is proposed and contrasted with existing models.

2. BACKGROUND

Of the modern solid insulation materials, Cross Linked PolyEthylene (XLPE) has proven to be tough, flexible, relatively light and a strong dielectric material compared to other options. The reasons for its strength, the cross linking between polymer chains, is also its greatest weakness in some ways. These cross-links are highly susceptible to damage from high electric field stress. This results in XLPE failing mere hours after an electrical tree has been initiated. It is a weakness almost all rubber based solid insulation face due to the way the polymer chains interact. It has also been found that electrical treeing is essentially the final failure mode of all insulation in some form or another [2].

Nanocomposite insulations may be a relatively new field but it has attracted the attention of many researchers worldwide. Most researchers are currently working with epoxy resin as the host material for several reasons such as simple manufacture procedure and it is still used throughout industry for jointings, motor and generators to name a few. Once the behaviours have been fully understood, the effects should correlate to more complex host materials such as XLPE.

2.1 Interface models

There are several models that have been developed to explain the modifications seen with nanocomposite material but the most recent and appropriate models are the Polymer Chain Alignment Model (PCAM) [3] and the recently proposed failure model proposed by Tanaka [4].

in the PCAM model, the nanoparticles act as anchor points which cause an interface region to be formed [3]. The interface region can be regarded as polymer strands radiating out from the nanoparticle due to the oxide hydroxide bonds that form. This interface region is also posited to exist around microparticles in microcomposite insulation and is thought to be the reason for the beneficial effects seen in composite insulations. Lewis has further modelled the interface region for both microcomposites and nanocomposites and shown that the interfacial volume of a nanoparticle is much greater than the microparticle interface volume [5]. This interface region is also hypothesised to act as a hole-electron recombination point [3], which may explain many of the beneficial effects. These long polymer strands that are not roughly parallel to the general growth direction of the electrical tree would cause an impediment to the electrical tree growth. This may also force the electrical tree to form around the interface region rather than through it, further delaying the growth rate and allowing the insulation to survive for longer. The much greater interface volume is thought to be what causes the unexpected and stronger effects than is seen in microcomposites [5].

Tanaka recently discovered that an electrical tree can fully bridge the insulation between the electrodes without failure occurring for many hours afterwards [6]. He has further hypothesised with more experimental data that the important aspect to the electrical tree is the width of the microtubules [4]. The electrical tree may breach the insulation but is not yet wide enough to allow for a short circuit to occur. This also implies that the spread rate of the microtubules can be greater than the microtubule widening rate.

In previous work by the authors, the PD time evolution plots were examined for nanocomposite epoxy samples. A PD time evolution plot in this case is the average PD magnitude plotted over entire life of the sample. The patterns displayed common as well as unusual characteristics such as corona-like PRPDPs. The parameter metrics of interest have been chosen as: the time to failure; the peak average PD magnitude; and the mean average PD magnitude. Such data allows detection of trends. The information generated enables the possible explanations of how nanoparticles improve the host material.

3. EXPERIMENTAL PROCEDURE

The samples used for this work were manufactured at TU Delft in the Netherlands. The production procedure is detailed in [7] and summarised as follows. Huntsman™type CY231 epoxy with hardener type HY925 were used for the host epoxy and precautions were taken to ensure uniform dispersion of the MgO nano-filler. The test samples were specifically designed with Ogura™needles that have a well defined 5 μm tip allowing for accurate electric field descriptions to be calculated. The gap distance between the base of the sample and the needle tip was set to 3 mm. This gap was chosen as representative of the distance between two conductors in a cable. Finally to ensure a smooth surface on the plane electrode, a silver conductive paint was applied to the bottom of the samples. A diagram of the general sample construction is shown in Figure 1.

The experiment was designed in accordance with the IEC 60270 standard's PD measurement circuit. The PD data is logged continuously using a computer throughout the process. The sample was connected to the test circuit using a customised connector to smooth all sharp points and avoid all possible corona and PDs except those inside the sample. As a final countermeasure to spurious PDs outside the area of interest, the sample is submerged in transformer oil. The voltage applied to the sample was slowly increased to the applied voltage, $V_{app} = 20\ kV_{RMS}$ and maintained until breakdown occurred. It is noted that the noise level within the testing environment is approximately 0.3 pC.

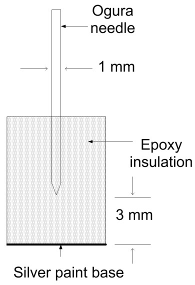

Figure 1 : Diagram of test sample structure.

4. RESULTS AND OBSERVATIONS

As the focus of this paper is on the characteristics of varying levels of MgO nanofiller in epoxy, there are several parameters that need to be analysed. Firstly, each nanofiller level will be analysed using a categorisation system. This will be done using PD time evolution graphs correlated with the recorded PRPDPs. Secondly the data will be quantified, compared and contrasted between different nanofiller levels to allow for analysis of any possible trends that may occur. From this analysis a refinement of the previously mentioned model is presented based on the new data and information.

4.1 Categorisation of electrical tree PD data

The nanofiller levels of the MgO used in the experiment were 0 % (clean or neat epoxy), 0.5 % by weight (%wt), 2 %wt and 5 %wt.

In a previous paper by the authors, a categorisation scheme was developed for the PD time evolution plots [8]. A brief description of this categorisation scheme is given below. It is noted that the PD time evolution behaviour is correlated with the PRPDP to further categorise the system.

4.1.1 Clean Epoxy: An example of a PD time evolution graph of clean epoxy is shown in Figure 2a. The plot plot the separation into categories A and B, which are further discussed as follows;

- *Category A*: This category represents the initiation phase of the electrical tree and is characterised by a slow, approximately linear increase in the average PD magnitude. This is believed to be due to the intense electric field stress causing an electrical bush tree to form. A typical PRPDP of this category is shown in Figure 3. At around 0.3 hours however, a rapid rise in average PD magnitude presents itself, prompting another category.
- *Category B*: As the electrical bush tree has grown,

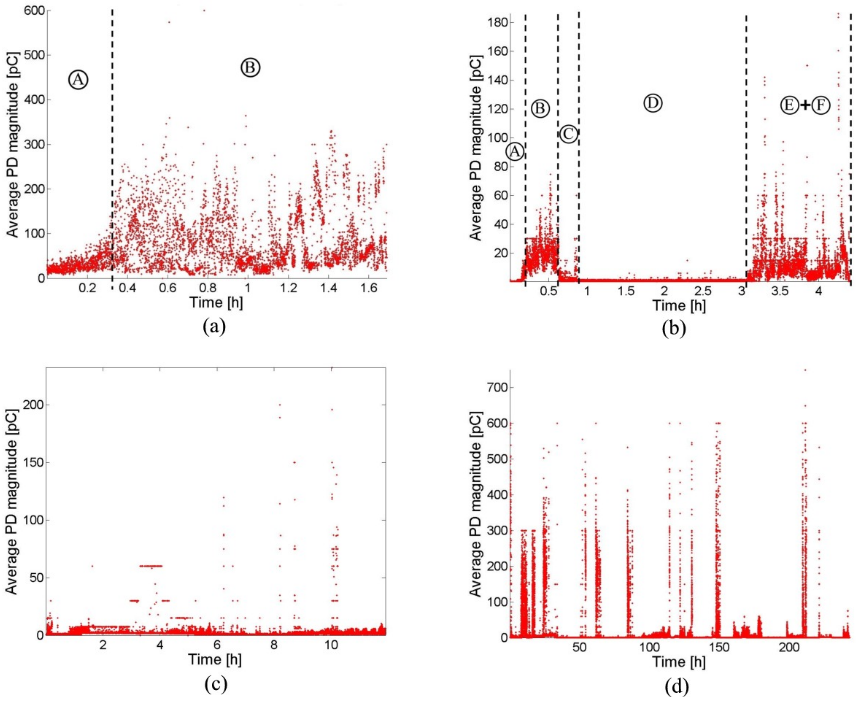

Figure 2 : PD time evolution plots for (a) clean epoxy, (b) 0.5 %wt MgO/Epoxy, (c) 2 %wt MgO/Epoxy and (d) 5 %wt MgO/Epoxy

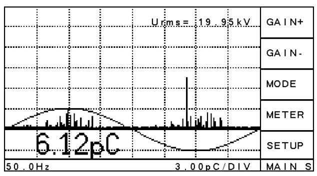

Figure 3 : Example PRPDP for category A.

it is theorised that an electrical branch tree has developed allowing larger PDs to occur. This phase is characterised by a rapid increase in the large PD magnitude. It should be noted that the small PD magnitudes are still present but are averaged out by the occurrence of so many large PDs. This can be seen from the PRPDPs for this time period as shown in Figure 4. This can be explained by the bush trees still experiencing PDs.

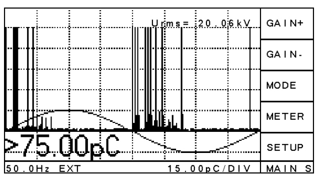

Figure 4 : Example PRPDP for category B.

Once the electrical branch tree has grown large enough, category B PD behaviour continues to occur until failure of the sample is reached. The PRPDPs are as expected for typical PDs in both categories, with the PDs occurring on the rising and falling edges of the sinusoid.

4.1.2 0.5 %wt MgO/Epoxy: The plot of PD time evolution plot for a 0.5 %wt filler level of MgO is shown in Figure 2b. As can be seen in Figure 2b, the categorisation marks, categories A and B still occur. This appears to remain true for all the clean epoxy and nanocomposite epoxy samples. This is accounted for by the model that is being developed as the nano-particles are unlikely to affect the initiation of the electrical tree as an electrical bush tree is a necessary first step. The cascade into an electrical branch tree is further unavoidable due to the stress induced by the needle. From that point onwards however nanocomposite insulation differs from standard clean epoxy due to the additional categories that occur.

- *Category C*: This additional category is characterised by a sudden drop to relatively small partial discharges. This loss of the large average PD magnitudes can only occur if the longer tubules of the electrical branch tree, that allow the large magnitudes, have at least partially carbonised. Some of these tubules may also have encountered nanoparticles or the interface region around it which impede progress. Whilst the nanoparticles are much smaller than the tubules, the leading edge of the tubule where propagation occurs is relatively small and may be interrupted by the nano-particle or the dense radial polymer strands close to it. A typical category C PRPDP is shown in Figure 5.

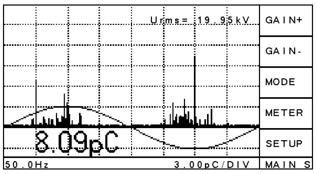

Figure 5 : Example PRPDP for category C.

- *Category D*: This category shows a complete cessation of all partial discharge activity above the noise level. This can only occur if all the tubules have completely carbonised or terminated due to the nanofiller. Figure 6 shows a typical PRPDP for category D.

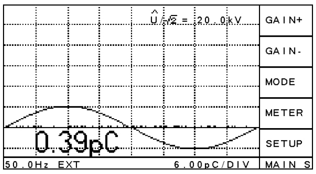

Figure 6 : Example PRPDP for category D.

- *Category E+F*: After category D has started, the stress may be actually increased in the regions where electrical trees have been terminated. This will be discussed further in the next section. As can be seen, no real clustering of data points occurs in the figure implying the spread of average PD magnitudes is more even. The reason for this can be deduced by looking at the PRPDP of the category in Figure 7. The PDPRP displays both PD patterns, that is activity on the rising and falling edges of the sinusoidal voltage, but with typical corona patterns. Corona PDPRPs show most of the activity occurring on the peaks and troughs of the sinusoid. This points to 2 events occurring simultaneously. As the micro-tubules have spread, the nanoparticles and their interfaces may protrude into the micro-tubule along it's length. Due to the protrusions having a different permittivity, as well as possible carbonisation, these protrusions will cause an electric field stress. The stress would cause corona to occur, resulting in widening of the tubule as well as promoting propagation as depicted in Figure 8. This widening causes PD activity to initiate again but with noticeably larger PD magnitudes due to the micro-tubules being wider.

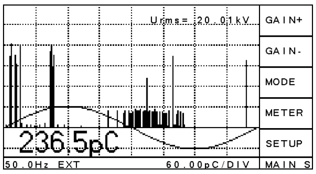

Figure 7 : Example PRPDP for categories E and F.

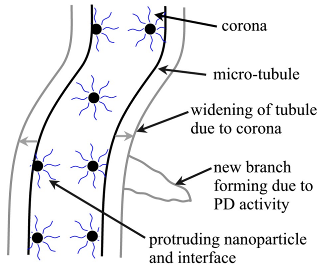

Figure 8 : Model for behaviour in categories E and F with grey depicting effects of corona. Not to scale.

4.1.3 2 %wt MgO/Epoxy: With the 2 %wt samples, similar behaviour was observed. This correlates to the previous paper were 2 %wt of both Al_2O_3 and Si_2O where investigated [8]. As in the previous 0.5 %wt samples, there is a clear pattern in the PD time evolution plot. Categories A and B are present as expected although a rapid drop in magnitude is seen at around 20 minutes before the large PDs start to occur. This can happen if the bush electrical tree carbonises before the branch electrical tree can gain sufficient length. This may also indicate nanoparticles close to the tip of the needle interfering with the growth of the electrical trees. Multiple cycles of categories C through F are visible in Figure 2c. This figure has not been demarcated as the widths are too small to easily mark them out but categories C to F can be seen by applying the system above.

4.1.4 5 %wt MgO/Epoxy: An example of a PD time evolution for the 5 %wt MgO/Epoxy samples is shown in Figure 2d. The 5 %wt sample behaves similar to other nanofiller levels but it is quite clear that more than one cycle of categories C to F can occur. The much longer duration compresses the categories making it difficult to demarcate but the amount of cycles makes the cyclical pattern quite apparent. This correlates with the model described in Section 4.1.2 as categories C to F occur when the electrical tree has encountered nanoparticles. This can be viewed as the electrical tree encountering a 3 dimensional shell layer of nanoparticles. This encounter can happen multiple times as the electrical tree passes the previous nanoparticles and encounters the next layer of nanoparticles. The much longer time to failure is notable for the 5 %wt sample lasted over 10 consecutive days. These observation correlate with

Table 1 : Table of metrics extracted from PD data.

Filler Material	Amount of Filler (% weight)	Sample	Time to failure (h)	Peak average PD magnitude (pC)	Mean average PD magnitude (pC)
Clean Epoxy	0.0	1	1.69	600.00	75.11
MgO	0.5	1	1.21	300.00	19.50
MgO	0.5	2	4.40	186.20	6.70
MgO	0.5	3	0.72	750.00	197.01
MgO	2.0	1	6.66	411.20	106.36
MgO	2.0	2	5.98	445.10	7.22
MgO	2.0	3	11.90	232.40	1.98
MgO	5.0	2	243.37	750.00	2.50

the data presented by colleagues at TU Delft [9].

5. DISCUSSION

Trends can be extracted from categorisations of the PD time evolution, PRPDP behaviours and statistical data from the samples. Table 1 shows the relevant statistical information extracted: time to failure; peak average PD magnitude; mean average PD magnitude; and the standard deviation of the average PD magnitude.

The clean epoxy sample is included here for comparison purposes. Other clean epoxy samples were only tested for time to failure, which when combined with this sixth sample, gives a mean time to failure of 8.74 hours. This is shown in Table 2. The 0.5 %wt samples have a significantly shorter lifespan than the clean epoxy. This may indicate that at these low filler levels, the nanoparticles act as electric field stress enhancements more than impedance to electrical tree growth.

Another interesting trend is the inverse relationship between time to failure and peak average PD magnitude. Most show that larger peaks in the average PD magnitudes give smaller time to failures. This is a small sample size but given the uniformity in behaviour exhibited with categorisation as well as correlation with other literature [8, 9], the behaviour cannot be ignored. More experiments are needed to validate these observations and expand them to other nanofiller materials. Furthermore clean epoxy samples will need to undergo the same experiments to give a firmer control samples to work from.

The 2 %wt samples show a similar time to failure but the 5 %wt show a significant increase from around 9 hours to 10 days before the sample failed. This value is also in keeping with other time to failures of 5 %wt Al_2O_3 and 5 %wt Si_20 from colleagues at TU Delft [9]. More nanofiller levels will need to be investigated to achieve an optimization graph for filler levels and this may vary according to both nanofiller material and the host material.

Table 2 : Table with time to failures of all six clean epoxy samples.

Sample	Time to failure (h)
1	12.0
2	15.5
3	7.0
4	11.0
5	5.26
6	1.69

5.1 Hypothesised electrical treeing model in nanocomposites

The background models point to the reason nanocomposites may be effective in retarding electrical tree formation. In neat or clean epoxy, the electrical tree can easily form between the polymer strands as only the weak Van der Waal's forces between polymer strands needs to be overcome. This is not in conflict with the proposed model as this model may be the underlying micro-model that explains the macro-model behaviour described in this paper.

This categorisation system prompted a model to be developed as delineated in a previous publication by the authors [8]. The most interesting portion of the categorisation section is categories E and F, where corona occurs in an insulation which is beyond expectations. This may be due to the nanoparticles protruding into the micro-tubule acting as a electric field stress enhancement feature. This stress enhancement in the tubule could cause corona which would lead to the micro-tubules widening and propagating further, as the grey depicts in Figure 8, explaining the PD behaviour that occurs simultaneously. This model has however been slightly updated to include Tanaka's conclusions. The model has been delineated above by slowly going through each of the categories and proposing the physical causes behind the recorded behaviour. The behaviour exhibited by the samples is primarily a factor of the interface region, which can impede the widening of the tubules slowing down breakdown. This model also works to explain the cyclical nature of the categories C to F, with each cycle representing a different layer of nano-particles. This also implies that the denser the nanoparticle dispersion, the more pronounced the effects such as increase in time to failure. There would be a turning point however where the interface regions start to overlap and interfere with each other causing gaps through which the electrical trees can spread and clumping of the polymer strands, possibly causing further electric field stress enhancement.

6. FUTURE WORK

Nanocomposite insulation can be considered to only just be entering its adolescence if not still in its infancy. This implies that there are multiple avenues still left unexplored without even considering possible new nanofiller materials. Several avenues of research are of interest to the authors. The two immediate avenues will be on further quantifying the behaviour over multiple filler levels of various materials. An imaging methodology is also still a major area of interest as this would allow at least partial verification of the proposed model. Beyond these focuses, different nanofiller materials outside the current standard materials are continuously being investigated.

7. CONCLUSION

Experiments monitoring the PD behaviour of MgO/Epoxy nanocomposite insulation have yielded very similar results when compared to the same experiments carried out on Al_2O_3 and Si_20. This shows similar treeing mechanisms occurring between materials. Furthermore this behaviour can be categorised and used to model the current stage of the electrical trees. This model does not contradict recently developed micro-models in literature lending credence to it. Trends are visible between different filler levels with the categories being the most obvious. Beyond that, there is a definite variation in time to failure with nanofiller levels. Furthermore once more experiments have been concluded the investigation into the link between peak average PD magnitudes and the associated time to failure may yield interesting developments in the model.

ACKNOWLEDGEMENTS

The authors would like to acknowledge Eskom for their support of the High Voltage Engineering Research Group through TESP. The authors would also like to express gratitude to the Department of Trade and Industry (DTI) for THRIP funding and to thank the National Research Foundation (NRF) for direct funding of the research group. Finally thanks must be given to the Technical University of Delft for their aid and resources in producing the test samples used in the experiments.

REFERENCES

[1] W. Zhu, P. Bartos, and A. Porro. "Application of nanotechnology in construction." *Materials and Structures*, vol. 37, pp. 649–658, 2004.

[2] L. A. Dissado. "Understanding Electrical Trees in Solids: From Experiment to Theory." *IEEE Transactions on Dielectrics and Electrical Insulation*, vol. 9, pp. 483–497, 2002.

[3] T. Andritsch. *Epoxy Based Nanocomposites for High Voltage DC Application - Synthesis, Dielectric Properties and Space Charge Dynamics*. Ph.D. thesis, Technical University of Delft, 2010.

[4] T. Tanaka. "Mechanisms of crossover phenomenon in tree length vs. applied voltage characeteristics between base epoxy and its nanocomposites." In *18th International Symposium on High Voltage Engineering*. 2013.

[5] T. Lewis. "Interfaces are the dominant feature of ddielectric at the nanometric level." *IEEE Transactions on Dielectrics and Electrical Insulation*, vol. 11, pp. 739–753, 2004.

[6] T. Tanaka. "Comprehensive understanding of treeing V-t characteristics of epoxy nanocomposites." In *Proceedings of the 17th International Symposium on High Voltage Engineering (ISH), Hannover, Germany*. 2011.

[7] C. Nyamupangedengu, R. Kochetov, P. H. F. Morshuis, and J. J. Smit. "A Study of Electrical Tree Partial Discharges in Nanocomposite Epoxy." *2012 Annual Report Conference on Electrical Insulation and Dielectric Phenomena (CEIDP)*, vol. 1, pp. 912–915, 2012.

[8] D. Cornish and C. Nyamupangedengu. "Electrical tree partial discharge characteristics in nanocomposites." In *18th Symposium on High Voltage Engineering*. 2013.

[9] R. Kohetov, T. Andritsch, U. Lafont, P. Morshuis, and J. Smit. "Electrical tree propogation time to breakdown for epoxy resin composites containing alumina and silica nanocparticles." In *18th Symposium on High Voltage Engineering*. 2013.